UNIVERSITY OF CALIFORNIA,
IRVINE

Cell-extrinsic and intrinsic regulation of *N*-glycosylation in health and disease

DISSERTATION

submitted in partial satisfaction of the requirements
for the degree of

DOCTOR OF PHILOSOPHY

in Biomedical Sciences

by

Haik Mkhikian

Dissertation Committee:
Professor Michael Demetriou, Chair
Professor Manuela Raffatellu
Professor Klemens J. Hertel

2014

DEDICATION

To

my parents,

Artem and Galia Mkhikian

TABLE OF CONTENTS

	Page
LIST OF FIGURES	iv
LIST OF TABLES	vi
ACKNOWLEDGMENTS	vii
CURRICULUM VITAE	viii
ABSTRACT OF THE DISSERTATION	x
CHAPTER 1: INTRODUCTION	1
CHAPTER 2: GENETICS AND THE ENVIRONMENT CONVERGE TO DYSREGULATE N-GLYCOSYLATION IN MULTIPLE SCLEROSIS	16
Summary	17
Introduction	18
Materials and Methods	20
Results	28
Discussion	57
References	61
Acknowledgments	68
CHAPTER 3: GOLGI PROOFREADING HOMEOSTATICALLY CONTROLS CELL GROWTH AND DIFFERENTIATION	69
Summary	70
Introduction	71
Materials and Methods	74
Results	78
Discussion	98
References	102
CHAPTER 4: CONCLUSIONS, IMPLICATIONS, AND FUTURE DIRECTIONS	105

LIST OF FIGURES

		Page
Figure 2.1	IL-2 and IL-7 signaling regulate N-glycan branching in T cells	29
Figure 2.2	N-glycan branching by IL-2 and IL-7	30
Figure 2.3	*IL2RA**T and *IL7RA**C MS risk alleles limit N-glycan branching in T cell blasts	33
Figure 2.4	sIL7RA-Fc antagonizes IL-7 signaling	34
Figure 2.5	*MGAT1* haplotypes reduce N-glycan branching	36
Figure 2.6	*MGAT1* haplotypes reduce N-glycan branching	37
Figure 2.7	Conditional regulation of N-glycan branching and T cell growth by *MGAT1* $IV_AV_{T\text{-}T}$	40
Figure 2.8	Conditional regulation of N-glycan branching and T cell growth by *MGAT1* $IV_AV_{T\text{-}T}$	41
Figure 2.9	Vitamin D_3 counters *IL2RA**T and *IL7RA**C mediated reduction in Mgat1 to promote N-glycan branching	50
Figure 2.10	*IL2RA**C and *IL7RA**T with Vitamin D3 in N-glycan branching	51
Figure 2.11	Vitamin D_3 regulates T cell growth and EAE	53
Figure 2.12	Vitamin D3 regulates N-glycan branching in activated mouse and human $CD4^+$ T cells	54
Figure 2.13	Vitamin D3 regulates CTLA-4 surface expression and N-glycan branching	55
Figure 2.14	A model for environmental and genetic dysregulation of N-glycosylation in Multiple Sclerosis	58
Figure 3.1	Hexosamine and N-glycan biosynthetic pathways in mammals	73

Figure 3.2	Compensation limits hyperactivity of Mgat2 deficient T cells	79
Figure 3.3	Branching deficiency induces poly-LacNAc on N-glycans	82
Figure 3.4	Mass spectrometry of N-glycans confirms poly-LacNAc induction by SW	84
Figure 3.5	Poly-LacNAc compensation opposes human T cell activation	86
Figure 3.6	Poly-LacNAc compensation opposes mouse T cell activation	87
Figure 3.7	Poly-LacNAc compensation inhibits severity of EAE and pro-inflammatory T cells *in vivo*	89
Figure 3.8	TCR signaling is neither necessary nor sufficient for poly-LacNAc induction	91
Figure 3.9	Poly-LacNAc induction is not dependent on increased UDP-GlcNAc levels	93
Figure 3.10	Poly-LacNAc induction cannot be accounted for by increased iGnT activity	97

LIST OF TABLES

		Page
Table 2.1	Genetic interaction in multiple sclerosis.	44
Table 2.2	Association analysis of single variants in multiple sclerosis	45
Table 2.3	Stratified analysis of *MGAT1* $IV_AV_{T\text{-}T}$ in multiple sclerosis	46
Table 3.1	List of top 50 differentially expressed genes	95
Table 3.2	List of N-glycan branching, poly-LacNAc production, and hexosamine pathway genes	96

ACKNOWLEDGMENTS

I would like to thank my thesis advisor, Dr. Michael Demetriou. Doing good science is a craft, which has to be learned through apprenticeship. I could not have asked for a better advisor or a more generous mentor. It will likely be years before I can appreciate everything he has imparted.

I would like to thank my committee members, Professor Manuela Raffatellu and Professor Klemens J. Hertel, who have given time, effort and especially support so willingly.

I would like to thank my lab mates throughout these years, Carey Li, Raymond Zhou, Lindsey Araujo, Ani Grigorian, Ken Hayama, Christie Mortales, Khachik Khachikyan and Barbara Newton for their help and friendship. I am also grateful for the help and friendship given by member of the Microbiology and Molecular Genetics department. More than a few experiments would not have been realized without encouragement, reagents, or guidance from my colleagues.

I would also like to thank my previous mentors, Dr. Philip Carpenter, Dr. Andreas Androutsellis-Theotokis and Dr. Ronald McKay. My foundation in biology was built under their guidance and their infectious enthusiasm is one of the main reasons that I enjoy science so much.

Finally, I would like to acknowledge my greatest mentor and friend, my father, Artem Mkhikian. Everything that is good in me is an imitation of his example.

Financial support was provided by the National Institutes of Health Medical Scientist Training Program at UC Irvine and the National Institutes of Health (National Heart Lung and Blood Institute) Ruth L. Kirschstein National Research Service Awards for Individual Predoctoral MD/PhD Fellows [F30 HL108451].

Curriculum Vitae

Haik Mkhikian
hmkhikian@gmail.com

EDUCATION

University of California, Irvine
Ph.D. Biomedical Sciences **2014**

University of California, Irvine
B.S. Biochemistry and Molecular Biology, Magna Cum Laude **2005**
B.A. Philosophy, Magna Cum Laude

AWARDS

- **NIH Individual MD/PhD Fellowship (F30)** - N-glycosylation as a downstream effector of Interleukin-7. NHLBI NRSA F30HL108451 **2011 – Present**
- **Medical Scientist Training Program award from NIH** **2006 – Present**
- **Laurence J. Mehlman Prize** - Awarded yearly by the UCI School of Biological Sciences to an undergraduate Biological Sciences student demonstrating outstanding achievement in both scholarship and service to the school **2005**
- **National Institutes of Health (NIH) Undergraduate Scholarship Program (UGSP)** - This is a prestigious and highly competitive program that awards only 15 new scholarships nationwide per year. In addition to the scholarship money (up to $20,000 per year), the program offers invaluable research training and experience at the NIH. **2005**
- **UCI School of Biological Science Excellence in Research Poster Award** **2004**
- **Phi Beta Kappa** **2004**
- **UROP undergraduate research grants** **2003 & 2004**

RESEARCH EXPERIENCE

Graduate Training **2008-2014**
Laboratory of Prof. Michael Demetriou, UCI
Glycosylation in human disease

NIH Undergraduate Scholar **2005-2006**
Laboratory of Dr. Ron McKay, NINDS, NIH
Signaling pathways regulating stem cell survival in vivo and in vitro

Undergraduate Research **2003-2005**
Laboratory of Prof. Philip Carpenter, UCI
Effects of tumor microenvironment on cancer cell motility

Undergraduate Research **2002-2003**
Laboratory of Prof. Michael Rose, UCI
Antagonistic pleiotropy as a mechanism of aging in Drosophila

PUBLICATIONS AND PAPERS

Yu, Z., Li, C.F., **Mkhikian, H**., Zhou, R.W., Newton, B.L., and Demetriou, M. Family studies of type 1 diabetes reveal additive and epistatic effects between MGAT1 and three other polymorphisms. **Genes and immunity.** (2014) Feb 27. doi: 10.1038/gene.2014.7.

Li CF, Zhou RW, **Mkhikian H**, Newton BL, Yu Z, Demetriou M. Hypomorphic MGAT5 polymorphisms promote multiple sclerosis cooperatively with MGAT1 and interleukin-2 and 7 receptor variants. **J Neuroimmunol. (2013) Mar 15;256(1-2):71-6**

Grigorian, A., **Mkhikian, H.** and Demetriou, M. Interleukin-2, Interleukin-7, T cell mediated autoimmunity and N-glycosylation. Ann N Y Acad Sci. (2012) **1253** 49-57

Grigorian A, **Mkhikian H**, Li CF, Newton BL, Zhou RW, Demetriou M. Pathogenesis of multiple sclerosis via environmental and genetic dysregulation of N-glycosylation. **Semin Immunopathol**. (2012) May;34(3):415-24

Mkhikian H, Grigorian A, Li CF, Chen HL, Newton B, Zhou RW, Beeton C, Torossian S, Tatarian GG, Lee SU, Lau K, Walker E, Siminovitch KA, Chandy KG, Yu Z, Dennis JW, Demetriou M. Genetics and the environment converge to dysregulate N-glycosylation in multiple sclerosis. **Nat Commun**. (2011) 2: 334. PMID: 21629267

Androutsellis-Theotokis A, Rueger MA, Park DM, **Mkhikian H**, Korb E, Poser SW, Walbridge S, Munasinghe J, Koretsky AP, Lonser RR, McKay RD. Targeting neural precursors in the adult brain rescues injured dopamine neurons. **Proc Natl Acad Sci U S A**. (2009) 106(32):13570-5. Epub 2009 Jul 23

Androutsellis-Theotokis A, Rueger MA, **Mkhikian H**, Korb E, McKay RD. Signaling pathways controlling neural stem cells slow progressive brain disease. **Cold Spring Harb Symp Quant Biol.** (2008) 73:403-10.

Mkhikian, H. The Effects of Normal Tissue on E-Cadherin Expression in Breast Cancer. **UCI Undergraduate Research Journal.** (2004) 7:53-59

ABSTRACT OF THE DISSERTATION

Cell-extrinsic and intrinsic regulation of *N*-glycosylation in health and disease

By

Haik Mkhikian

Doctor of Philosophy in Biomedical Sciences

University of California, Irvine, 2014

Professor Michael Demetriou, Chair

Essential biological systems are tightly regulated and their dysregulation is often associated with disease states. Recently, plasma membrane dynamics that globally control cell growth and differentiation have been shown to be regulated by the interaction of galectins with branched N-glycans at the cell surface. Galectins bind N-acetyllactosamine units (LacNAc: Galβ1,4GlcNAc) in branched N-glycans attached to surface glycoproteins, forming a molecular lattice that controls receptor clustering/surface-retention/signaling. LacNAc density and galectin avidity for N-glycans increase proportional to the number of LacNAc branches initiated via the sequential action of the medial Golgi branching enzymes Mgat1, 2, 4, and 5. Mgat5 deficiency marginally reduces LacNAc content by limiting N-glycans to three branches, yet results in T-cell hyperactivity and autoimmunity in mice. Despite its importance, little is known about endogenous mechanisms that regulate N-glycosylation and the galectin-glycoprotein lattice.

Here we show that multiple MS risk modulators converge to alter N-glycosylation and/or CTLA-4 surface retention conditional on metabolism and Vitamin D_3, including genetic variants in interleukin-7 receptor-α (*IL7RA**C), interleukin-2 receptor-α (*IL2RA**T),

MGAT1 (IV_AV_{T-T}) and *CTLA-4* (Thr17Ala). Down-regulation of Mgat1 by *IL7RA**C and *IL2RA**T is opposed by *MGAT1* (IV_AV_{T-T}) and Vitamin D_3, optimizing branching and mitigating MS risk when combined with enhanced CTLA-4 N-glycosylation by *CTLA-4* Thr17. Our data suggest a molecular mechanism in MS whereby multiple environmental and genetic inputs lead to dysregulation of a final common pathway, namely N-glycosylation.

We also report a startling homeostatic mechanism that maintains cell surface LacNAc content when branching is severely disrupted. Based on the model of galectin-glycoprotein lattice, restricting N-glycans to a single branch via Mgat2 deficiency or mannosidase II inhibition is expected to result in a dramaticly hyperactive state, when compared to Mgat5 deficiency. However, we find that a marked increase in poly-LacNAc extension maintains LacNAc content and galectin binding to N-glycans, thereby preventing further increases in T cell activity and autoimmunity; phenotypes reversed by targeted deficiency of the poly-LacNAc extension enzyme B3GnT2 or complete blockade of branching. Homeostatic maintenance of LacNAc content in N-glycans appears to be a general mechanism, being present in epithelial, mesenchymal and stem cells. These data define Golgi proofreading and LacNAc content, rather than unique N-glycan structures, as critical regulators of the galectin lattice, cell homeostasis and autoimmunity.

Chapter1

Introduction

Portions of this chapter are taken from:

Grigorian, A., Mkhikian, H**.** and Demetriou, M. Interleukin-2, Interleukin-7, T cell mediated autoimmunity and N-glycosylation. *Ann N Y Acad Sci*. (2012) **1253** 49-57

T cells are the master regulators of the antigen-specific adaptive immune response and play a central role in the delicate balance between protective immunity and tolerance of self-antigen. T cell activation and self-tolerance are tightly regulated and have evolved to provide effective host defense against foreign antigens while deflecting inappropriate inflammatory and autoimmune responses directed against the host [1,2]. The T cell growth cycle has distinct phases comprised of basal signaling in the absence of antigen, antigen - major histocompatibility complex (MHC) induced activation signaling, multiple rounds of cell division, growth arrest followed by differentiation into effector T cells and finally apoptosis. Dysregulation at any of these phases can lead to aberrant T cell function and autoimmune pathogenesis. The common cytokine receptor **γ-**chain (γ_c) family cytokines have important functions in T cell proliferation, differentiation and survival. Interleukin-2 (IL-2) and interleukin-7 (IL-7) are both potent T cell growth factors and have been widely considered to be key cytokines controlling the effector and regulatory arms of the immune system, yet the underlying mechanisms are not entirely clear [3,4]. Although T cell fate and function have largely been considered to be dictated by changes in gene expression and protein production, alterations in protein glycosylation is increasingly recognized as a major regulatory mechanism.

IL-2 and IL-7 regulation of T cell growth

The common cytokine receptor γ-chain (γ_c) family cytokines have central roles in the regulation of T cell growth and function, including development, proliferation, survival and peripheral tolerance. The Interleukin-2 receptor (IL-2R) is the prototypical

member of this family and consists of three subunits: the α-chain, the β-chain, and the γ_c-chain that is shared by IL-4R, IL-7R, IL-9R, IL-15R and IL-21R. IL-2 is a potent T cell growth factor identified nearly 30 years ago [5] that is well-known to induce the proliferation and survival of TCR-activated mouse and human T cells [6,7] and is required to sustain expansion of T cell populations [8]. Its crucial role in promoting T cell-dependent immune responses became questionable when it was unexpectedly found that IL-2 deficiency in mice resulted in lymphoproliferation followed by lethal autoimmunity [9-11]. These findings indicate that a critical function of IL-2 is to regulate peripheral T cell tolerance. Subsequent studies revealed that IL-2/IL-2R signaling is essential for regulatory T cell (T_{reg}) development and peripheral homeostasis [12-14]. The reduction of T_{reg} cells is thought to be a major factor in the autoimmunity associated with IL-2/IL-2R deficiency as studies show that transfer of T_{reg} cells or their reconstitution with IL-2 in these mice prevents lymphoproliferation and autoimmunity [15-17]. However, it has also been shown that transgenic overexpression of CTLA-4 can control the lymphoproliferation in IL-2 deficient mice, suggesting an important role for IL-2 in CTLA-4 mediated effector cell growth arrest [18].

Extensive studies indicate IL-2 is responsible for both generating and subsequently, limiting the T cell-dependent immune response by regulating clonal expansion, effector and T_{reg} cell development and contraction of antigen-specific T cells. The use of IL-2 in the past to boost immune responses and the current status of evaluating its use to inhibit immune responses highlights the need to re-evaluate the current understanding of the biology of IL-2. It is evident that IL-2 has a wide range of

actions with multi-faceted roles, promoting growth early in T cell activation but limiting expansion later; yet the underlying molecular mechanisms remain unclear.

`The Interleukin-7 (IL-7) receptor (IL-7R) is another member of the γ_c family and is a heterodimer comprised of IL-7Rα and the γ_c. IL-7/IL-7R is critical for the development [19] and survival [20,21] of several blood cell types. Mice mutant for IL-7 [20] or either component of its receptor [19] have major hematopoietic abnormalities and exhibit T-cell-negative (T-), B-cell-negative (B-), natural killer cell-negative (NK-) severe combined immunodeficiency (SCID). In humans, loss of function mutations in the IL-7Rα gene have been found to cause T-cell-negative (T-), B-cell-positive (B+), natural killer cell-positive (NK+) SCID [22]. In addition, IL-7 has also been found to be critical for the survival and homeostatic cycling of T-cells in the periphery [21,23,24]. Maintenance of the peripheral T-cell pool requires a low level proliferative cycling of naïve and memory cells. Under lymphopoenic conditions, this proliferative rate is dramatically increased in an effort to reconstitute the T-cell pool, and is referred to as homeostatic peripheral expansion (HPE) [25,26]. HPE has been shown to be largely deficient in the absence of IL-7 [21,23]. Several studies indicate that TCR signal strength is also critical for HPE, with IL-7 neutralization having greatest effect on the slower proliferating pool characteristic of responses to low affinity antigens, but little effect on the most rapidly proliferating pool with high affinity TCR [24,27]. However, the effector mechanisms underpinning IL-7 signaling and in particular the crosstalk with TCR signaling remain ill-defined.

Regulation of T cells by N-glycosylation

Most cell surface receptors and transporters are co- and post-translationally modified with asparagine (N)-linked glycans in the endoplasmic reticulum and Golgi apparatus following sequential but incomplete action of a series of glycohydrolases and glycosyltransferases[28,29]. Eukaryotic cell surfaces are heavily glycosylated and the size, abundance and complexity of these glycan structures provide information encoding distinct from the genome[30]. In contrast to proteins and nucleic acids, production of complex carbohydrates is not template driven. Instead, N-glycan biosynthesis depends on the nutrient environment of the cell, metabolic supply of substrates and enzymatic activities of the ER/Golgi enzymes. Cell surface N-glycans serve as ligands for a number of carbohydrate binding protein families, including galectins, siglecs and selectins, all of which play important roles in immunity. Here we focus on the role of N-glycosylation in titrating binding to galectins, interactions that regulate glycoprotein distribution and concentration at the cell surface to affect T cell function and autoimmunity[31-33].

Galectins are ubiquitously expressed at the cell surface and extracellular matrix and bind multivalent glycan ligands to form microdomains or molecular “lattices” at the cell surface[32,34,35]. The minimal binding structure for galectins is N-acetyllactosamine (LacNAc: Galactose β1,4N-acetylglucosamine)[36] and binding avidity for individual glycoproteins increase in proportion to the degree of LacNAc content within the attached N-glycans. LacNAc density is determined by the degree of N-acetylglucosamine (GlcNAc) branching per N-glycan (nutrient/environment dependent) as well as the number of N-glycans per glycoprotein (gene-encoded; occupied N-X-S/T

sites)[30]. N-glycan branching and structural diversity produced in the Golgi is dependent upon the expression and activity of N-acetylglucosaminyltransferases I, II, IV, and V (encoded by *Mgat*1, 2, 4 and 5) and the metabolic supply of the substrate uridine diphosphate N-acetylglucosamine (UDP-GlcNAc) via the hexosamine pathway [31,37,38].

The multivalent galectin-glycoprotein lattice controls the function of cell surface receptors by regulating membrane localization, lateral mobility, clustering, cell surface retention and endocytosis rates [31-33,39-46]. Growth-promoting receptors (e.g. T cell receptor (TCR) and receptor tyrosine kinases) typically have high numbers of N-glycans ($n > 5$) while growth inhibitory receptors (e.g. transforming growth factor-β receptor and cytotoxic T-lymphocyte antigen-4, CTLA-4) have few N-glycans ($n \leq 4$). Higher density of N-glycans within a glycoprotein generates significant avidity for galectins at low levels of branching, resulting in significant surface retention under basal Golgi conditions. In contrast, a low density of N-glycans falls below the threshold for stable association under basal Golgi activity and requires high levels of branching activity to incorporate into the galectin lattice and maintenance at the cell surface. For example, with increased Golgi branching activity, surface levels of glycoproteins with high N-glycan density increase with a steady, modest incline, whereas glycoproteins with low N-glycan density increase with a sharp, steep incline.

Golgi branching activity depends on both the activity of Golgi enzymes and metabolic supply of UDP-GlcNAc. As such, the strength of the galectin-glycoprotein lattice reflects both genetic and metabolic conditions to modulate receptor and transporter surface levels and cellular sensitivity to ligands and cytokines. The distinct N-glycan profile of each glycoprotein allows for differential association with the galectin

lattice dependent on Golgi branching activity, thereby determining the intricate balance between growth stimulatory and inhibitory receptors at the cell surface. In this manner, the Golgi can globally set growth characteristics of cells, controlling cellular transitions from growth to arrest/differentiation[31].

T cell expansion and inhibition are tightly regulated to ensure effective immune responses. Full T cell activation requires TCR clustering above a certain threshold, determined by engagement of the TCR with a specific MHC-peptide complex and co-signals via CD28. Binding of galectins to the multiple N-glycans of the TCR complex prevents spontaneous TCR oligomerization in the absence of antigen and subsequent filamentous (F)-actin-mediated transfer to lipid microdomains and activation of CD4-lymphocyte protein tyrosine kinase (Lck)[39]. Concurrently, galectin binding to the tyrosine phosphatase CD45 blocks F-actin-mediated movement of CD45 out of the lipid microdomain, thus maintaining a negative regulator of TCR-Lck signaling within signaling microdomains. In this manner, N-glycan branching directly controls basal TCR signaling. The same molecular mechanisms serve to set T cell activation thresholds in response to peptide-MHC. Galectin binding to the TCR complex inhibits ligand-dependent TCR clustering while concurrently promoting CD45 at the immune synapse[32,39,45,47]. For example, mice deficient in the branching enzyme β1,6-N-acetylglucosaminyltransferase V (Mgat5) or β1,3-N-acetylglucosaminyltransferase (β3GnT2), an enzyme that extends branched N-glycans with poly-LacNAc, display lower thresholds to TCR clustering, T cell activation and autoimmune disease[32,48]. Moreover, removal of N-glycan sites in the TCR results in increased receptor diffusion, clustering

and activation[45]. Galectin binding to the TCR also inhibits CD8 binding, hindering complex formation[40].

Inhibitory regulators of the T cell response are critical for T cell growth arrest, differentiation and T cell tolerance. CTLA-4 is an inhibitory receptor that competes with CD28 for CD80/CD86 co-stimulatory ligand on antigen presenting cells (APCs) and is induced to the cell surface 4-5 days following T cell activation to initiate growth arrest [49]. The levels of CTLA-4 transcript and intracellular stores of the protein increase with TCR signaling during the early T cell growth phase. However, endosomal trafficking limits CTLA-4 expression at the cell surface and therefore CTLA-4 is predominantly located in endosomes. Similar to other growth-inhibitory receptors, CTLA-4 has a low number of N-glycans (two N-X-S/T sites) and is highly sensitive to UDP-GlcNAc and N-glycan branching by the Golgi to increase binding avidity for galectins. Integration of CTLA-4 into the lattice enhances surface retention by opposing endocytic loss, resulting in sustained and increased growth arrest signaling. TCR signaling increases metabolic flux to N-glycan branching, contributing to the incorporation of CTLA-4 into the galectin lattice to sustain arrest signaling[31]. T cells deficient in Mgat5 or deficient in the galectin lattice (i.e. chemical inhibitors of branching) have decreased levels of CTLA-4 at the cell surface, but high levels inside the cells indicating a deficiency in surface retention. Cell surface levels can be enhanced by metabolic supplementation to UDP-GlcNAc as well as maximal CD28 co-stimulation, which drives metabolism.

Consistent with serving as a critical regulator of early and late T cell growth, deficiency in N-glycan branching promotes spontaneous autoimmunity. On the 129/Sv background, Mgat5 deficiency induces spontaneous kidney autoimmunity and increased

susceptibility to Experimental Autoimmune Encephalomyelitis (EAE), a model of multiple sclerosis [32]. Several mouse strains highly susceptible to EAE (PL/J, SJL and NOD) display intrinsic deficiency in N-glycan branching in T cells when compared with resistant strains (129/Sv, BALB/c, and B10.S) [50]. The PL/J strain, with the lowest levels of N-glycan branching, contains natural deficiencies in multiple N-glycan branching enzymes (i.e. Mgat1, 2, and 5) as observed by mass spectroscopy and enzyme assays. PL/J mice with targeted deficiency in Mgat5 develop a spontaneous, late-onset clinical MS-like disease manifested by inflammatory demyelination and neurodegeneration [50]. A much milder form of disease is observed in wild-type PL/J mice, consistent with the defective N-glycan branching inherent to this inbred strain.

N-glycan branching in T cells is directly influenced by metabolism, nutrient status and environmental factors, providing a potential explanation and underlying molecular mechanism for the environmental influence of T-cell mediated autoimmune disease. Golgi Mgat1, 2, 4, and 5 catalyze N-glycan branching using the same sugar-nucleotide donor (i.e. UDP-GlcNAc), but with declining efficiency [30]. Mgat1 and Mgat2 activities are limited by low affinity for N-glycan acceptors, whereas Mgat4 and Mgat5 activities are limited by UDP-GlcNAc concentrations. Therefore, initiation of branching by Mgat1 and 2 depends on rates of bulk protein synthesis while branching by Mgat4 and 5 is sensitive to metabolic production of UDP-GlcNAc. Biosynthesis of UDP-GlcNAc by the hexosamine pathway requires highly regulated intermediates of carbohydrate, nitrogen, and fatty acid metabolism [37]. Indeed, increased supply of glucose, glutamine (a critical nitrogen metabolite), acetyl-CoA (final metabolite of free fatty acids), glucosamine and N-acetylglucosamine (GlcNAc) increases N-glycan branching in T cells in culture,

suppressing T cell growth. GlcNAc supplementation in mice also increases N-glycan branching and results in inhibition of Th1 and Th17 responses, EAE and autoimmune diabetes [37,51]. Simon Murch and colleagues observed that oral GlcNAc therapy in children with treatment-resistant inflammatory bowel disease inhibited clinical disease in 8 out of 12 cases [52].

Despite the importance of the galectin-glycoprotein lattice in health and disease little is known about endogenous regulatory mechanism that maintain its normal function. As previously stated, the N-glycan branching pathway can be manipulated with inhibitors or supplementation with hexosamine pathway metabolites. In addition, a great deal is known about the glycosylation machinery, its products, and their downstream effects on cell function, pointing to many possible foci of regulation. However, the upstream signaling and mechanism responsible to computing, setting, and maintaining galectin-glycoprotein lattice strength remain largely unexplored and are the major focus of this work.

References

1 Abbas, A. K. & Janeway, C. A., Jr. Immunology: improving on nature in the twenty-first century. *Cell* **100**, 129-138 (2000).

2 Medzhitov, R. & Janeway, C. A., Jr. How does the immune system distinguish self from nonself? *Semin Immunol* **12**, 185-188; discussion 257-344, doi:10.1006/smim.2000.0230 (2000).

3 Ma, A., Koka, R. & Burkett, P. Diverse functions of IL-2, IL-15, and IL-7 in lymphoid homeostasis. *Annu Rev Immunol* **24**, 657-679, doi:10.1146/annurev.immunol.24.021605.090727 (2006).

4 Malek, T. R. The biology of interleukin-2. *Annu Rev Immunol* **26**, 453-479, doi:10.1146/annurev.immunol.26.021607.090357 (2008).

5 Taniguchi, T. *et al.* Structure and expression of a cloned cDNA for human interleukin-2. *Nature* **302**, 305-310 (1983).

6 Kim, H. P., Imbert, J. & Leonard, W. J. Both integrated and differential regulation of components of the IL-2/IL-2 receptor system. *Cytokine Growth Factor Rev* **17**, 349-366, doi:10.1016/j.cytogfr.2006.07.003 (2006).

7 Morgan, D. A., Ruscetti, F. W. & Gallo, R. Selective in vitro growth of T lymphocytes from normal human bone marrows. *Science* **193**, 1007-1008 (1976).

8 D'Souza, W. N. & Lefrancois, L. IL-2 is not required for the initiation of CD8 T cell cycling but sustains expansion. *J Immunol* **171**, 5727-5735 (2003).

9 Sadlack, B. *et al.* Ulcerative colitis-like disease in mice with a disrupted interleukin-2 gene. *Cell* **75**, 253-261 (1993).

10 Sadlack, B. *et al.* Generalized autoimmune disease in interleukin-2-deficient mice is triggered by an uncontrolled activation and proliferation of CD4+ T cells. *Eur J Immunol* **25**, 3053-3059, doi:10.1002/eji.1830251111 (1995).

11 Sadlack, B. *et al.* Development and proliferation of lymphocytes in mice deficient for both interleukins-2 and -4. *Eur J Immunol* **24**, 281-284, doi:10.1002/eji.1830240144 (1994).

12 Setoguchi, R., Hori, S., Takahashi, T. & Sakaguchi, S. Homeostatic maintenance of natural Foxp3(+) CD25(+) CD4(+) regulatory T cells by interleukin (IL)-2 and induction of autoimmune disease by IL-2 neutralization. *J Exp Med* **201**, 723-735, doi:10.1084/jem.20041982 (2005).

13 Fontenot, J. D., Rasmussen, J. P., Gavin, M. A. & Rudensky, A. Y. A function for interleukin 2 in Foxp3-expressing regulatory T cells. *Nat Immunol* **6**, 1142-1151, doi:10.1038/ni1263 (2005).

14 D'Cruz, L. M. & Klein, L. Development and function of agonist-induced CD25+Foxp3+ regulatory T cells in the absence of interleukin 2 signaling. *Nat Immunol* **6**, 1152-1159, doi:10.1038/ni1264 (2005).

15 Malek, T. R., Yu, A., Vincek, V., Scibelli, P. & Kong, L. CD4 regulatory T cells prevent lethal autoimmunity in IL-2Rbeta-deficient mice. Implications for the nonredundant function of IL-2. *Immunity* **17**, 167-178 (2002).

16 Almeida, A. R., Legrand, N., Papiernik, M. & Freitas, A. A. Homeostasis of peripheral CD4+ T cells: IL-2R alpha and IL-2 shape a population of regulatory cells that controls CD4+ T cell numbers. *J Immunol* **169**, 4850-4860 (2002).

17 Furtado, G. C., Curotto de Lafaille, M. A., Kutchukhidze, N. & Lafaille, J. J. Interleukin 2 signaling is required for CD4(+) regulatory T cell function. *J Exp Med* **196**, 851-857 (2002).

18 Hwang, K. W. *et al.* Transgenic expression of CTLA-4 controls lymphoproliferation in IL-2-deficient mice. *J Immunol* **173**, 5415-5424 (2004).

19 Peschon, J. J. *et al.* Early lymphocyte expansion is severely impaired in interleukin 7 receptor-deficient mice. *J Exp Med* **180**, 1955-1960 (1994).

20 von Freeden-Jeffry, U. *et al.* Lymphopenia in interleukin (IL)-7 gene-deleted mice identifies IL-7 as a nonredundant cytokine. *J Exp Med* **181**, 1519-1526 (1995).

21 Maraskovsky, E. *et al.* Impaired survival and proliferation in IL-7 receptor-deficient peripheral T cells. *J Immunol* **157**, 5315-5323 (1996).

22 Puel, A., Ziegler, S. F., Buckley, R. H. & Leonard, W. J. Defective IL7R expression in T(-)B(+)NK(+) severe combined immunodeficiency. *Nat Genet* **20**, 394-397, doi:10.1038/3877 (1998).

23 Schluns, K. S., Kieper, W. C., Jameson, S. C. & Lefrancois, L. Interleukin-7 mediates the homeostasis of naive and memory CD8 T cells in vivo. *Nat Immunol* **1**, 426-432, doi:10.1038/80868 (2000).

24 Tan, J. T. *et al.* IL-7 is critical for homeostatic proliferation and survival of naive T cells. *Proc Natl Acad Sci U S A* **98**, 8732-8737, doi:10.1073/pnas.161126098 (2001).

25 Stutman, O. Postthymic T-cell development. *Immunol Rev* **91**, 159-194 (1986).

26 Jameson, S. C. Maintaining the norm: T-cell homeostasis. *Nat Rev Immunol* **2**, 547-556, doi:10.1038/nri853 (2002).

27 Min, B. *et al.* Neonates support lymphopenia-induced proliferation. *Immunity* **18**, 131-140 (2003).

28 Schachter, H. The 'yellow brick road' to branched complex N-glycans. *Glycobiology* **1**, 453-461 (1991).

29 Kornfeld, R. & Kornfeld, S. Assembly of asparagine-linked oligosaccharides. *Annu Rev Biochem* **54**, 631-664, doi:10.1146/annurev.bi.54.070185.003215 (1985).

30 Dennis, J. W., Nabi, I. R. & Demetriou, M. Metabolism, cell surface organization, and disease. *Cell* **139**, 1229-1241, doi:10.1016/j.cell.2009.12.008 (2009).

31 Lau, K. S. *et al.* Complex N-glycan number and degree of branching cooperate to regulate cell proliferation and differentiation. *Cell* **129**, 123-134, doi:10.1016/j.cell.2007.01.049 (2007).

32 Demetriou, M., Granovsky, M., Quaggin, S. & Dennis, J. W. Negative regulation of T-cell activation and autoimmunity by Mgat5 N-glycosylation. *Nature* **409**, 733-739, doi:10.1038/35055582 (2001).

33 Partridge, E. A. *et al.* Regulation of cytokine receptors by Golgi N-glycan processing and endocytosis. *Science* **306**, 120-124, doi:10.1126/science.1102109 (2004).

34 Brewer, C. F., Miceli, M. C. & Baum, L. G. Clusters, bundles, arrays and lattices: novel mechanisms for lectin-saccharide-mediated cellular interactions. *Curr Opin Struct Biol* **12**, 616-623 (2002).

35 Ahmad, N. *et al.* Galectin-3 precipitates as a pentamer with synthetic multivalent carbohydrates and forms heterogeneous cross-linked complexes. *The Journal of biological chemistry* **279**, 10841-10847, doi:10.1074/jbc.M312834200 (2004).

36 Hirabayashi, J. *et al.* Oligosaccharide specificity of galectins: a search by frontal affinity chromatography. *Biochimica et biophysica acta* **1572**, 232-254 (2002).

37 Grigorian, A. *et al.* Control of T Cell-mediated autoimmunity by metabolite flux to N-glycan biosynthesis. *J Biol Chem* **282**, 20027-20035, doi:10.1074/jbc.M701890200 (2007).

38 Sasai, K., Ikeda, Y., Fujii, T., Tsuda, T. & Taniguchi, N. UDP-GlcNAc concentration is an important factor in the biosynthesis of beta1,6-branched oligosaccharides: regulation based on the kinetic properties of N-acetylglucosaminyltransferase V. *Glycobiology* **12**, 119-127 (2002).

39 Chen, I. J., Chen, H. L. & Demetriou, M. Lateral compartmentalization of T cell receptor versus CD45 by galectin-N-glycan binding and microfilaments coordinate basal and activation signaling. *J Biol Chem* **282**, 35361-35372, doi:10.1074/jbc.M706923200 (2007).

40 Demotte, N. *et al.* Restoring the association of the T cell receptor with CD8 reverses anergy in human tumor-infiltrating lymphocytes. *Immunity* **28**, 414-424, doi:10.1016/j.immuni.2008.01.011 (2008).

41 Pace, K. E., Lee, C., Stewart, P. L. & Baum, L. G. Restricted receptor segregation into membrane microdomains occurs on human T cells during apoptosis induced by galectin-1. *J Immunol* **163**, 3801-3811 (1999).

42 Lajoie, P. *et al.* Plasma membrane domain organization regulates EGFR signaling in tumor cells. *J Cell Biol* **179**, 341-356, doi:10.1083/jcb.200611106 (2007).

43 Ohtsubo, K. *et al.* Dietary and genetic control of glucose transporter 2 glycosylation promotes insulin secretion in suppressing diabetes. *Cell* **123**, 1307-1321, doi:10.1016/j.cell.2005.09.041 (2005).

44 Cha, S. K. *et al.* Removal of sialic acid involving Klotho causes cell-surface retention of TRPV5 channel via binding to galectin-1. *Proc Natl Acad Sci U S A* **105**, 9805-9810, doi:10.1073/pnas.0803223105 (2008).

45 Kuball, J. *et al.* Increasing functional avidity of TCR-redirected T cells by removing defined N-glycosylation sites in the TCR constant domain. *J Exp Med* **206**, 463-475, doi:10.1084/jem.20082487 (2009).

46 Grigorian, A., Torossian, S. & Demetriou, M. T-cell growth, cell surface organization, and the galectin-glycoprotein lattice. *Immunol Rev* **230**, 232-246, doi:10.1111/j.1600-065X.2009.00796.x (2009).

47 Chung, C. D., Patel, V. P., Moran, M., Lewis, L. A. & Miceli, M. C. Galectin-1 induces partial TCR zeta-chain phosphorylation and antagonizes processive TCR signal transduction. *J Immunol* **165**, 3722-3729 (2000).

48 Togayachi, A. *et al.* Polylactosamine on glycoproteins influences basal levels of lymphocyte and macrophage activation. *Proc Natl Acad Sci U S A* **104**, 15829-15834, doi:10.1073/pnas.0707426104 (2007).

49 Alegre, M. L., Frauwirth, K. A. & Thompson, C. B. T-cell regulation by CD28 and CTLA-4. *Nat Rev Immunol* **1**, 220-228, doi:10.1038/35105024 (2001).

50 Lee, S. U. *et al.* N-glycan processing deficiency promotes spontaneous inflammatory demyelination and neurodegeneration. *The Journal of biological chemistry* **282**, 33725-33734, doi:10.1074/jbc.M704839200 (2007).

51 Grigorian, A. *et al.* N-Acetylglucosamine Inhibits T-helper 1 (Th1)/T-helper 17 (Th17) Cell Responses and Treats Experimental Autoimmune Encephalomyelitis. *J Biol Chem* **286**, 40133-40141, doi:10.1074/jbc.M111.277814 (2011).

52 Salvatore, S. *et al.* A pilot study of N-acetyl glucosamine, a nutritional substrate for glycosaminoglycan synthesis, in paediatric chronic inflammatory bowel disease. *Aliment Pharmacol Ther* **14**, 1567-1579 (2000).

Chapter 2

Genetics and the environment converge to dysregulate *N*-glycosylation in multiple sclerosis

From:

Mkhikian H, Grigorian A, Li CF, Chen HL, Newton B, Zhou RW, Beeton C, Torossian S, Tatarian GG, Lee SU, Lau K, Walker E, Siminovitch KA, Chandy KG, Yu Z, Dennis JW, Demetriou M. Genetics and the environment converge to dysregulate N-glycosylation in multiple sclerosis. **Nat Commun**. (2011) 2: 334. PMID: 21629267

Statement of contribution

In this study, I designed and performed experiments, analyzed data, and interpreted results. My data contributes to Figures 2.1, 2.2, 2.3, 2.4, 2.7 and Tables 2.1, 2.2 and 2.3.

Summary

How environmental factors combine with genetic risk at the molecular level to promote complex trait diseases such as Multiple Sclerosis (MS) is largely unknown. In mice, N-glycan branching by the Golgi enzymes Mgat1 and/or Mgat5 prevents T cell hyper-activity, cytotoxic T-lymphocyte antigen 4 (CTLA-4) endocytosis, spontaneous inflammatory demyelination and neurodegeneration, the latter pathologies characteristic of MS. Here we show that multiple MS risk modulators converge to alter N-glycosylation and/or CTLA-4 surface retention conditional on metabolism and Vitamin D_3, including genetic variants in interleukin-7 receptor-α (*IL7RA**C), interleukin-2 receptor-α (*IL2RA**T), *MGAT1* ($IV_AV_{T\text{-}T}$) and *CTLA-4* (Thr17Ala). Down-regulation of Mgat1 by *IL7RA**C and *IL2RA**T is opposed by *MGAT1* ($IV_AV_{T\text{-}T}$) and Vitamin D_3, optimizing branching and mitigating MS risk when combined with enhanced CTLA-4 N-glycosylation by *CTLA-4* Thr17. Our data suggest a molecular mechanism in MS whereby multiple environmental and genetic inputs lead to dysregulation of a final common pathway, namely N-glycosylation.

Introduction

Multiple Sclerosis (MS) is an autoimmune and neurodegenerative disorder influenced by genetics, female gender and Vitamin D_3[1-3]. Molecular mechanisms demonstrating how gene-gene and gene-environmental interactions combine to regulate disease risk remain largely unknown. Genome wide association studies (GWAS) of common polymorphisms have identified only a proportion of the genetic variation responsible for familial disease clustering in complex trait diseases such as MS[4], leading some to suggest that rare and highly penetrant variants account for the missing heritability[5-8]. However, rare and highly penetrant variants often display Mendelian type inheritance and are relatively insensitive to environmental influences (e.g. Cystic Fibrosis). An alternative is epistatic interactions[9] between multiple independent alleles and the environment that affect a common biochemical pathway, whereby each factor has only a minor genetic and/or biological effect, but when combined results in severe deficiencies. Consistent with this, MS concordance rates in monozygotic twins are only ~30%[10], despite recent evidence that discordant twins do not harbor significant sequence differences in their genome, epigenome and transcriptome[11]. This implies direct environmental impact on genetic risk.

Virtually all cell surface and secreted proteins in metazoans are modified by co- and/or post-translational addition of complex carbohydrates in the endoplasmic reticulum (ER)/Golgi secretory pathway[12,13], providing information encoding distinct from the genome[14]. Unlike DNA/RNA/protein, production of complex carbohydrates is not template-driven, but rather is controlled by the activity of ER/Golgi enzymes and metabolic supply of their substrates. The branching and number of N-glycans per

protein molecule cooperate to regulate binding to galectins, forming a molecular lattice at the cell surface that controls the concentration and endocytosis of surface glycoproteins[14]. N-glycan number is gene-encoded while branching is conditional to activity of the Golgi α-mannosidases, N-acetylglucosaminyltransferases I, II, IV and V (Mgat1, 2, 4 and 5) and hexosamine pathway production of the substrate Uridine diphosphate N-acetylglucosamine (UDP-GlcNAc)[15,16] (Figure 2.1a). In mice, genetic deficiencies in N-glycan branching promote neurodegeneration, spontaneous inflammatory demyelination, T cell receptor clustering/signaling, T helper 1 (T_H1) differentiation and endocytic loss of the growth and autoimmune inhibitor Cytotoxic T-Lymphocyte Antigen 4 (CTLA-4), phenotypes that can be reversed by metabolic supplementation to UDP-GlcNAc biosynthesis[15-21]. Here we investigate whether similar mechanisms are active in MS through detailed biological characterization of known polymorphisms and a unique candidate gene approach. Our data suggests that N-glycosylation provides the first unifying molecular mechanism in MS, whereby convergent genetic dysregulation is modulated by multiple environmental inputs such as metabolism and sunlight/Vitamin D_3.

Materials and Methods

Reagents and Flow Cytometry

Isolated PBMCs (Histopaque-1077^{TM}; Sigma) were stimulated with soluble anti-CD3 (Biomeda). $CD3^+$ T cells purified by negative selection (RosetteSep, StemCell Technologies) were stimulated with plate-bound anti-CD3 (OKT3, eBioscience). $CD25^+$ cells were positively selected by EasySep (StemCell Technologies). Procedures with human subjects were approved by the Institutional Review Board of the University of California, Irvine. IL-2 (stock#002252) and IL7RA (stock#002295) deficient mice (Jackson Laboratories) were used between 4-8 weeks of age. $IL7R^{-/-}Mgat5^{-/-}$ mice were obtained by crossing IL7RA-deficient mice with C57BL/6 $Mgat5^{-/-}$ mice. All mice were selected randomly for experiments and approved by the Institutional Animal Care and Use Committee of the University of California, Irvine. IL2RA antagonist Ro26-4550 (Calbiochem), anti-IL-2 (clone#5334), anti-IL-7 (clone#7417), rhIL2, rhIL7, sIL2RA, sIL7RA/Fc (R&D systems) and rmIL-2 (eBioscience) were used. Human cells were stained with anti-CD4, anti-CTLA-4, anti-CD69 (eBioscience) and/or L-PHA-FITC (*Phaseolus Vulgaris* Leukoagglutinin, Vector Labs) as previously described[15,16,20]. Intracellular pStat5 staining used anti-Stat5pY694 (BDPharmingen, clone#47). Mouse cells were stained with anti-CD4 (RM 4-5), anti-CD8 (53-6.7), anti-CTLA-4 (UC10-4B9), anti-CD69 (H1.2F3), anti-B220 (RA3-6B2), anti-CD11b (M1/70), anti-CD11c (N418), and anti-CD49b (DX5) (eBioscience). Proliferation was assessed by 3H-Thymidine incorporation or 5,6-carboxyfluorescein diacetate succinimidyl ester (CFSE; Molecular Probes) at 1uM in PBS (20 min., 4^{o}C) and stimulated with plate-bound anti-CD3e (2C11, eBioscience). Cells were cultured in RPMI-1640 media supplemented with 10%

fetal bovine serum, 2μM L-glutamine, 100 U/ml penicillin/streptomycin and 2μM 2-mercaptoethanol. For CTLA-4 internalization, cells were stained for surface CTLA-4 (30 min., 4^{o}C), washed, incubated at 37^{o}C at indicated times, washed in cold FACS buffer or acid for 4 min. (0.133M citric acid, 0.0666M sodium carbonate, pH3.3). % internalization=100 x (MFI acid wash/MFI PBS wash).

Quantitative Real Time PCR and Differential Allelic Expression

RNA from transfected Lec1 cells and human PBMCs/T cells isolated by RNeasy kit (Qiagen) were reverse-transcribed by M-MLV Reverse Transcriptase (Ambion) and analyzed by real-time PCR using TaqMan Gene Expression Assays with *MGAT1* (Hs00159121_m1), *MGAT4a* (Hs00923412_m1), *MGAT4b* (Hs00365001_m1), *MGAT5* (Hs00159136_m1), *MAN1A1* (Hs00195458_m1), *MAN1A2* (Hs00198611_m1), *MAN1C1* (Hs00220595_m1), *MAN2A1* (Hs00159007_m1), *MAN2A2* (Hs00196172_m1), *GAPDH* (Hs9999905_m1), and *ACTIN* (Hs99999903_m1) primers (Applied Biosystems). Relative mRNA expression was determined by ΔΔCt method and normalized for *GAPDH* or *ACTIN* expression. Differential allelic expression was performed using two competing TaqMan probes targeting the common and VT-T polymorphisms of *MGAT1* in cDNA and gDNA isolated from two individuals heterozygous for *MGAT1* IVAVT-T haplotype. Reference curves for analyzing allelic ratios were generated using plasmid containing either common or VT-T haplotype.

DNA Sequencing and SNP Analysis

Exon2 of *MGAT*, including ~20-100 nucleotides (nt) of intronic sequence at 5' and 3' ends, was PCR-amplified from genomic DNA isolated from PBMCs and sequenced by Seqwright. SNPs were identified from chromatograms and derived sequences. All

previously unknown SNPs were sequenced in both directions at least once, and confirmed with TaqMan allelic discrimination assay (Applied Biosystems). SNP genotyping was performed using TaqMan Genotyping Assays (Applied Biosystems), except for the controls from the greater Toronto area, which used the Sequenom Mass Array platform for genotyping the two SNPs in *MGAT1* $V_{T\text{-}T}$ (rs2070924 and rs2070925). These two *MGAT1* $V_{T\text{-}T}$ SNPs are 10nt apart and were genotyped in all other cohorts using a custom TaqMan probe designed to detect both (sequence submitted to ABI was CCTCGCCCGCGTCTACGGTGCTCCCCAGCTGCAGGTGGAGAAAGTGAGGACCAA TGACCGGAAGGAG[C/T]TGGGGGAGGT[G/T]CGGGTGCAGTATACGGGCAGGGAC AGCTTCAAGGCTTTCGCCAAGGCTCTGGGTGTCATGGATGACCTTAAGTCGGGGG TTCCGAGAG). *MGAT1* IV_A (rs7726005) was also genotyped using a custom TaqMan probe (sequence: CACTACCGCTGGGCGCTGGGCCAGGTCTTCCGGCAGTTTCGCTTCCCCGCGGCC GTGGTGGTGGAGGATGACCTGGAGGTGGCCCCGGACTTCTTCGAGTACTTTC[G/A] GGCCACCTATCCGCTGCTGAAGGCCGACCCCTCCCTGTGGTGCGTCTCGGCCTG GAATGACAACGGCAAGGAGCAGATGGTGGACGCCAGCAGGCCTGAGCTGCTCTA). Accuracy of the custom TaqMan assays was confirmed by sequencing genomic DNA from 7 subjects genotyped as heterozygous for both IV_A and $V_{T\text{-}T}$ and sequencing cloned genomic DNA. Moreover, sequenom genotyping of 1387 subjects for the two separate SNPs in $V_{T\text{-}T}$ revealed 100% concordance. Human subjects are defined as positive or negative for *MGAT1* $IV_AV_{T\text{-}T}$ by genotyping IV_A and $V_{T\text{-}T}$ polymorphisms. TaqMan Genotpying Assay primers for *CTLA-4* (rs231775), *IL-2RA* (rs2104286), and *IL-7R* (rs6897932) are C___2415786_20, C__16095542_10, and C___2025977_10,

respectively. The genotyping success rate for all 5 SNPs examined was >99% in all cohorts except for *IL2RA* in control cohort 2 (98.8%). Concordance for duplicate genotyping was determined by re-genotyping all 5 SNPs in 735 samples and revealed 100% concordance for all SNPs except *CTLA-4* (99.46%).

Cloning of human *MGAT1* and *CTLA-4* variants

MGAT1 and *CTLA-4* variants were cloned into pCMV-Script (Stratagene), which utilizes human cytomegalovirus (CMV) immediate early promoter to drive expression in mammalian systems. For *MGAT1*, primers 5'-CCCCCATTTCCTCTACCTGT-3' and 5'-CCCTCCCACTCATCTGCTTTC-3' were used to PCR-amplify exon2 from genomic DNA of subjects +/- IV_A and V_{T-T} polymorphisms followed by sequencing of PCR products. Full length cDNA clones for *CTLA-4*Thr17 and Ala17 from Mammalian Gene Collection (http://mgc.nci.nih.gov/) were subcloned into pCMV vector following PCR amplification with primers 5'-TGAACACCGCTCCCATAAAG-3' and 5'-CCTCAGCTCTTGGAAATTGAA-3'. Genotypes were confirmed by allelic discrimination assay.

Transient Transfections

1×10^5 Mgat1-defective Lec1 cells seeded 24h earlier were incubated (5 hrs, 37°C) with 3ug plasmid DNA and 15 ul LIPOFECTAMINE™ (Invitrogen) serum-free DMEM and cultured for 72 hrs. Cells were stained with L-PHA-FITC (4ug/ml) +/- anti-human CTLA-4-PE (eBioscience) (30 min., 4^oC); MFIs determined on L-PHA^+ population.

Enzymatic assays

Mgat1 enzyme activity was measured using the synthetic, specific acceptor αMan(1,3)βMan-O(CH2)7CH3 (Toronto Research Chemicals). 10ul cell lysate (0.9%

NaCl, 1% Triton X-100, centrifuged 5000g, 15 min., 4°C) was added to 1mM acceptor, 1mM [63H]-UDP-GlcNAc (Amersham) in 50mM MES pH6.5, 0.1mM GlcNAc and 25mM AMP in total of 20µl. Mgat1 reactions containing 5mM $MnCl_2$, were incubated for 1 hr and stopped with ice-cold water. Enzyme products were separated from radioactive substrates by binding to 50mg C18 cartridges (Alltech) preconditioned with methanol rinsing/water washing. Radiolabeled products were eluted directly into scintillation vials with two 0.5 ml aliquots of methanol; radioactivity was determined by liquid scintillation counting.

MALDI-TOF mass spectroscopy

This was done as a service by Glycotechnology Core Facility at University of California, San Diego. PBMCs were lysed with 1% SDS in 100mM Tris pH7.4, dialyzed to remove SDS, digested with trypsin to generate glycopeptides and treated with PNGaseF to release N-glycans. N-glycans were desialylated by mild acid digestion prior to permethylation and mass spectroscopy. Monoisotopic peaks were identified using GlycanMass/GlycoMod software.

Computational model

Computational modeling of Golgi N-glycan processing and lattice-mediated glycoprotein surface retention was previously described[15]. Briefly, biochemical reaction network for N-glycan processing was represented by a series of ordinary differential equations (ODE) constructed using generalized mass action (GMA) formulation and generated structures up to a maximum size of tetra-antennary with N-acetyllactosamine and (Galβ1-4GlcNAcβ1-3)$_2$ extensions. The fraction of each N-glycan type was utilized to calculate the glycoform fractions of CTLA-4 in a combinatorial manner dependent on

number of N-glycosylation sites. Glycoform avidity for galectin lattice is represented as a linear summation of the affinity of each N-glycan, with avidity enhancements as described previously.

Vitamin D3 and Experimental Autoimmune Encephalomyelitis

To induce *in vivo* deficiency of Vitamin D3, age-matched littermate female PL/J mice were randomly selected and fed 4g/day of chow containing varying amounts of Vitamin D3 (500-625 ng, 250 ng, 125 ng; Prolab RMH 2500, LabDiet) or a diet deficient in Vitamin D3 (0 ng; specially formulated for our laboratory) for 5–21 days. 1,25(OH)2D3 (100ng) was administered *in vivo* to age-matched littermate female PL/J mice (fed diet containing 500-625ng Vitamin D3) by intraperitoneal injection every other day for the duration of the study. EAE was induced by subcutaneous immunization of randomly selected female PL/J mice at days 0 and 15 with 100μg of bovine MBP (Sigma) emulsified in Complete Freund's Adjuvant containing 4mg/ml heat-inactivated *Mycobacterium tuberculosis* (H37RA;Difco). Mice were examined daily for clinical signs of EAE over the next 40 days with observer blinded to treatment conditions. Mice were scored daily as follows: 0, no disease; 1, loss of tail tone; 2, hindlimb weakness; 3, hindlimb paralysis; 4, forelimb weakness or paralysis and hindlimb paralysis; 5, moribund or dead. All EAE mice were maintained on a diet low in Calcium and Vitamin D3 (Certified Rodent Diet 5002*;LabDiet). 100ng of 1,25(OH)2D3 was administered by intraperitoneal injection every other day and swainsonine was given orally via the drinking water starting 3 days before immunization. All mice were housed with 12 hr light/dark cycles.

DNA Datasets

We analyzed two independent randomly selected non-Hispanic Caucasian MS case-control cohorts and an African American MS cohort from North America. Cohort 1 cases consisted of unrelated, non-Hispanic Caucasians with clinically definite MS[52] obtained at University of California, Irvine (n=82) or from across the United States by Multiple Autoimmune Disease Genetics Consortium (n=176, MADGC, www.madgc.org) and Accelerated Cure Project for Multiple Sclerosis (n=943, www.acceleratedcure.org). Controls were un-related, non-diabetic, non-Hispanic, Caucasians obtained at University of California, Irvine (n=102) and from across North America by North American Rheumatoid Arthritis Consortium (n=192, NARAC, www.naracdata.org) and Type1 Diabetes Genetics Consortium (n=1199, TIDGC, www.t1dgc.com). Cohort 2 cases were un-related, non- Hispanic Caucasians with clinically definite MS obtained from across United States by BioServe (n=1030, www.bioserve.com) and University of California, San Francisco (n=1050). Cohort 2 controls were non-diabetic, non-Hispanic and un-related Caucasians obtained from across North America (BioServe (n=2972), Genetics of Kidneys in Diabetes (GoKinD) (n=746, www.niddkrepository.org), NARAC (n=1159), UCSF (n=796) and greater Toronto area (n=1387). GoKinD DNA samples were obtained from National Institute of Diabetes and Digestive and Kidney Diseases (NIDDK). The African-American MS cohort has previously been described[53] and comprises 758 unrelated MS patients and 480 unrelated controls. All study participants are self-reported African-Americans, but European ancestry was documented in the majority of individuals based on genotyping of 186 SNPs highly informative for African vs. European ancestry. Global estimation of European ancestry using these markers

indicated similar mean admixture proportions in cases and controls (21%). Individual and combined control cohorts were in Hardy Weinberg Equilibrium.

Results

IL-2 and IL-7 regulate T cell growth via N-glycan branching

Interleukin-2 receptor (*IL2R*) and interleukin-7 receptor (IL-7R) are members of the common γ chain cytokine receptor family and employ signal transduction through Stat5. Recently, genetic alterations in the IL-2 and IL-7 signaling pathways have been implicated in MS[3,22,23]. To examine whether these pathways alter N-glycan branching, we utilized flow cytometry with L-PHA (*Phaseolus vulgaris*, leukoagglutinin), a plant lectin that binds specifically to β1,6GlcNAc-branched N-glycans, the product of Mgat5 (Figure 2.1a)[18,24]. Addition of exogenous IL-2 or IL-7 to resting human T cells reduced L-PHA binding structures (hereafter termed branching) in $CD25^{-}CD4^{+}$ T cells by ~20-30% (Figure 2.1b and Figure 2.2a). Analysis of IL-2 and IL-7RA deficient *ex vivo* $CD25^{-}CD4^{+}$ mouse T cells revealed ~50% and >2-fold increases in branching, respectively, confirming that autocrine IL-2 and IL-7 signaling regulates branching *in vivo* (Figure 2.1c). As ~15-20% change in L-PHA binding is sufficient to alter T cell function, growth and autoimmune risk[16,20], these alterations are highly significant and in the case of IL-7RA deficiency, represents the largest change observed outside of direct manipulation of the Golgi branching pathway. Indeed, addition of exogenous IL-2 or IL-7 both induce ~2-fold increase in Golgi *MGAT1* mRNA as well as ~1.5 - 3 fold decreases in Golgi *MGAT5*, *MGAT4B*, mannosidase II and IIx (*MAN2A1*, *MAN2A2*) and mannosidase Ia and b (*MAN1A1*, *MAN1A2*) (Figure 2.1d, e). These mRNA changes are opposite of that induced by T cell receptor (TCR) signaling, which enhances branching[25]. Mgat1 has a ~250 fold higher affinity for UDP-GlcNAc than Mgat5 and over expression of Mgat1,

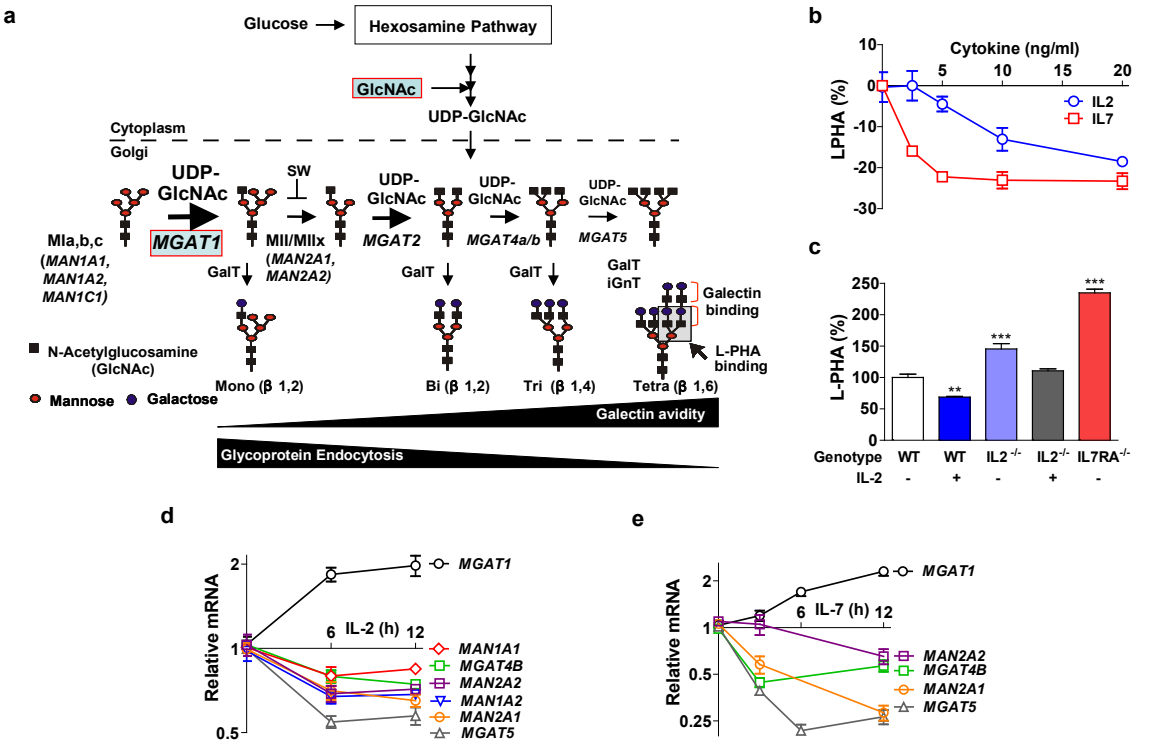

Figure 2.1. IL-2 and IL-7 signaling regulate N-glycan branching in T cells
(a) Hexosamine and N-Glycan branching pathway in mammals. Medial Golgi enzymes Mgat1, 2, 4a/b, and 5 generate mono-, bi-, tri-, and tetra-antennary branched N-glycans, respectively, in a sequential fashion that is dependent on the supply of a common substrate, UDP-GlcNAc. GlcNAc branches are further modified to create N-acetyllactosamine units which serve as binding sites for galectins and L-PHA. Mgat1, 2, 4 and 5 = N-acetylglucosaminyltransferases I, II IV and V; MII/MIIx = mannosidase II/IIx, MIa,b,c = mannosidase I,a,b,c, SW = swainsonine. Additional structural diversity via addition of sialic acid, fucose, N-acetylgalactosamine and/or sulfate is not shown[12]. **(b)** Resting human PBMCs were treated for 3 days as indicated and analyzed for L-PHA binding by FACS, gating on $CD4^+$ $CD25^-$ resting populations based on forward vs. side scatter. Mean fluorescence intensity (MFI) for control cells was used to normalize data. **(c)** Resting mouse splenocytes with the indicated genotypes were treated with IL-2 (20ng/ml) and analyzed as in (b). **(d)** Quantitative RT-PCR on cDNA derived from resting human $CD3^+$ T cells treated with IL-2 (20ng/ml) in triplicate. **(e)** Resting Human PBMCs were treated with IL-7 (20ng/ml) and analyzed as in (d). Genotypes for human cells were *IL2RA**TC and *IL7RA**CC except for panel d, which was *IL2RA**TT. P-values by ANOVA and the Newman-Keuls Multiple Comparison Test. ***p<0.001, **p<0.01 in all panels. Error bars are standard error of triplicate or greater values in all pnaels.

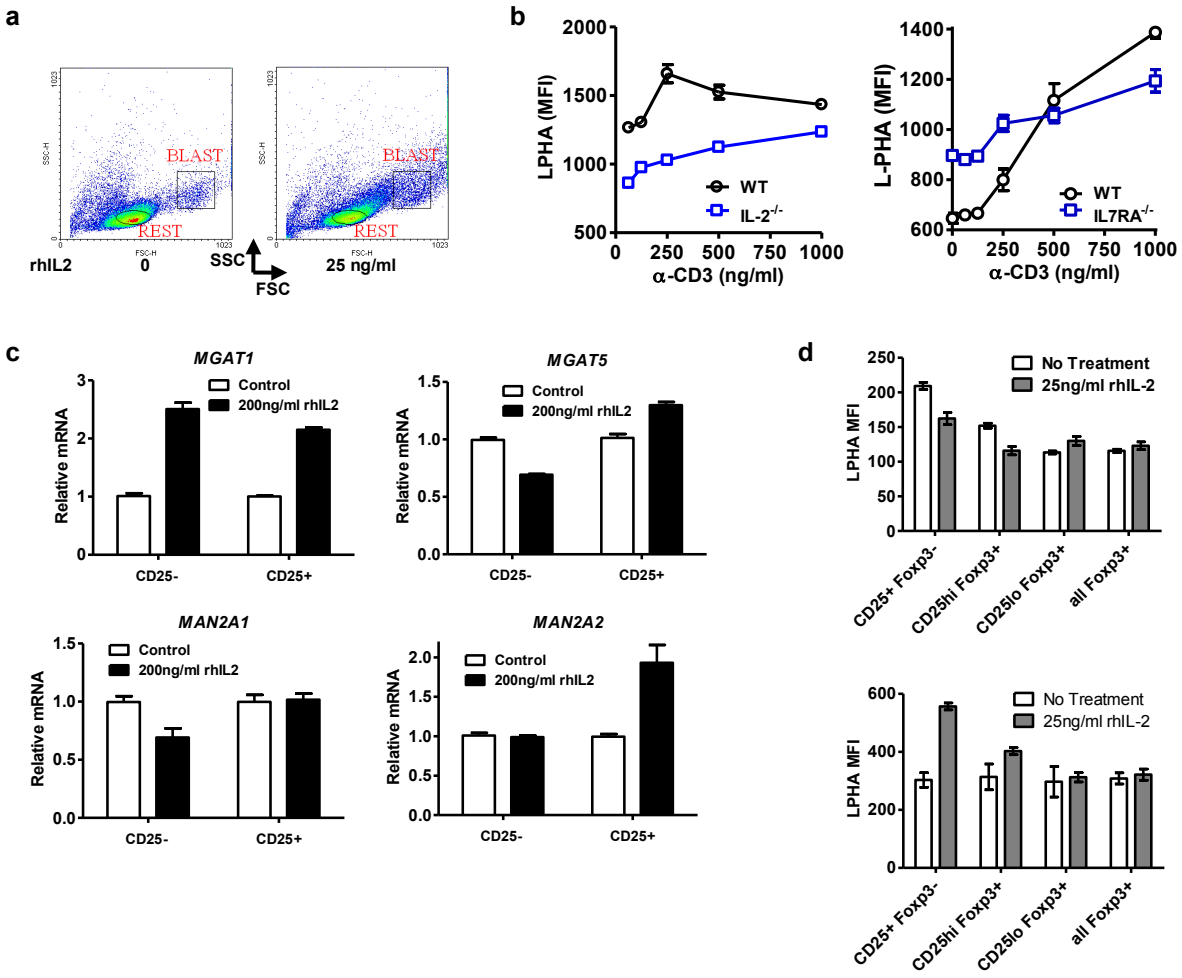

Figure 2.2. N-glycan branching by IL-2 and IL-7

(a) Human $CD3^+$ T cells treated with the indicated concentrations of rhIL-2 for four days. The gated regions indicate cells considered at rest or blasting. FCS – forward scatter, SSC – side scatter. **(b)** Mouse splenocytes of the indicated genotypes were stimulated with anti-CD3 for 5 days (right panel) or 3 days (left panel). $CD25^+CD4^+$ T cell blasts were analyzed by FACS for L-PHA binding. **(c)** Quantitative RT-PCR on cDNA derived from human T cells (*IL2RA**CT and *IL7RA**CT). Purified $CD3^+$ T cells were stimulated with plate bound anti-CD3 (1ug/ml) for 2 days in the presence of 10ug/ml anti-IL2 to induce CD25 expression in the absence of IL-2 signaling. $CD25^+$ and $CD25^-$ cells were then isolated by the EasySep human CD25 positive selection kit and treated with rhIL2 (200ng/ml) for 12 hours prior to isolation of RNA. **(d)** L-PHA FACS analysis of the indicated T cell subsets (*IL2RA**CT and *IL7RA**CC) with and without rhIL2 treatment for four days, gated on resting (top) or blasting (bottom) cells as shown in (a). MFI = mean fluorescence intensity.

particularly in the presence of reduced Mgat4 and Mgat5, decreases branching by limiting UDP-GlcNAc supply to Mgat4 and Mgat5[15,25].

T cell activation enhances branching as well as IL-2 and IL-2RA expression; therefore we next examined the effects of IL-2 and IL-7 signaling in T cell blasts. Remarkably, exogenous IL-2 enhanced TCR signaling-induced increases in branching in $CD25^+CD4^+$ mouse and human T cell blasts, while anti-IL-2 neutralizing antibody, the IL-2RA antagonist Ro26-4550 and/or IL-2 deficiency had the opposite effect (Figure 2.3a and Figure 2.2b). Similarly, addition of exogenous IL-7 increased branching in human $CD25^+CD4^+$ T cell blasts while deficiency of IL-7RA limited up-regulation of branching in mouse $CD25^+CD4^+$ T cell blasts (Figure 2.3b and Figure 2.2b). IL-2 treatment significantly enhanced transcripts of *MGAT1* > *MAN2A2* > *MGAT5* in TCR-activated $CD25^+CD3^+$ T cells (Figure 2.2c). These data are consistent with the ultra-sensitive kinetics of the Golgi branching pathway[15], where *MGAT1* hyperactivity limits branching in resting T cells with low UDP-GlcNAc and Mgat5 activity but enhances branching in T cell blasts where UDP-GlcNAc, Mgat5 and mannosidase IIx are enhanced. CD25 is also constitutively expressed by $FoxP3^+$ T regulatory cells (Treg); however IL-2 enhanced branching to a much greater extent in $CD25^+FoxP3^-$ T cell blasts (Figure 2.2d). Thus, IL-2 and IL-7 co-regulate multiple Golgi genes to reduce branching in resting T cells; but promote branching in T cell blasts.

Cytokine induced alterations in branching are expected to initially promote TCR mediated growth[18], followed by enhanced growth arrest of T cell blasts via increased CTLA-4 surface expression[15]. Indeed, pre-treatment of resting human T cells with IL-2 significantly enhanced TCR signaling mediated up-regulation of CD69 in the absence

but not presence of N-Acetylglucosamine (GlcNAc) and uridine (Figure 2.3c). GlcNAc and uridine enhance branching by increasing UDP-GlcNAc supply to the Golgi[15,16], and rescued reductions induced by IL-2 (Figure 2.3c inset). Similarly, analysis of IL7RA$^{-/-}$ Mgat5$^{-/-}$ double knockout mice revealed that suppression of TCR activation by IL7RA deficiency requires Mgat5 (Figure 2.3d). In CD25^{+}CD4^{+} T cell blasts, anti-IL-2 neutralizing antibody and IL-2 deficiency reduced CTLA-4 surface expression (Figure 2.3e, f), the latter reversed by the addition of exogenous IL-2 in the absence but not presence of swainsonine (SW) (Figure 2.3f). SW is an inhibitor of Golgi α-mannosidase II/IIx that reduces branching downstream of Mgat1 (Figure 2.1a)[26], confirming that IL-2 promotes CTLA-4 surface retention by increasing branching.

IL2RA and *IL7RA* MS risk alleles reduce *MGAT1* and branching

The *IL2RA**T (rs2104286) and *IL7RA**C (rs6897932) MS risk alleles are the common alleles in Caucasian populations (frequency ~75%) and are associated with enhanced secretion of soluble receptors (i.e. sIL2RA and sIL7RA) that bind cognate cytokines and antagonize signaling (Figure 2.4a-c)[22,27-29]. Exogenous sIL2RA and sIL7RA/Fc chimera both reduced branching in CD25^{+}CD4^{+} T cells blasts, an effect that was additive when combined and rescued by exogenous IL-7 or GlcNAc (Figure 2.3a, b). Blocking IL-2 and IL-7 signaling with sIL2RA + sIL7RA or anti-IL-2 + anti-IL-7 neutralizing antibodies both reduced *MGAT1* mRNA in CD25^{+}CD4^{+} T cells blasts while having little effect on *MGAT5* expression (Figure 2.3g and Figure 2.4d). sIL2RA reduced CTLA-4 surface levels in T cell blasts to a similar degree as anti-IL-2 neutralizing antibody (Figure 2.3e). Directly comparing T cell blasts with or without the

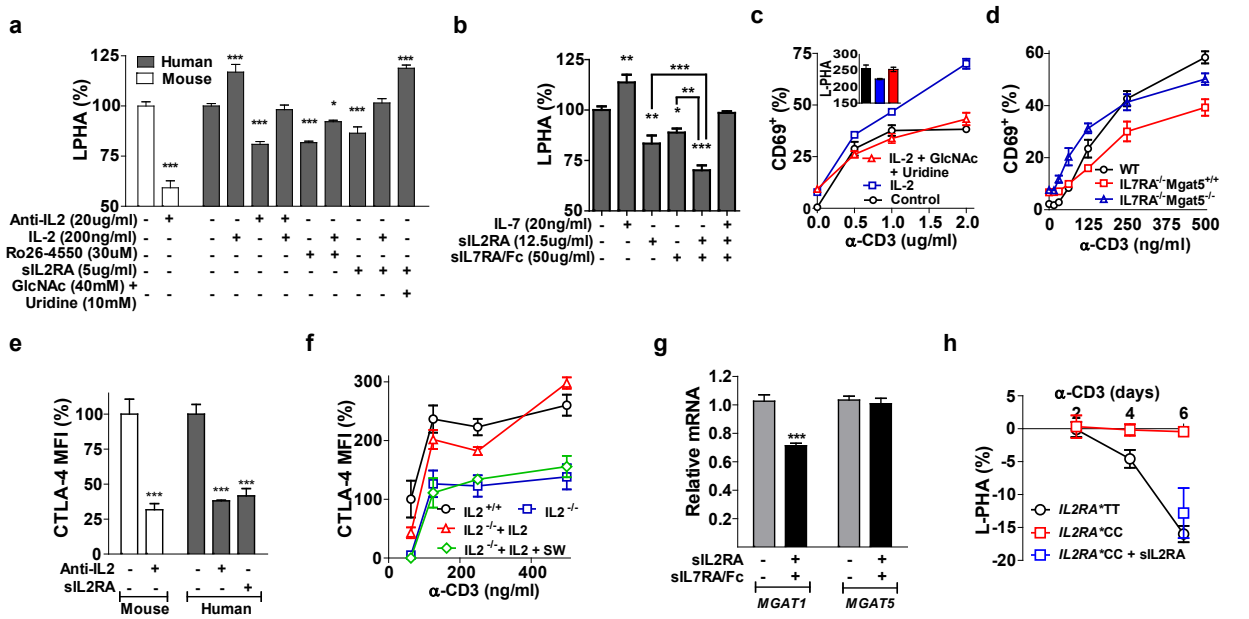

Figure 2.3. ***IL2RA*T and *IL7RA*C MS risk alleles limit N-glycan branching in T cell blasts**
(a) Human CD3$^+$ T cells or mouse splenocytes were stimulated with anti-CD3 (200ng/ml) and treated as indicated for 5 days. CD25$^+$CD4$^+$ T cell blasts were analyzed for L-PHA binding by FACS. Ro26-4550 is an IL-2RA antagonist. **(b)** Human T cells were stimulated with anti-CD3 (200ng/ml) and treated as indicated for 5 days. CD25$^+$CD4$^+$ T cell blasts were analyzed as in (a). **(c)** Purified human T cells were pre-treated for 3 days with IL-2 (20ng/ml) and/or GlcNAc (40mM) + uridine (10mM), and then stimulated with anti-CD3 for 24 hrs. CD4$^+$ T cells were analyzed for CD69 expression and L-PHA binding by FACS. **(d)** Mouse splenocytes with the indicated genotypes were stimulated with anti-CD3 for 3 days. CD4+ T cells were analyzed as in (c). **(e)** Human T cells or mouse splenocytes were stimulated with anti-CD3 (200ng/ml) and treated with anti-IL2 (20ug/ml) or sIL2RA (5ug/ml) for 5 days. CD25$^+$CD4$^+$ T cell blasts were analyzed for CTLA-4 surface expression. Data are normalized to control and by subtracting background from unstimulated CD4$^+$ T cells. **(f)** Mouse splenocytes with the indicated genotypes were stimulated with anti-CD3 for 5 days, with or without IL-2 (20ng/ml) and/or SW (150nM) addition at day 3. CD25$^+$CD4$^+$ T cell blasts were analyzed for CTLA-4 surface expression as in (e). **(g)** Human CD25$^+$CD4$^+$ T cells were stimulated with anti-CD3 (200ng/ml) and treated with sIL2RA (12.5ug/ml) and/or sIL7RA/Fc (50ug/ml) for 3 days. Relative mRNA levels were measured by quantitative RT-PCR (normalized to actin). **(h)** Human T cells (*IL7RA*CC) with the indicated genotypes were stimulated with anti-CD3 (200ng/ml) for 2-6 days, with or without sIL2RA (12.5ug/ml). CD25$^+$CD4$^+$ T cell blasts were analyzed for L-PHA binding by FACS as in (a). Genotypes were *IL2RA*CC and *IL7RA*CC in panel a; *IL2RA*CT and *IL7RA*CT in panels b, e and g; *IL2RA*CT and *IL7RA*CT in panels c and d; all lacked the *MGAT1* $IV_AV_{T\text{-}T}$ haplotype. MFI = mean fluorescence intensity. P-values by ANOVA and the Newman-Keuls Multiple Comparison Test. ***p<0.001, **p<0.01, *p<0.05 in all panels. Error bars are standard error of triplicate or greater values in all panels.

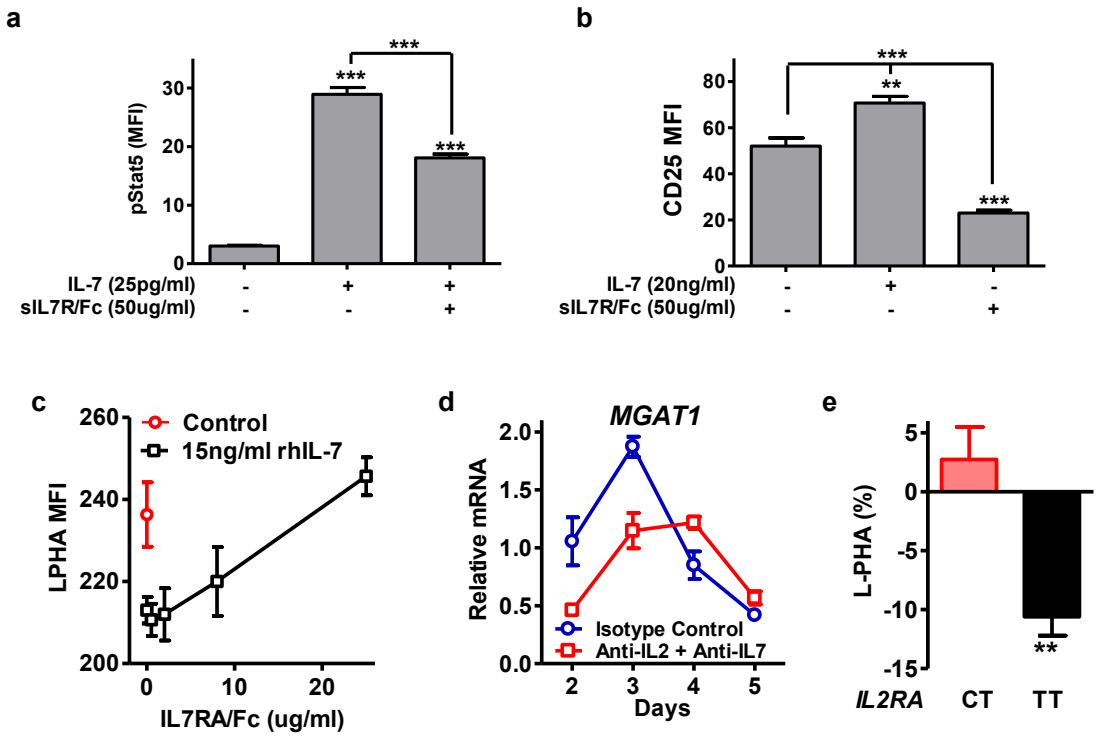

Figure 2.4. **sIL7RA-Fc antagonizes IL-7 signaling**
(a) Resting human CD3$^+$ T cells (*IL2RA**CT and *IL7RA**CC) were treated in triplicate as indicated for 15 minutes, then fixed and analyzed for intracellular Stat5 phosphorylation by FACS, gating on CD4$^+$ cells. **(b)** Human CD3$^+$ T cells (*IL2RA**CT and *IL7RA**CT) were stimulated with plate bound anti-CD3 (400ng/ml) and treated as indicated for 5 days. CD25 expression in CD4$^+$ T cells were analyzed by FACS. **(c)** L-PHA FACS analysis of resting human CD3$^+$ T cells (*IL2RA**CT and *IL7RA**CT) treated as indicated for 3 days. Data are gated on CD4$^+$ T cells. **(d)** Quantitative RT-PCR on cDNA derived from human T cells (*IL2RA**CT and *IL7RA**CT). Purified CD4$^+$ T cells were stimulated with plate bound anti-CD3 for the indicated times in the presence or absence of anti-IL-2 + anti-IL-7 neutralizing antibody. CD25$^+$ cells were used to isolate RNA. Relative mRNA levels were normalized to actin. **(e)** Human CD3$^+$ T cells of the indicated genotypes and matched for *IL7RA* (CC) and *MGAT1* (common variant) were stimulated with anti-CD3 (4ug/ml) for 6 days and analyzed for L-PHA staining by FACS. CD25$^+$CD4$^+$ T cell blasts were gated based on forward vs. side scatter. MFI = mean fluorescence intensity.

*IL2RA**T risk allele revealed minimal differences in branching during early stages of activation; however by day 6, branching in *IL2RA**TT and *IL2RA**TC blasts was significantly reduced relative to *IL2RA**CC blasts (Figure 2.3h, Figure 2.4e), consistent with enhanced endogenous sIL2RA production by the T allele. Addition of exogenous sIL2RA to *IL2RA**CC T cell cultures lowered branching at day 6 to that observed in *IL2RA**TT blasts (Figure 2.3h), confirming differences in branching arose from reduced endogenous sIL2RA in *IL2RA**CC T cell cultures. Thus, soluble receptors associated with the *IL2RA**T and *IL7RA**C risk alleles combine to down-regulate *MGAT1* and branching in T cell blasts.

MGAT1 variants alter branching conditional on metabolism

Next we directly screened the *MGAT1* gene for functional variants. Sequencing the *MGAT1* coding region (exon 2) in 42 MS patients identified a high frequency of variants suitable for functional testing (Figure 2.6a). Directly cloning PCR-amplified genomic DNA revealed multiple haplotypes that rescued cell surface binding to L-PHA when transiently transfected into Lec1 cells[30], an Mgat1-deficient Chinese Hamster Ovary (CHO) cell line (Figure 2.5a and Figure 2.6b,c). All variant haplotypes were less effective than the common haplotype, with those harboring both the IV_A (rs7726005) and $V_{T\text{-}T}$ (rs2070924 and rs2070925) polymorphisms reducing branching ~20%. The IV_A and $V_{T\text{-}T}$ polymorphisms appear to exert additive effects, as separately each displayed a ~10% reduction in branching. Consistent with this, anti-CD3 and myelin-activated T cells heterozygous for the IV_A and $V_{T\text{-}T}$ polymorphisms (hereafter referred as the *MGAT1* $IV_AV_{T\text{-}T}$ haplotype) displayed reduced up-regulation of branching (Figure 2.5b,c).

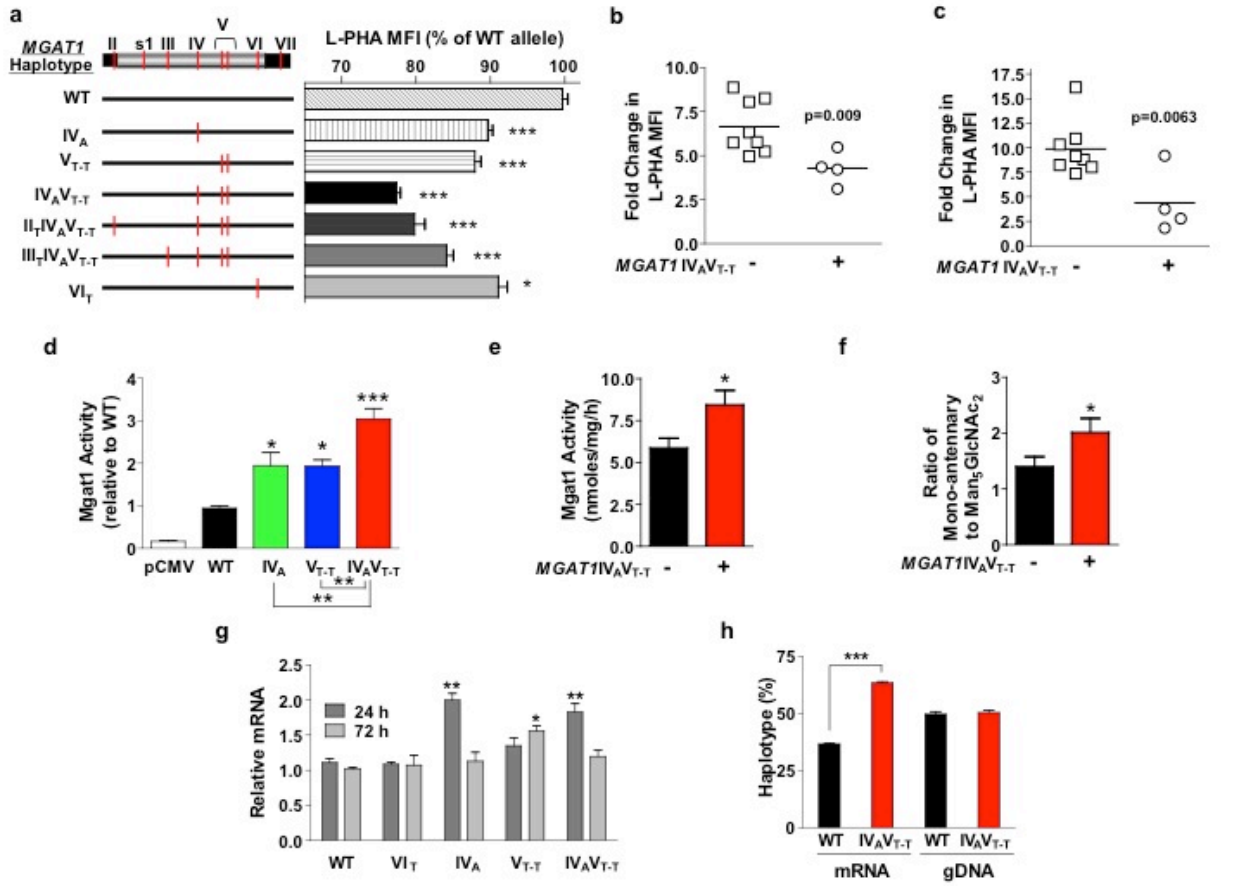

Figure 2.5. ***MGAT1*** **haplotypes reduce N-glycan branching**
(**a**) *MGAT1* exon 2 was amplified by PCR from genomic DNA, cloned into the pCMV vector, sequenced to identify haplotypes, transiently transfected into Mgat1-deficient CHO cells (Lec1) in triplicate and analyzed 3 days later by L-PHA FACS. MFI was determined on the L-PHA$^+$ population and normalized to the common haplotype (WT). (**b**) Anti-CD3 or (**c**) myelin peptide was used to stimulate PBMCs from healthy human controls for 48hr. Fold increase in L-PHA MFI in CD4$^+$ T cells following stimulation was determined by comparing unstimulated resting cells with blasting cells in each subject. All subjects had ≥3 *IL2RA**T + *IL7RA**C risk alleles except one subject in each group heterozygous for both. **(d)** Mgat1-deficient Lec1 cells were transiently transfected with the indicated *MGAT1* haplotypes and lysed to assess Mgat1 enzyme activity. Average Mgat1 activity for WT (common haplotype) was 6.45 nmoles/mg/hr. Activities were normalized for transfection efficiency. **(e)** Human PBMCs with the indicated genotypes (n=4 per genotype) were lysed to assess Mgat1 enzyme activity as in (d). Subjects had ≥3 *IL2RA**T + *IL7RA**C risk alleles. (**f**) N-glycans in human PBMCs with the indicated genotypes (n=6 per genotype) were analyzed by MALDI-TOF mass spectroscopy and normalized by taking the ratio of the intensity of mono-antennary ((Gal)GlcNAc$_1$Man$_5$GlcNAc$_2$) to Man$_5$GlcNAc$_2$, the product and acceptor of Mgat1, respectively. Subjects had ≥3 *IL2RA**T + *IL7RA**C risk alleles except for two *MGAT1* IV$_A$V$_{T\text{-}T}$ subjects that were double heterozygotes; removal of which does not alter the result (i.e. 2.01 vs. 1.97). (**g**) Lec1 cells transfected with the indicated *MGAT1* haplotypes were analyzed for relative mRNA levels by quantitative RT-PCR. Expression was normalized for transfection efficiency. **(h)** Human PBMCs from two heterozygous *MGAT1* IV$_A$V$_{T\text{-}T}$ subjects were examined for differential allelic expression by comparing the relative abundance of mRNA and genomic DNA (gDNA) for each haplotype *in vivo*. MFI = mean fluorescence intensity. P values in panels b, c, e, f, h by t-test and panels a, d, g by ANOVA and the Newman-Keuls Multiple Comparison Test. *p<0.05, **p<0.01, ***p<0.001 in all panels. Error bars are standard error of triplicate or greater values in all panels.

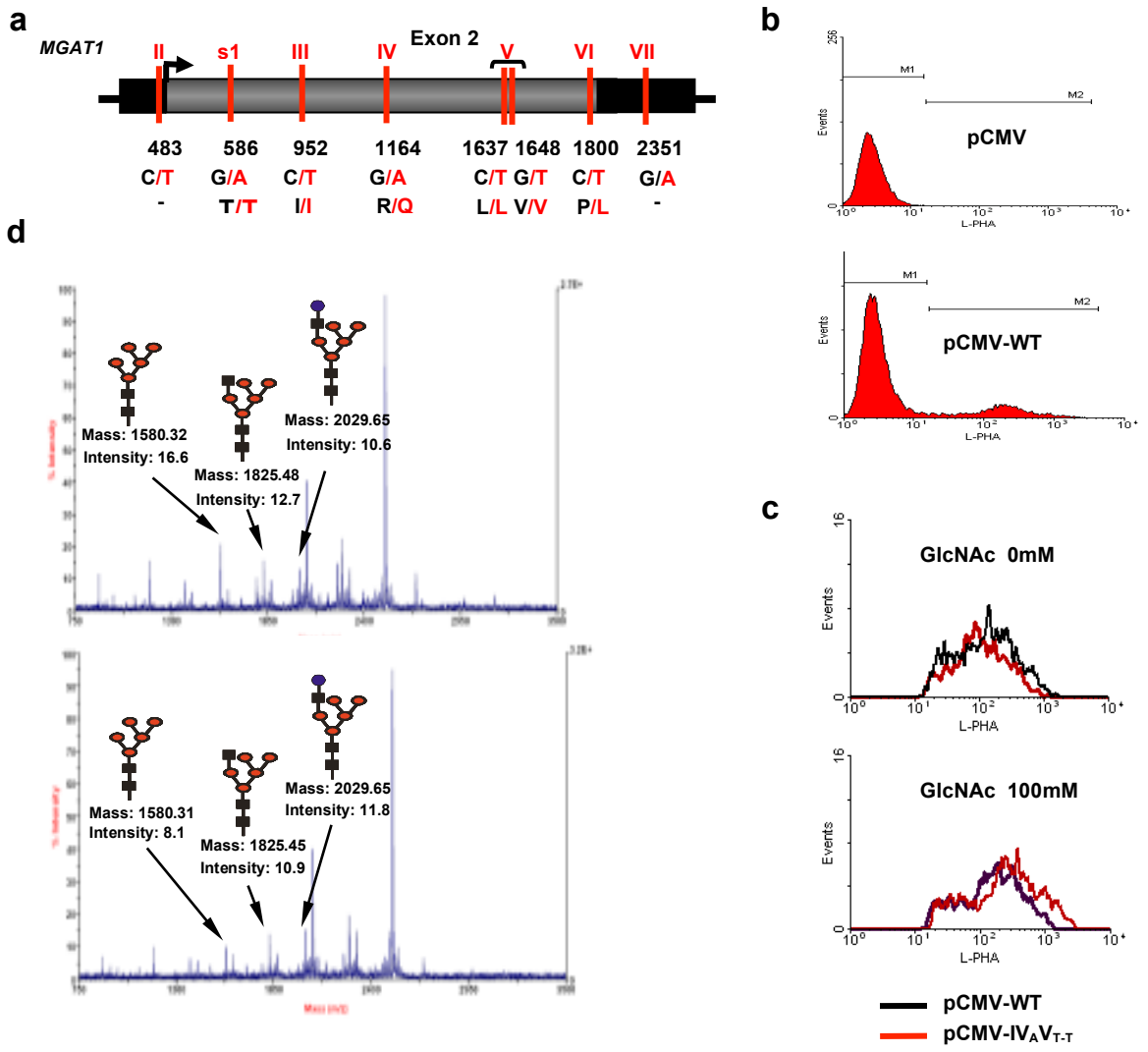

Figure 2.6. *MGAT1* haplotypes reduce N-glycan branching
(a) SNPs in *MGAT1* identified by sequencing 42 MS patients. II – ss104807085, III - ss104807087, IV - rs7726005, V – rs2070924 and rs2070925, VI – rs634501, VII - ss104807088 and s1-ss104807086. **(b)** Examples of L-PHA FACS histograms used to generate data for Lec1 transfection experiments measuring L-PHA binding. Mgat1-deficient Lec1 cells transiently transfected in triplicate with empty vector (pCMV) or various *MGAT1* haplotypes were stained with L-PHA and analyzed by FACS. The M2 gait, representing all transfected cells, was used to determine MFI for all data, with error bars representing standard error of triplicate values. **(c)** Examples of L-PHA FACS histograms used to generate data for GlcNAc supplementation experiments with transfected Lec1 cells. **(d)** Examples of two spectra from donors with the *MGAT1* common (top) or IVAVT-T (bottom) haplotype used to calculate the ratio of mono-antennary (i.e. (Gal)GlcNAc1Man5GlcNAc2) to Man5GlcNAc2. To normalize the data, the peak intensities of mass ion 1825 (GlcNAc1Man5GlcNAc2) and 2029 (Gal1GlcNAc1Man5GlcNAc2) were added together and divided by the peak intensity of mass ion 1580 (Man5GlcNAc2). This ratio was obtained from spectra of 6 individuals with and 6 individuals without the *MGAT1* IVAVT-T haplotype (i.e. 12 samples in total) and analyzed by t-test.

Transient transfection into Lec1 cells demonstrated that the IV_A, V_{T-T} and IV_AV_{T-T} haplotypes increased Mgat1 activity ~2, 2 and 3 fold, respectively, a phenotype also associated with peripheral blood mononuclear cells (PBMCs) harboring the *MGAT1* IV_AV_{T-T} haplotype (Figure 2.5d,e). MALDI-TOF mass spectroscopy confirmed the N-glycan product of Mgat1 (mono-antennary) was increased relative to its N-glycan acceptor ($Man_5GlcNAc_2$) in PBMCs with the *MGAT1* IV_AV_{T-T} haplotype (Figure 2.5f and Figure 2.6d).

The *MGAT1* IV_AV_{T-T} haplotype harbors three polymorphisms in exon 2: an upstream non-synonymous coding single-nucleotide polymorphism (SNP) (IV_A: G1164A encoding Arg223Gln) and two synonymous coding SNPs that are 10 nucleotides apart (V_{T-T}: C1637T and G1648T). Based on the Mgat1 enzyme crystal structure, Arg223Gln is a surface-exposed residue far from the active site and therefore unlikely to effect enzyme activity[31]. However, IV_A increases *MGAT1* mRNA levels relative to the common haplotype in Lec1 transfected cells (Figure 2.5g). The two synonymous SNPs in V_{T-T}, with or without IV_A, also increase mRNA expression following transfection, although with differing kinetics. Analysis of heterozygous PBMCs confirms mRNA levels of the *MGAT1* IV_AV_{T-T} haplotype are ~2 fold higher than the common haplotype *in vivo* (Figure 2.5h).

The Km of Mgat5 for UDP-GlcNAc is significantly higher than Mgat1 (~11 mM vs ~0.04 mM), whereas this difference is reversed for their respective N-glycan acceptors (~0.087 mM vs ~2 mM)[15]. The ~2-3 fold increase in Mgat1 expression induced by the *MGAT1* IV_AV_{T-T} haplotype increases Mgat1 product (Figure 2.5f) while also reducing UDP-GlcNAc supply to downstream Mgat5. The latter is predicted to reduce

β1,6GlcNAc branching by Mgat5 and indeed, this is observed both experimentally (Figure 2.5a,b) and with computational modeling (Figure 2.7a)[15]. Thus, *MGAT1* IV_AV_{T-T} acts dominantly to reduce branching under basal UDP-GlcNAc levels, but with increasing UDP-GlcNAc and/or Mgat5 levels, enhanced Mgat1 expression is expected to become less effective in limiting supply of UDP-GlcNAc to Mgat5, thereby allowing Mgat5 to act upon the increased supply of N-glycan acceptors from Mgat1 to first equalize then super-rescue β1,6GlcNAc branching. Indeed, these pathway dynamics are revealed by computational modeling (Figure 2.8a) and confirmed experimentally by increasing UDP-GlcNAc levels in transiently transfected Lec1 cells and $CD4^+$ T cells via GlcNAc supplementation (Figure 2.7b and Figure 2.8b). Consistent with this model, the magnitude of super-rescue by GlcNAc for the IV_A, V_{T-T} and IV_AV_{T-T} haplotypes was proportional to baseline enzyme activities. Thus, the gain-of-function haplotypes of *MGAT1* reduce branching under basal conditions, but enhance levels when UDP-GlcNAc and/or Mgat5 are increased beyond a threshold.

Consistent with reduced branching, resting PBMCs heterozygous for the *MGAT1* IV_AV_{T-T} haplotype are more sensitive to TCR agonist than cells homozygous for the common *MGAT1* haplotype (Figure 2.7c). Blocking branching with SW enhanced proliferation of cells with the common *MGAT1* haplotype but had little effect on cells heterozygous for the *MGAT1* IV_AV_{T-T} haplotype, the latter consistent with the pre-existing deficiency in branching (Figure 2.7c).

The Thr17Ala polymorphism in human *CTLA-4* encodes a non-synonymous SNP (49A/G, rs231775) in the signal peptide that reduces average N-glycan occupancy at the two N-X-S/T sites from two to one, limiting CTLA-4 surface levels and promoting T

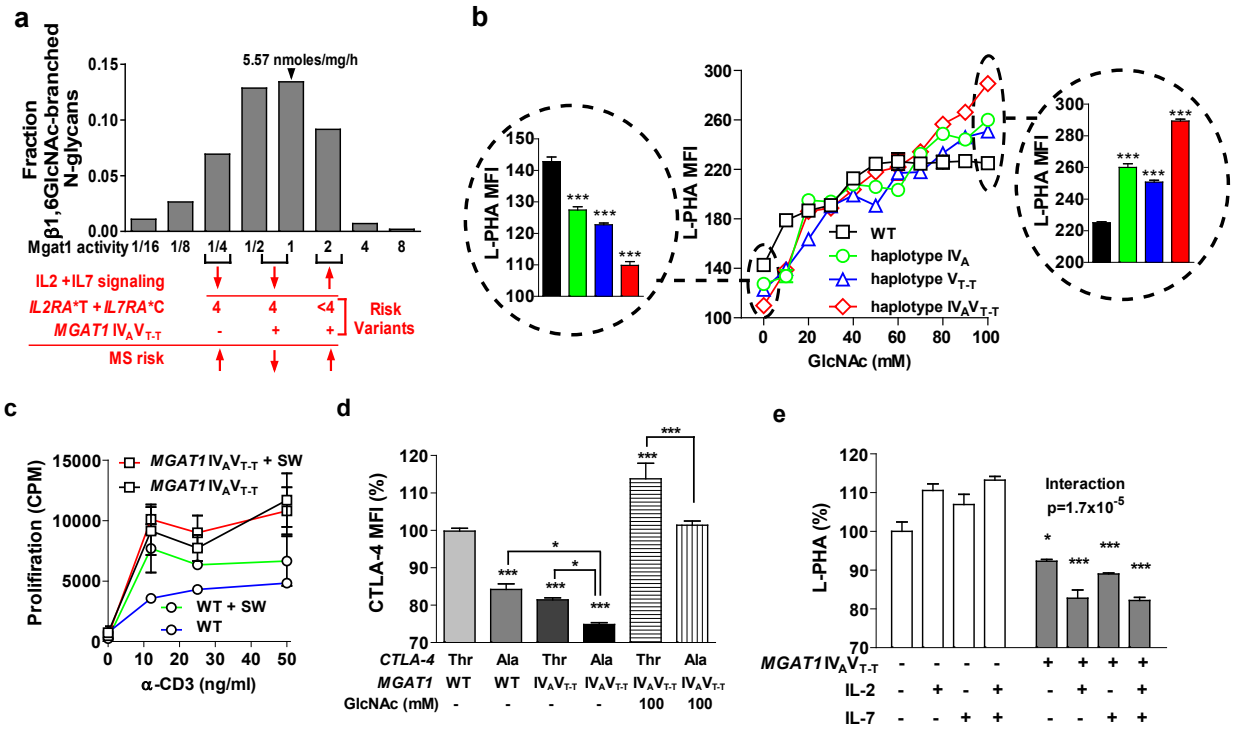

Figure 2.7. Conditional regulation of N-glycan branching and T cell growth by *MGAT1* IV_AV_{T-T}

(a) Ordinary differential equation (ODE) model of medial Golgi enzyme reactions showing predicted alterations in β1,6GlcNAc branching when varying Mgat1 activity in the presence of fixed activities in Mgat2, 4 and 5. Activities in resting mouse 129/Sv T cells were used for Mgat1, Mgat2, Mgat5[20], while Mgat4 was estimated. In red, predicted effects of IL2/IL7 signaling and various genetic combinations of *IL2RA*T* + *IL7RA*C* risk alleles (4 alleles or less than 4) on Mgat1 activity, β1,6GlcNAc branching and MS risk in the absence or presence of the *MGAT1* IV_AV_{T-T} haplotype. **(b)** Mgat1-deficient Lec1 cells transiently transfected as indicated were co-incubated with or without GlcNAc for 3 days and then analyzed by FACS for L-PHA binding. P-values by ANOVA and Newman-Keuls Multiple Comparison Test. **(c)** PBMCs heterozygous for the *MGAT1* IV_AV_{T-T} haplotype (n=2 subjects assayed in triplicate) or homozygous for the common haplotype (WT) (n=1 subject assayed in triplicate) were stimulated with anti-CD3 and analyzed for proliferation as indicated for 2 days. Subjects used were *IL2RA**T/C, *IL7RA**CC, and CTLA-4 Thr/Ala. Error bars represent range of all values. **(d)** Transiently transfected Lec1 cells with or without GlcNAc treatment (3 days) were analyzed for CTLA-4 expression by FACS. P-values by ANOVA and Newman-Keuls Multiple Comparison Test. **(e)** PBMCs with the indicated genotype (n=2) were stimulated with anti-CD3 (200ng/ml) and treated with IL-2 (20ng/ml) and IL-7 (20ng/ml) for 5 days. Subjects used were *IL2RA**T/C, *IL7RA**CC, and CTLA-4 Thr/Thr. Data is the average of triplicate values for each subject. MFI = mean fluorescence intensity. P-values by 2-way ANOVA and Bonferoni's multiple comparison test. *p<0.05, **p<0.01, ***p<0.001 in all panels. Error bars are standard error of triplicate or greater values in all panels unless otherwise stated.

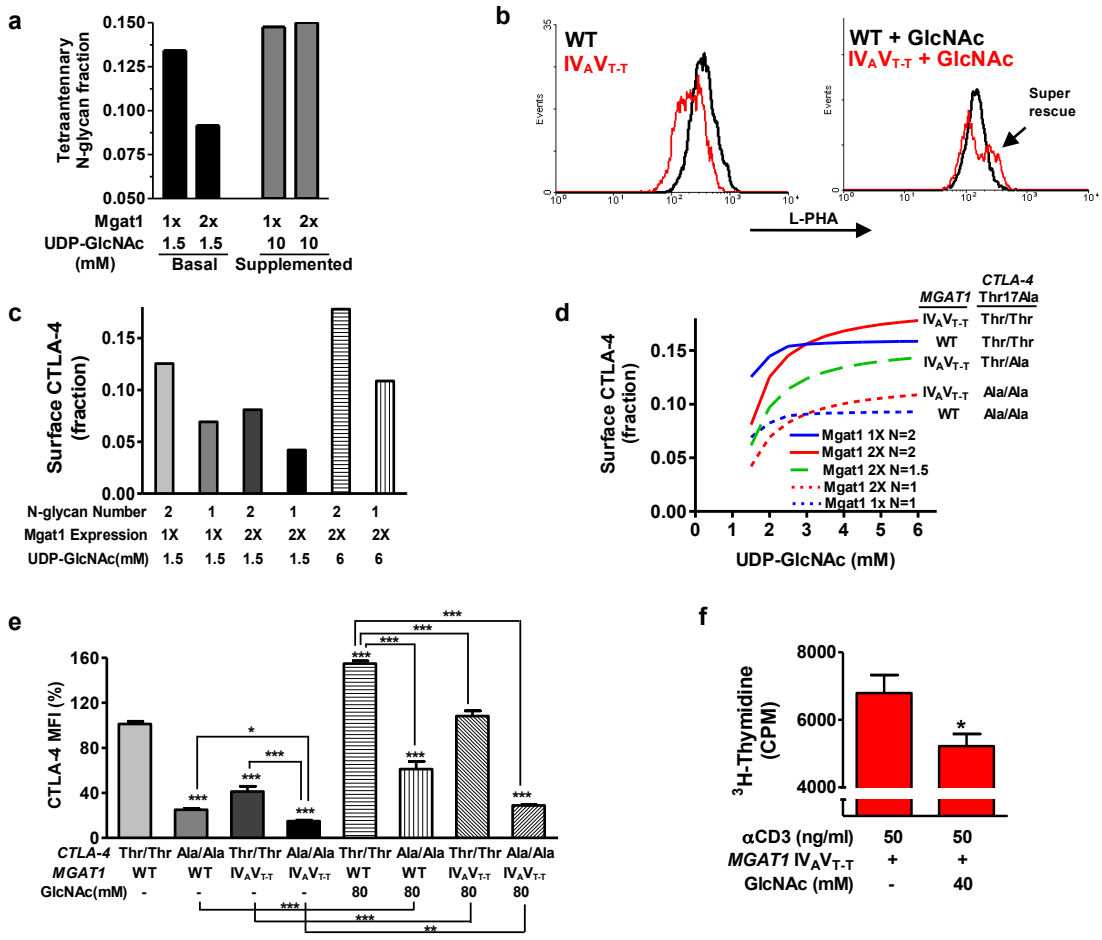

Figure 2.8. Conditional regulation of N-glycan branching and T cell growth by *MGAT1* IV_AV_{T-T}

(a) Ordinary Differential Equation (ODE) model of medial Golgi enzyme reactions and the galectin lattice showing predicted alterations in β1,6GlcNAc branching. Mgat1, 2 and 5 activities were modeled with measurements made in 129/Sv mouse T cells. **(b)** Human PBMCs of the indicated genotypes were rested with or without GlcNAc and examined by FACS for L-PHA binding in $CD4^+$ T cells at day 3. Subjects (n=2) were homozygous for the common alleles of *CTLA-4*, *IL2RA**T and *IL7RA**C. **(c)** ODE model showing predicted alterations in surface retention of CTLA-4 under varying conditions (i.e. number of N-glycans attached to CTLA-4, increases in Mgat1 activity and UDP-GlcNAc levels). **(d)** ODE model showing predicted alterations in surface retention of CTLA-4 in the indicated genotypes as UDP-GlcNAc levels change. **(e)** Human PBMCs of the indicated genotypes were stimulated with or without GlcNAc and examined by FACS at day 5. CTLA-4 MFI was assessed in $CD4^+$ T cell blasts with background subtracted from resting cells and normalized to cells homozygous for both common variants. n=2 for Ala/Ala+WT and Ala/Ala+IV_AV_{T-T}; n=1 for Thr/Thr+WT and Thr/Thr+IV_AV_{T-T}; subjects are carriers for *IL2RA**T and *IL7RA**C except one Ala/Ala+IV_AV_{T-T} subject with unknown genotype. P-values by ANOVA and the Newman-Keuls Multiple Comparison Test. ***p<0.001. **(f)** Human PBMCs with the *MGAT1* IVAVT-T haplotype were stimulated with anti-CD3 with or without GlcNAc and examined for proliferation at day 2. P values by t-test. *p<0.05. Error bars are standard error of triplicate or greater values. MFI = mean fluorescence intensity.

cell proliferation[32,33]. Such alterations in N-glycan number are expected to interact with the *MGAT1* $IV_AV_{T\text{-}T}$ haplotype to control CTLA-4 surface expression[15]. Indeed, computational modeling, co-transfection of Lec1 cells and analysis of T cell blasts confirmed previous observations[32,33] of significantly lower surface *CTLA-4* Ala17 (i.e. one N-glycan) compared to *CTLA-4* Thr17 (i.e. two N-glycans) when co-expressed with the common *MGAT1* haplotype (Figure 2.7d and Figure 2.8c-e). The *MGAT1* $IV_AV_{T\text{-}T}$ haplotype also limited CTLA-4 surface levels when expressed with the common *CTLA*-4 Thr17 allele (two N-glycans) while combining the *MGAT1* $IV_AV_{T\text{-}T}$ haplotype with *CTLA-4* Ala17 (one N-glycan) further reduced CTLA-4 surface levels. These phenotypes were rescued by increasing UDP-GlcNAc levels and/or GlcNAc supplementation, confirming that these phenotypes are sensitive to metabolism. GlcNAc also inhibited proliferation of T cells heterozygous for the *MGAT1* $IV_AV_{T\text{-}T}$ haplotype (Figure 2.8f).

Soluble receptors associated with the *IL2RA**T and *IL7RA**C MS risk alleles reduce Mgat1 mRNA and should interact with Mgat1 up-regulation by the *MGAT1* $IV_AV_{T\text{-}T}$ haplotype to control branching (Figure 2.7a). Indeed, addition of exogenous IL-2 or IL-7 enhanced branching in control cells but reduced branching in *MGAT1* $IV_AV_{T\text{-}T}$ heterozygous cells (Figure 2.7e, interaction $p=1.7x10^{-5}$). These results are predicted by computational modeling, with up-regulation of Mgat1 by IL-2 or IL-7 enhancing or reducing branching depending on baseline Mgat1 activity (Figure 2.7a).

Taken together, these data indicate that the *MGAT1* $IV_AV_{T\text{-}T}$ haplotype lowers branching, T cell activation thresholds and CTLA-4 surface retention in a manner that is sensitive to metabolic conditions (i.e. UDP-GlcNAc), activity of other Golgi branching

enzymes (e.g. Mgat5), the number of N-glycans attached to CTLA-4 (i.e. *CTLA-4* Thr17Ala) and IL-2 and IL-7 signaling.

Genetic interaction of *IL2RA*, *IL7RA*, *MGAT1* and *CTLA-4* in MS

The biological interactions defined above for *IL2RA* (rs2104286), *IL7RA* (rs6897932), *MGAT1* IV_AV_{T-T} (rs7726005, rs2070924 and rs2070925) and *CTLA-4* Thr17Ala (rs231775) are expected to result in genetic interaction in MS. To test this hypothesis, we first examined point association of the four variants in two Caucasian MS case-control cohorts from North America (n=2705 and n=9132, respectively). We replicated association of *IL2RA* (rs2104286) and *IL7RA* (rs6897932) as well as the lack of association of CTLA-4 (rs231775) in both cohorts (Table 2.1, Table 2.2)[3,22,23,34]. Although the *MGAT1* IV_AV_{T-T} haplotype is relatively rare (carrier freq. ~7.2%), we observed a novel association for carrier status in both cohorts, with $p=1.51x10^{-5}$ and odds ratio (OR)=1.36 in combined data of 3280 cases and 8557 controls (Table 2.1, Table 2.2). Allelic analysis yielded a trend p-value (Cochran-Armitage) of $1.90x10^{-5}$ (1 tail) for combined data. Pearson's correlation (r) confirmed that the IV_A (rs7726005) and V_{T-T} (rs2070924 and rs2070925) polymorphisms are in strong linkage disequilibrium ($r=0.633695$, p-value < $2.2x10^{-16}$), as first observed by physical cloning and sequencing of genomic DNA (Figure 2.5a). Analysis of the IVA and VT-T polymorphisms irrespective of haplotype revealed association of VT-T (rs2070924 and rs2070925; $p=1.67x10^{-4}$, OR=1.29) and marginal association of IVA (rs7726005, $p=1.66x10^{-2}$, OR=1.13 (Table 2.2).

Table 2.1. Genetic interaction in multiple sclerosis.

		Ethnicity	Variant frequency		*P* value	OR (95% CI)
			Control (*n*)	MS (*n*)		
*IL2RA**T (rs2104286)		Caucasian	0.740 (6507)	0.770 (3168)	2.44×10^{-6}	1.18 (1.10–1.26)
*IL7RA**C (rs6897932)		Caucasian	0.747 (6506)	0.767 (3172)	1.05×10^{-3}	1.12 (1.04–1.20)
*CTLA-4**Thr17 (rs237155)		Caucasian	0.613 (6506)	0.620 (3173)	0.184	1.03 (0.97–1.09)
		African-American	0.639 (480)	0.642 (758)	0.453	1.01 (0.86–1.20)
*MGAT1*IV_AV_{T-T}		Caucasian	0.0713 (8557)	0.0942 (3280)	1.51×10^{-5}	1.36 (1.17–1.56)
		African-American	0.110 (480)	0.125 (758)	0.215	1.15 (0.81–1.65)
Stratified analysis						
		Ethnicity	*MGAT1* IV_AV_{T-T} frequency		*P* value	OR (95% CI)	Interaction *P* value (empiric *P* value, power)
			Control (*n*)	MS (*n*)			
*IL2RA**T + *IL7RA**C	<4	Caucasian	0.0708 (4491)	0 0993 (2084)	3.60×10^{-5}	1.45 (1.21–1.74)	6.75×10^{-2} (7.1×10^{-2}, 0.32)
	=4		0.0744 (2015)	0.0831 (1083)	0.206	1.13 (0.86–1.48)	
*CTLA-4**Thr17	<2	Caucasian	0.0707 (4031)	0.104 (1940)	4.95×10^{-6}	1.53 (1.26–1.85)	1.20×10^{-2} (1.3×10^{-2}, 0.62)
	=2		0 0746 (2465)	0.0787 (1232)	0.329	1.06 (0.82–1.37)	
	<2	African-American	0.0860 (279)	0.146 (438)	8.40×10^{-3}	1.82 (1.11–2.98)	2.29×10^{-3} (2.5×10^{-3}, 0.81)
	=2		0.144 (201)	0.0969 (320)	4.95×10^{-2}	0.64 (0.37–1.10)	
			Combined *P* values: <2		7.48×10^{-7}		3.16×10^{-4}
*IL2RA**T + *IL7RA**C + *CTLA-4**Thr17	<6	Caucasian	0.0712 (5732)	0.101 (2754)	1.62×10^{-6}	1.46 (1.24–1.71)	9.48×10^{-4} (9×10^{-4}, 0.87)
	=6		0.0791 (771)	0.0523 (421)	4.08×10^{-2}	0.64 (0.39–1.06)	

Combined data from two independent North American Caucasian case–control MS cohorts and an African-American MS cohort. Reported is one-sided P values computed using the Cochran-Armitage test with *MGAT1* IV_AV_{T-T} (rs7726005, r2070924 and rs2070925) coded 0 or 1 for carrier status and IL2RA*T (rs2104286), IL7RA*C (rs6897932) and CTLA-4 Thr17 (rs231775) coded as 0, 1 or 2 for the number of alleles. *MGAT1* IV_AV_{T-T} homozygosity is 0.0016 and 0.0021 for Caucasian controls and MS, respectively. Compound heterozygosity for the IV_A and V_{T-T} variants is estimated at ~1 in 5,800 in Caucasians; therefore, subjects genotyped as heterozygous for both are treated as the *MGAT1* IV_AV_{T-T} haplotype. All control cohorts are in Hardy-Weinberg Equilibrium. CI, confidence intervals ; OR, odds ratio.

Table 2.2. Association analysis of single variants in Multiple Sclerosis

		Variant Frequency			
		Control (n)	Disease (n)	p-value	Odds Ratio [95% CI]
***IL2RA**T (rs2104286)**	Cohort 1	0.745 (1484)	0.770 (1196)	1.95×10^{-2}	1.14 [1.01-1.30]
	Cohort 2	0.729 (5023)	0.771 (1972)	3.81×10^{-5}	1.19 [1.09-1.30]
	Combined Data	**0.740 (6507)**	**0.770 (3168)**	$\mathbf{2.44 \times 10^{-6}}$	**1.18 [1.10-1.26]**
	Combined p-values			$\mathbf{1.12 \times 10^{-5}}$	
***IL7RA**C (rs6897932)**	Cohort 1	0.737 (1485)	0.762 (1200)	1.66×10^{-2}	1.15 [1.01-1.30]
	Cohort 2	0.750 (5024)	0.771 (1972)	5.67×10^{-3}	1.12 [1.03-1.22]
	Combined Data	**0.747 (6509)**	**0.767 (3172)**	$\mathbf{1.05 \times 10^{-3}}$	**1.12 [1.04-1.20]**
	Combined p-values			$\mathbf{9.67 \times 10^{-4}}$	
***CTLA-4**Thr17 (rs237155)**	Cohort 1	0.611 (1489)	0.629 (1200)	9.75×10^{-2}	1.08 [0.96-1.20]
	Cohort 2	0.614 (5017)	0.614 (1973)	4.66×10^{-1}	1.00 [0.93-1.08]
	Combined Data	**0.613 (6506)**	**0.620 (3173)**	$\mathbf{1.84 \times 10^{-1}}$	**1.03 [0.97-1.09]**
	Combined p-values			$\mathbf{1.86 \times 10^{-1}}$	
MGAT1 $\mathbf{IV_AV_{T\text{-}T}}$	Cohort 1	0.0673 (1501)	0.0947 (1204)	4.43×10^{-3}	1.45 [1.10-1.92]
	Cohort 2	0.0721 (7056)	0.0939 (2076)	5.33×10^{-4}	1.33 [1.12-1.59]
	Combined Data	**0.0713 (8557)**	**0.0942 (3280)**	$\mathbf{1.52 \times 10^{-5}}$	**1.36 [1.17-1.56]**
	Combined p-values			$\mathbf{3.30 \times 10^{-5}}$	
MGAT1 $\mathbf{IV_A}$	Cohort 1	0.161 (1490)	0.187 (1202)	3.74×10^{-2}	1.20 [0.98-1.47]
	Cohort 2	0.162 (5697)	0.174 (2077)	1.11×10^{-1}	1.09 [0.95-1.24]
	Combined Data	**0.162 (7187)**	**0.179 (3279)**	$\mathbf{1.66 \times 10^{-2}}$	**1.13 [1.01-1.26]**
	Combined p-values			$\mathbf{2.69 \times 10^{-2}}$	
MGAT1 $\mathbf{V_{T\text{-}T}}$	Cohort 1	0.0725 (1489)	0.101 (1196)	4.14×10^{-3}	1.44 [1.10-1.89]
	Cohort 2	0.0805 (7085)	0.0987 (2077)	4.29×10^{-3}	1.25 [1.06-1.48]
	Combined Data	**0.0791 (8574)**	**0.0996 (3273)**	$\mathbf{1.67 \times 10^{-4}}$	**1.29 [1.12-1.48]**
	Combined p-values			$\mathbf{2.12 \times 10^{-4}}$	

Variant frequency in non-latino Caucasians with MS and controls from North America. Reported is one-sided p-value computed using the Cochran-Armitage test with the *MGAT1* $IV_AV_{T\text{-}T}$ haplotype (rs7726005, rs2070924 and rs2070925), the *MGAT1* IV_A polymorphism (rs7726005) and the *MGAT1* $V_{T\text{-}T}$ polymorphisms (rs2070924 and rs2070925) coded 0 or 1 for carrier status and *IL2RAT (rs2104286), *IL7RA**C (rs6897932) and *CTLA-4* Thr17 (rs231775) coded as 0, 1 or 2 for the number of alleles. For 1387 controls in cohort 2, the *MGAT1* IV_A polymorphism was genotyped only in those positive for the *MGAT1* $V_{T\text{-}T}$ polymorphisms; therefore frequencies of the former are not reported for these samples. Combined p-values by Fishers method. OR = Odds Ratio; 95% CI = 95% Confidence Intervals. All control cohorts are in HWE.**

Table 2.3. Stratified analysis of *MGAT1* IV_AV_{T-T} in Multiple Sclerosis

			***MGAT1* IV_AV_{T-T} Frequency**			
			Control (n)	**Disease (n)**	**p-value**	**Odds Ratio [95% CI]**
***IL2RA**T + *IL7RA**C**	**< 4**	Cohort 1	0.0619 (1017)	0.1041 (788)	5.47×10^{-4}	1.76 [1.25-2.48]
		Cohort 2	0.0734 (3474)	0.0965 (1296)	4.46×10^{-3}	1.35 [1.08-1.69]
		Combined Data	**0.0708 (4491)**	**0.0993 (2084)**	$\mathbf{3.60 \times 10^{-5}}$	**1.45 [1.21-1.74]**
		Combined p-values			$\mathbf{3.40 \times 10^{-5}}$	
	= 4	Cohort 1	0.0799 (463)	0.0760 (408)	4.15×10^{-1}	0.95 [0.58-1.56]
		Cohort 2	0.0728 (1552)	0.0874 (675)	1.18×10^{-1}	1.22 [0.88-1.69]
		Combined Data	**0.0744 (2015)**	**0.0831 (1083)**	$\mathbf{1.95 \times 10^{-1}}$	**1.13 [0.86-1.48]**
		Combined p-values			$\mathbf{1.97 \times 10^{-1}}$	
***CTLA-4**Thr17**	**< 2**	Cohort 1	0.0634 (931)	0.109 (714)	4.22×10^{-4}	1.81 [1.27-2.58]
		Cohort 2	0.0729 (3100)	0.101 (1226)	1.07×10^{-3}	1.43 [1.14-1.80]
		Combined Data	**0.0707 (4031)**	**0.104 (1940)**	$\mathbf{4.95 \times 10^{-6}}$	**1.53 [1.26-1.85]**
		Combined p-values			$\mathbf{7.05 \times 10^{-6}}$	
	= 2	Cohort 1	0.0764 (550)	0.0742 (485)	4.48×10^{-1}	0.97 [0.61-1.54]
		Cohort 2	0.0742 (1915)	0.0817 (747)	2.56×10^{-1}	1.11 [0.81-1.52]
		Combined Data	**0.0746 (2465)**	**0.0787 (1232)**	$\mathbf{3.29 \times 10^{-1}}$	**1.06 [0.82-1.37]**
		Combined p-values			$\mathbf{3.63 \times 10^{-1}}$	
***IL2RA**T + *IL7RA**C + *CTLA-4**Thr17**	**< 6**	Cohort 1	0.0641 (1310)	0.101 (1039)	5.42×10^{-4}	1.64 [1.22-2.21]
		Cohort 2	0.0733 (4422)	0.100 (1715)	2.45×10^{-4}	1.41 [1.16-1.71]
		Combined Data	**0.0712 (5732)**	**0.101 (2754)**	$\mathbf{1.62 \times 10^{-6}}$	**1.46 [1.24-1.71]**
		Combined p-values			$\mathbf{2.24 \times 10^{-6}}$	
	= 6	Cohort 1	0.0941 (170)	0.0552 (163)	8.90×10^{-2}	0.56 [0.24-1.31]
		Cohort 2	0.0749 (601)	0.0504 (258)	9.49×10^{-2}	0.66 [0.35-1.24]
		Combined Data	**0.0791 (771)**	**0.0523 (421)**	$\mathbf{4.08 \times 10^{-2}}$	**0.64 [0.39-1.06]**
		Combined p-values			$\mathbf{4.88 \times 10^{-2}}$	

Stratified analysis in 2 independent North American Caucasian case-control MS cohorts. Reported is one-sided p-value computed using the Cochran-Armitage test with *MGAT1* IV_AV_{T-T}(rs7726005, rs2070924 and rs2070925) coded 0 or 1 for carrier status and *IL2RAT (rs2104286), *IL7RA**C (rs6897932) and *CTLA-4* Thr17 (rs231775) coded as 0, 1 or 2 for the number of alleles. OR = Odds Ratio; 95% CI = 95% Confidence Intervals. All control cohorts are in HWE.**

As gene-gene interaction analysis requires large sample sizes (power calculations in Table 2.1), especially when alleles are rare, we conducted stratified analysis in both Caucasian cohorts and interaction analyses only in combined data. Consistent with opposing effects on Mgat1 that optimize enzyme activity and branching when combined, stratified analysis of the Caucasian data reveals that *MGAT1* IV_AV_{T-T} significantly increases MS risk when there are less than four copies of the *IL2RA**T and *IL7RA**C risk alleles ($p=3.60x10^{-5}$, OR=1.45), while no association was observed in the presence of four copies of the *IL2RA**T and *IL7RA**C (p=0.195, OR=1.13) (Table 2.1, Table 2.3). The p-value for interaction is $6.75x10^{-2}$.

Next, we tested for interaction of *MGAT1* IV_AV_{T-T} with *CTLA-4* Thr17Ala (rs231775). *CTLA-4* Thr17 harbors twice as many N-glycans as *CTLA-4* Ala17 and therefore should compensate for reduced branching by *MGAT1* IV_AV_{T-T} to mitigate MS risk. Indeed, *MGAT1* IV_AV_{T-T} significantly associated with MS in *CTLA-4* Ala17 carriers ($p=4.95x10^{-6}$, OR=1.53) but not *CTLA-4* Thr/Thr homozygotes (p=0.329, OR=1.06) with an interaction p-value of $1.20x10^{-2}$ (Table 2.1, Table 2.3). Stratifying the data based on six or less than six alleles of *CTLA-4* Thr17, *IL2RA**T and *IL7RA**C strengthened the interaction, with *MGAT1* IV_AV_{T-T} promoting MS in the latter ($p=1.62x10^{-6}$, OR=1.46) while appearing to be protective in the former ($p=4.08x10^{-2}$, OR=0.64), giving an interaction p-value of $9.48x10^{-4}$.

Finally, we examined an independent African-American MS cohort (758 cases, 480 controls). Based on HapMap data, *IL2RA**T and *IL7RA**C risk alleles are much more common in Sub-Saharan Africans/African-Americans (risk allele frequencies of ~0.90-.95 vs ~0.75 in Caucasians). Indeed, analysis of a subset of the African-American

MS cases (n=478) revealed *IL2RA**T and *IL7RA**C allele frequencies of 0.94 and 0.88, respectively. As these high frequencies limit power, we restricted further analysis of the African-American cohort to *MGAT1* $IV_AV_{T\text{-}T}$ and *CTLA-4* Thr17Ala. *MGAT1* $IV_AV_{T\text{-}T}$ did not display association in African-American MS (p=0.215), with an OR similar to Caucasians with *IL2RA**T + *IL7RA**C = 4 (i.e. 1.15 vs 1.13, respectively), a result consistent with the much higher frequencies of *IL2RA**T and *IL7RA**C in African-Americans (Table 2.1). However, stratifying the data based on *CTLA-4* Thr17Ala replicated the Caucasian MS data, with *MGAT1* $IV_AV_{T\text{-}T}$ promoting MS in *CTLA-4* Ala17 carriers ($p=8.40x10^{-3}$, OR=1.82) but appearing to be protective in *CTLA-4* Thr/Thr homozygotes ($p=4.95x10^{-2}$, OR=0.64), with an interaction p-value of $2.29x10^{-3}$. The OR in *CTLA-4* Thr/Thr homozygotes is similar to that in Caucasians with 6 alleles of *CTLA-4* Thr17, *IL2RA**T and *IL7RA**C (i.e. 0.64 and 0.64, respectively), again consistent with the much higher frequencies of *IL2RA**T and *IL7RA**C in African-Americans. Combining the African-American and Caucasian p-values gives $p=7.48x10^{-7}$ for *CTLA-4* Ala17 carriers and $p=3.16x10^{-4}$ for interaction. Importantly, this interaction is observed despite lack of point association and marginal effects of *CTLA-4* Thr17Ala in both the Caucasian and African-American data, indicating an epistatic interaction. Thus, the Caucasian and African-American MS data are concordant and when combined with the demonstrated biological interactions, provide strong evidence that the four variants converge on N-glycosylation to differentially regulate MS risk.

Vitamin D_3 enhances Mgat1 to inhibit demyelinating disease

Deficiency of Vitamin D_3, which is synthesized from 7-dehydrocholesterol in the skin upon ultra-violet sun exposure, strongly associates with MS[2,35,36]. Vitamin D_3 and/or its active metabolite 1α,25-Dihydroxyvitamin D_3 ($1,25(OH)_2D_3$) inhibit T cell activation[37], Interferon-γ (INF-γ) production[38] and T cell-mediated demyelinating disease[38]; however molecular mechanisms are unclear. $1,25(OH)_2D_3$ enhanced *MGAT1* mRNA levels in human male and female $CD4^+CD25^+$ T cell blasts, a phenotype similar to the *MGAT1* $IV_AV_{T\text{-}T}$ haplotype but opposite of the *IL2RA**T + *IL7RA**C risk alleles (Figure 2.9a). $1,25(OH)_2D_3$ also increased *MAN1A1*, but had little effect on other Golgi branching genes. In the presence of the *IL2RA**T and *IL7RA**C risk alleles, $1,25(OH)_2D_3$ should enhance branching by reversing Mgat1 down-regulation resulting from reduced IL-2 and IL-7 signaling. In contrast, up-regulation of Mgat1 by $1,25(OH)_2D_3$ in T cell blasts lacking the *IL2RA**T and *IL7RA**C risk alleles is expected to have little or negative effect. Indeed, while $1,25(OH)_2D_3$ enhanced branching in T cell blasts with two or more copies of the *IL2RA**T and *IL7RA**C risk alleles (Figure 2.9b), branching was unchanged or reduced (depending on TCR stimulation strength) in blasting T cells homozygous for both protective alleles (Figure 2.9c and Figure 2.10). Addition of exogenous sIL2RA and sIL7RA to the latter cells, thereby mimicking the *IL2RA**T and *IL7RA**C risk alleles, restored the ability of $1,25(OH)_2D_3$ to enhance branching (Figure 2.9c). As a very small minority of Caucasians are homozygous for the *IL2RA**C and *IL7RA**T protective alleles (~ 0.5%), Vitamin D_3 is expected to promote branching in the majority of the population.

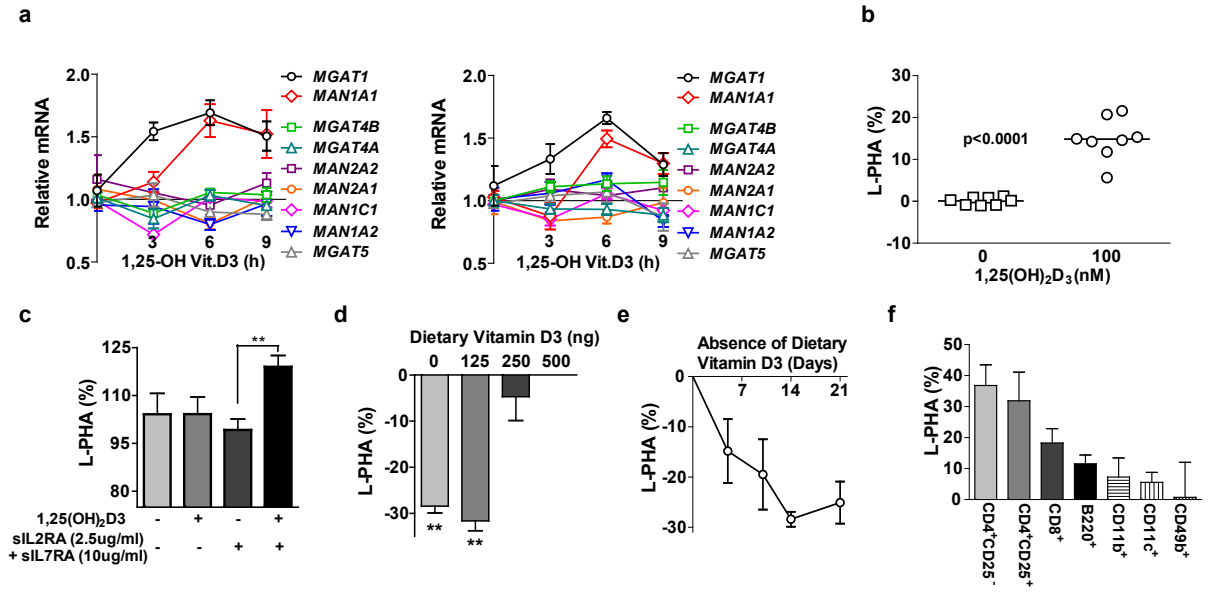

Figure 2.9. Vitamin D_3 counters *IL2RAT and *IL7RA**C mediated reduction in Mgat1 to promote N-glycan branching**

(a) Male (right) or female (left) purified human $CD4^+$ T cells were pre-stimulated with plate bound anti-CD3 for 4 days (1ug/ml) then treated with 100nM $1,25(OH)_2D_3$ for 3, 6 and 9 hrs. Blasting $CD25^+$ T cells were isolated and harvested for mRNA extraction and cDNA synthesis. Relative mRNA levels of indicated genes were performed by quantitative RT-PCR analysis and normalized to actin. **(b)** Human $CD3^+$ T cells harboring two or more *IL2RA*T* + *IL7RA*C* risk alleles (i.e. *IL2RA**T + *IL7RA**C ≥ 2) were pre-stimulated with anti-CD3 for 2 days (1ug/ml) then treated with 100nM $1,25(OH)_2D_3$ for 3 days before FACS analysis for L-PHA binding in $CD4^+$ cells. All donors are negative for *MGAT1* $IV_AV_{T\text{-}T}$. Horizontal bar represents the average L-PHA MFI of each treatment group. **(c)** Human $CD3^+$ T cells lacking the *IL2RA**T and *IL7RA**C risk alleles (i.e. *IL2RA**T + *IL7RA**C = 0, common haplotype for *MGAT1*) were pre-stimulated with anti-CD3 (400ng/ml) and pre-treated with sIL2RA/sIL7RA for 2 days before addition of 100nM $1,25(OH)_2D_3$ for another 3 days. L-PHA binding was analyzed as in (b). P-value by t-test. **p<0.01 **(d)** PL/J mice were fed 4g/day of chow containing varying amounts of Vitamin D_3 for 14 days. Splenocytes were isolated and analyzed for L-PHA binding in $CD4^+$ T cells as in (b). n=2 mice for each group with each mouse stained in triplicate. Error bars represent the range of biological replicates **(e)** PL/J mice were maintained on either a regular mouse diet obtaining ~500-625ng Vitamin D_3 per day or on a diet deficient in Vitamin D_3 for the indicated number of days. Splenocytes were harvested and analyzed as in (d). n=6 and n=4 mice per time point for the first and last two times points, respectively, with each mouse stained in triplicate. Error bars represent the range of biological replicates. **(f)** Mice consuming ~500-625ng dietary Vitamin D_3 per day were injected with 100ng $1,25(OH)_2D_3$ by intraperitoneal injection every other day for a total of three times. Splenocytes were harvested 24 hours after the last injection and analyzed for L-PHA binding in the indicated cell types by FACS. n=8 mice stained in triplicate with error bars representing standard error of biological replicates. CD11b+: macrophages, CD11c+: dendritic cells, CD49b+: NK cells. MFI = mean fluorescence intensity. Error bars are standard error of triplicate or greater values unless otherwise stated.

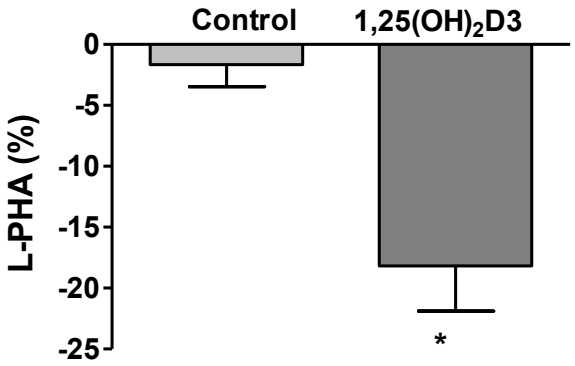

Figure 2.10. *IL2RAC and *IL7RA**T with Vitamin D3 in N-glycan branching**
Purified human $CD3^+$ T cells homozygous for both protective *IL2RA**C and *IL7RA**T alleles were pre-stimulated with plate-bound anti-CD3 for 2 days (400ng/ml) and then treated with 100nM $1,25(OH)_2D_3$ for 3 days. L-PHA binding was analyzed by FACS in $CD4^+$ T cell blasts. P-value was determined by t-test. *$p<0.05$. MFI = mean fluorescence intensity. Error bars are standard error of triplicate or greater values.

T cells from the PL/J mouse strain are deficient in Mgat1 activity (i.e. ~3.3nmol/mg/hr vs 5.57nmol/mg/hr in 129/Sv) and branching[20], providing a model for Mgat1 deficiency similar to the *IL2RA**T and *IL7RA**C MS risk alleles. The Vitamin D_3 receptor (VDR) is minimally expressed in naïve *ex vivo* T cells and up-regulated by TCR or Vitamin D_3 signaling[39]. Addition of $1,25(OH)_2D_3$ to resting PL/J mouse or human T cells had little affect on branching (Figure 2.12a,b), whereas addition to TCR-activated female PL/J mouse T cells enhanced branching (Figure 2.12c). Consistent with previous observations that $1,25(OH)_2D_3$ inhibits experimental autoimmune encephalomyelitis (EAE) in C57BL/6 female but not male mice, $1,25(OH)_2D_3$ had minimal effects on branching in male PL/J mouse T cell blasts (Figure 2.12d); however both male and female human T cell blasts responded similarly with enhanced branching (Figure 2.12e,f). C57BL/6 mice are also deficient in Mgat1 activity, however branching is reduced to a much smaller degree than PL/J mice[20]. Reducing dietary supply of Vitamin D_3 in female PL/J mice decreased branching in $CD4^+$ T cells *in vivo* in a dose- and time-dependent manner (Figure 2.9d,e). Intra-peritoneal injection of $1,25(OH)_2D_3$ in female PL/J mice enhanced branching in $CD4^+$ T cells > $CD8^+$ T cells > B-cells ($B220^+$) but had little effect in $CD11b^+$ cells (macrophages), $CD11c^+$ cells (dendritic cells) or $CD49b^+$ cells (NK cells) (Figure 2.9f). Blocking branching with SW reversed $1,25(OH)_2D_3$ induced T cell hypo-proliferation in response to TCR stimulation (Figure 2.11a). $1,25(OH)_2D_3$ enhanced CTLA-4 cell surface expression in PL/J mouse and human T cell blasts (Figure 2.11b and Figure 2.13a,b) and markedly reduced CTLA-4 endocytosis rates (Figure 2.11c). Intra-peritoneal injection of $1,25(OH)_2D_3$ inhibited myelin basic protein (MBP)-induced EAE in PL/J female mice in the absence but not

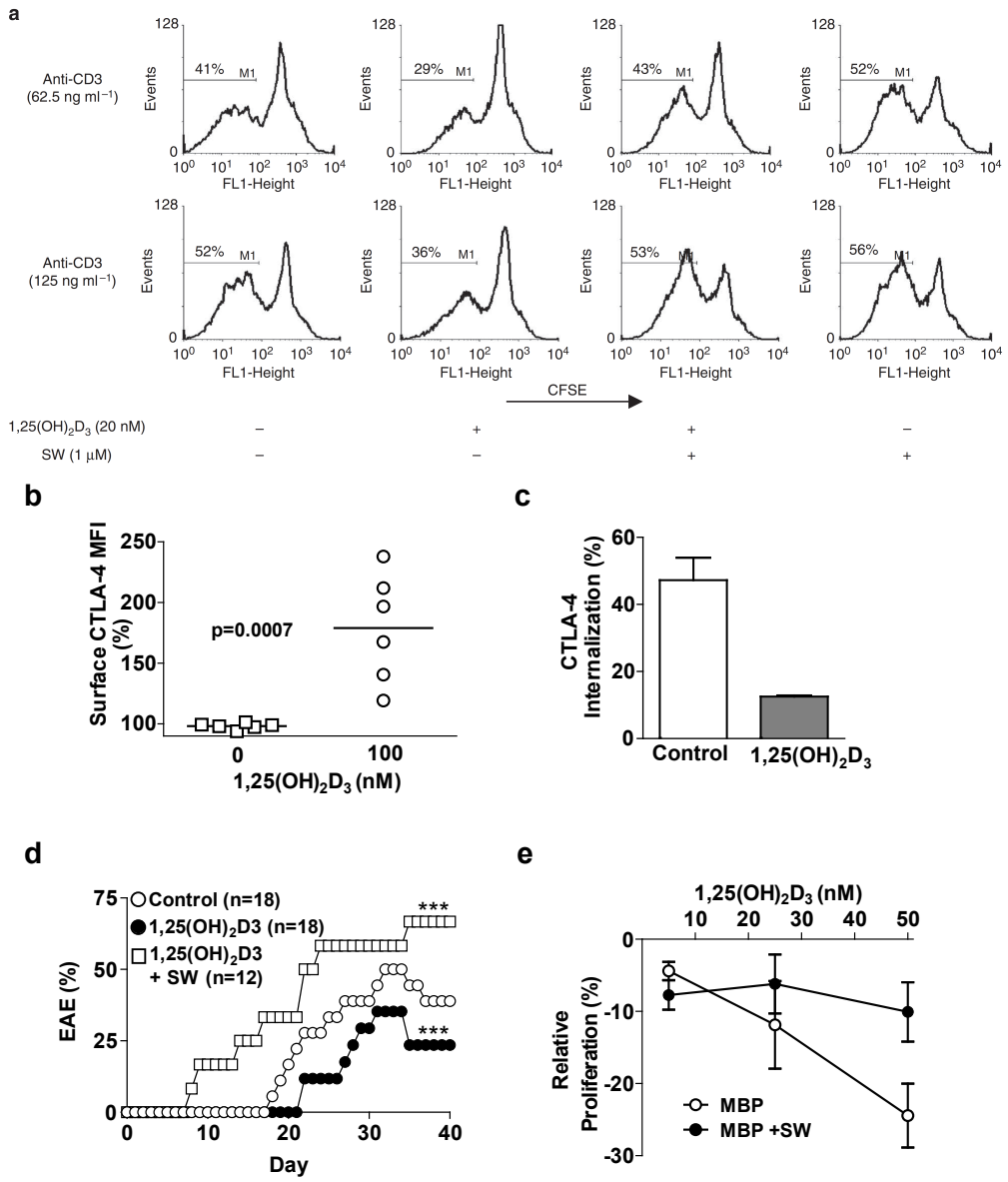

Figure 2.11. Vitamin D_3 regulates T cell growth and EAE

(a) Purified mouse $CD3^+$ T cells were stained with CFSE, stimulated with plate bound anti-CD3 antibody in the presence or absence of $1,25(OH)_2D_3$ (20nM) for 3 days and analyzed by FACS for CFSE dilution/proliferation in $CD4^+$ T cells. Horizontal bars mark the population of proliferating cells, with the percentage of proliferating cells noted above. **(b)** Purified human $CD3^+$ T cells (n=8 donors per group) were pre-stimulated with plate bound anti-CD3 for 2 days (1ug/ml) then treated with 100nM $1,25(OH)_2D_3$ for 3 days. $CD25^+CD4^+$ blasting T cells were analyzed for surface CTLA-4 expression by FACS. Horizontal bar represents the average L-PHA MFI of each treatment group. P-value determined by t-test. MFI = mean fluorescence intensity. **(c)** Purified mouse $CD3^+$ T cells were stimulated with plate-bound anti-CD3 (250ng/ml) in the presence or absence of $1,25(OH)_2D_3$ (150nM) for 5 days and analyzed by FACS for internalization rates of cell surface CTLA-4 in $CD4^+$ T cells. **(d)** PL/J mice treated as indicated were immunized with MBP+CFA and examined daily for clinical EAE. 100ng $1,25(OH)_2D_3$ was administered by intra-peritoneal injection every other day starting at day -3. SW was provided in drinking water and reduced L-PHA staining ~50%. P values by Fisher's Exact Test. ***$p<0.0001$ **(e)** Female mice were immunized with 100ug MBP+CFA by intra-peritoneal injection and after 10 days, splenocytes were harvested and re-stimulated *in vitro* with MBP in the presence or absence of $1,25(OH)_2D_3$ and/or SW as indicated. Proliferation was assessed by CFSE dilution and analyzed by FACS. Error bars are standard error of triplicate or greater values in all panels.

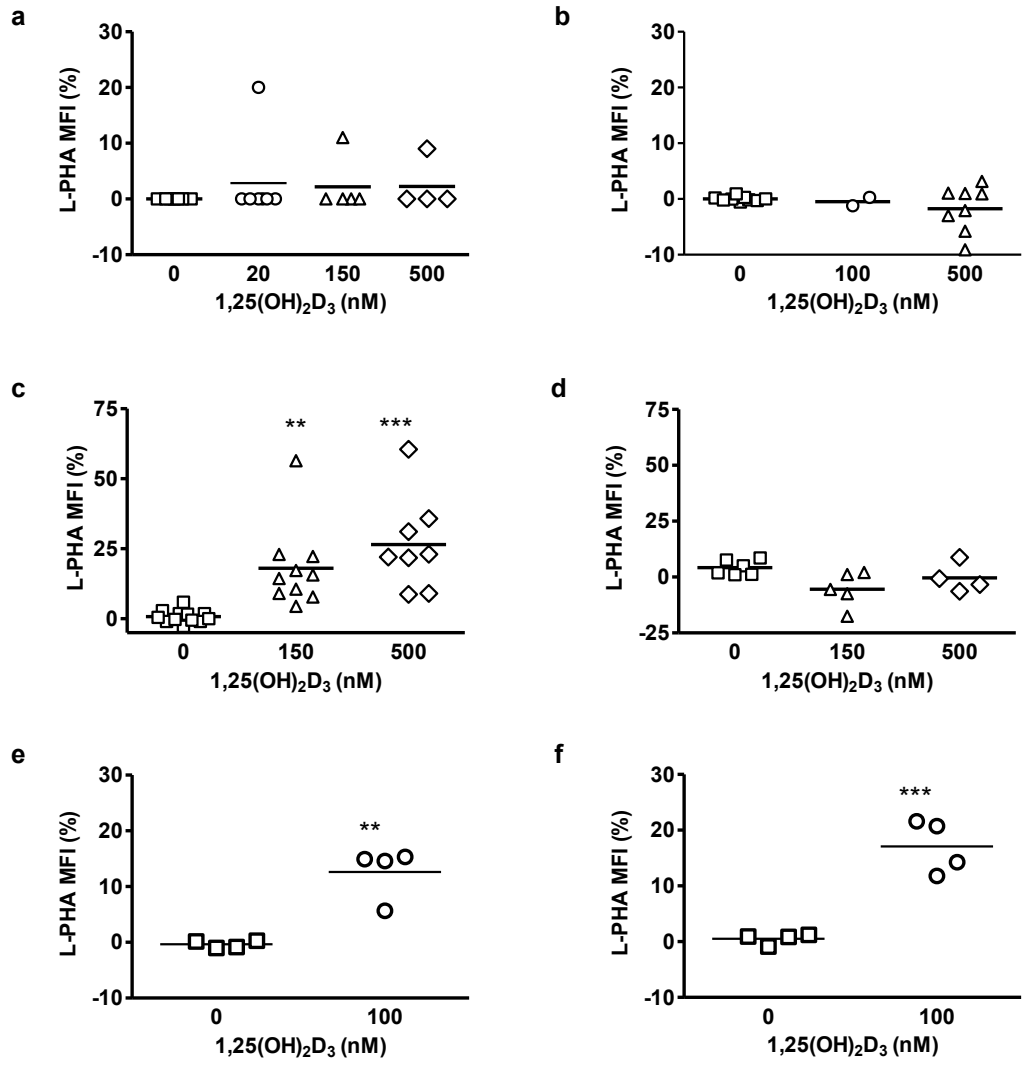

Figure 2.12. Vitamin D3 regulates N-glycan branching in activated mouse and human CD4$^+$ T cells
(a) Resting mouse or **(b)** resting human CD3$^+$ T cells were cultured with the indicated concentrations of $1,25(OH)_2D_3$, stained with L-PHA in triplicate, and analyzed by FACS (gated on CD4$^+$ T cells). **(c)** Male or **(d)** female mouse CD3$^+$ T cells were pre-stimulated with plate bound anti-CD3 for 2 days then treated with $1,25(OH)_2D_3$ for 3 days as indicated, stained with L-PHA in triplicate, and analyzed by FACS (gated on CD4$^+$ T cells). P-values by ANOVA and the Newman-Keuls Multiple Comparison Test. **p<0.01, ***p<0.001. **(e)** Male or **(f)** female human CD3$^+$ T cells were stimulated, treated, and analyzed as in (c). P-values by t-test in (e) and (f). **p<0.01, ***p<0.001. Horizontal bars represent the average MFI (mean fluorescence intensity) of each treatment group in all panels.

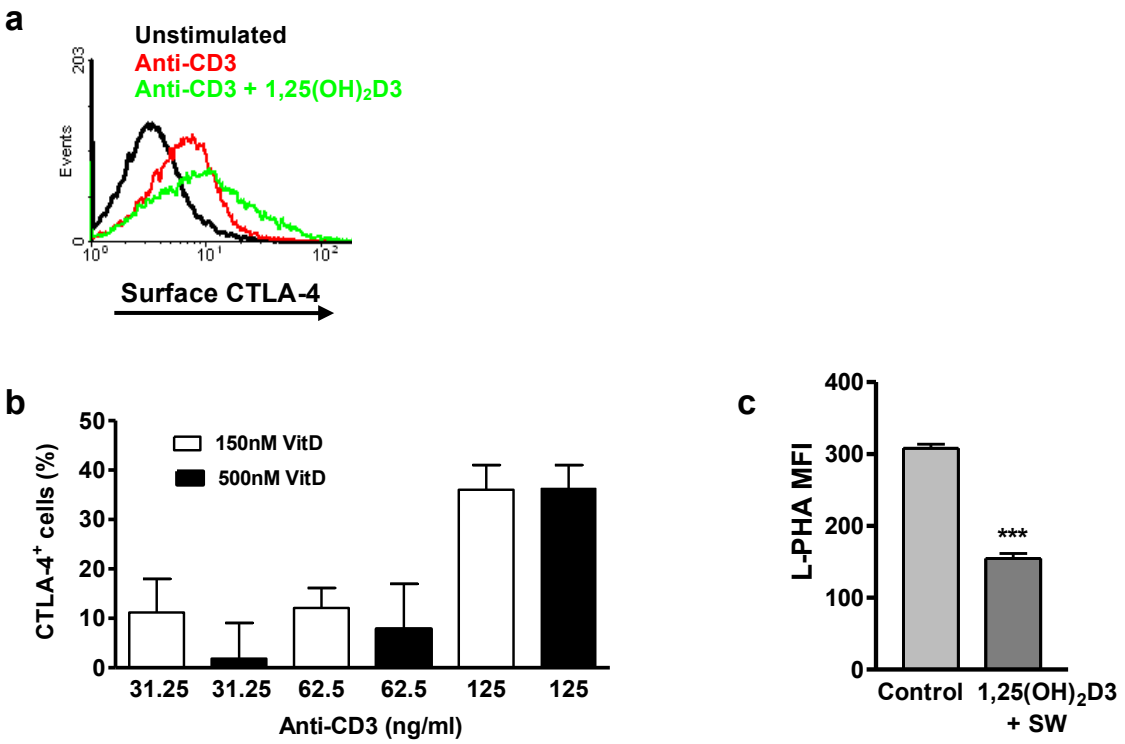

Figure 2.13. Vitamin D3 regulates CTLA-4 surface expression and N-glycan branching
(a) Purified mouse $CD3^+$ T cells were stimulated with plate-bound anti-CD3 (0 or 250ng/ml) with or without $1,25(OH)_2D_3$ (150nM) for 5 days and analyzed by FACS for cell surface CTLA-4 expression in $CD4^+$ T cells. **(b)** Purified mouse $CD3^+$ T cells were stimulated and treated as indicated for 5 days. CTLA-4 surface expression was analyzed as in (a). **(c)** Splenocytes from female mice immunized with 100ug MBP+CFA to induce EAE were stained with L-PHA and analyzed by FACS to assess for effectiveness of SW in reducing N-glycan branching in $CD4^+$ T cells. Error bars are standard error of triplicate or greater values. MFI = mean fluorescence intensity.

presence of SW in the drinking water (Figure 2.11d), where SW reduced branching in $CD4^+$ T cells ~50% (Figure 2.13c). SW also reversed $1,25(OH)_2D_3$ induced hypo-proliferation in MBP-stimulated T cells isolated from MBP-immunized PL/J mice (Figure 2.11e). Thus, Vitamin D_3 promotes branching and CTLA-4 surface retention to suppress T cell growth and autoimmune demyelinating disease when Mgat1 activity is suppressed, as occurs with the *IL2RA**T and *IL7RA**C risk alleles and in the C57BL/6 and PL/J mouse strains.

Discussion

Defining how environmental factors combine with genetic risk at the molecular level to promote complex trait diseases such as MS has remained a great challenge. Here we suggest a unifying molecular mechanism in MS, whereby multiple environmental factors (sunlight/Vitamin D_3 and metabolism) converge with multiple genetic variants (*IL-7RA*, *IL-2RA*, *MGAT1* and *CTLA-4*) to dysregulate a final common pathway, Golgi N-glycosylation (Figure 2.14). A causal role for defective N-glycosylation is supported by the development of spontaneous inflammatory demyelination and neurodegeneration in Mgat1 and/or Mgat5-deficient mice[17,20] as well as the observed biological and genetic interactions that appear to differentially control N-glycosylation and MS risk. The ability of environmental factors such as Vitamin D_3/sunshine and/or metabolism to directly compensate for genetic down-regulation of branching is consistent with concordance rates in monozygotic twins of only ~30% and their lack of significant detectable genomic, epigenomic or transcriptome differences[10,11]. Therapeutic supplementation to N-glycan biosynthesis may serve as a simple therapy to suppress phenotypic expression of MS risk factors. Indeed, Vitamin D_3 ($1,25(OH)_2D_3$) and GlcNAc are orally active, rescue branching deficiency on mouse T cells *in vivo* and inhibit EAE and spontaneous autoimmune diabetes in mice[16,38,40]. In humans, oral GlcNAc improved disease in 8 of 12 children with treatment-resistant inflammatory bowel disease[41].

Defective N-glycosylation likely promotes MS by multiple mechanisms. Reduced N-glycosylation lowers T cell activation thresholds and surface expression of the autoimmune inhibitor CTLA-4, promoting loss of self-tolerance. Mgat1 dysfunction may expose cryptic mannose linkages on the cell surface of oligodendrocytes that mimic

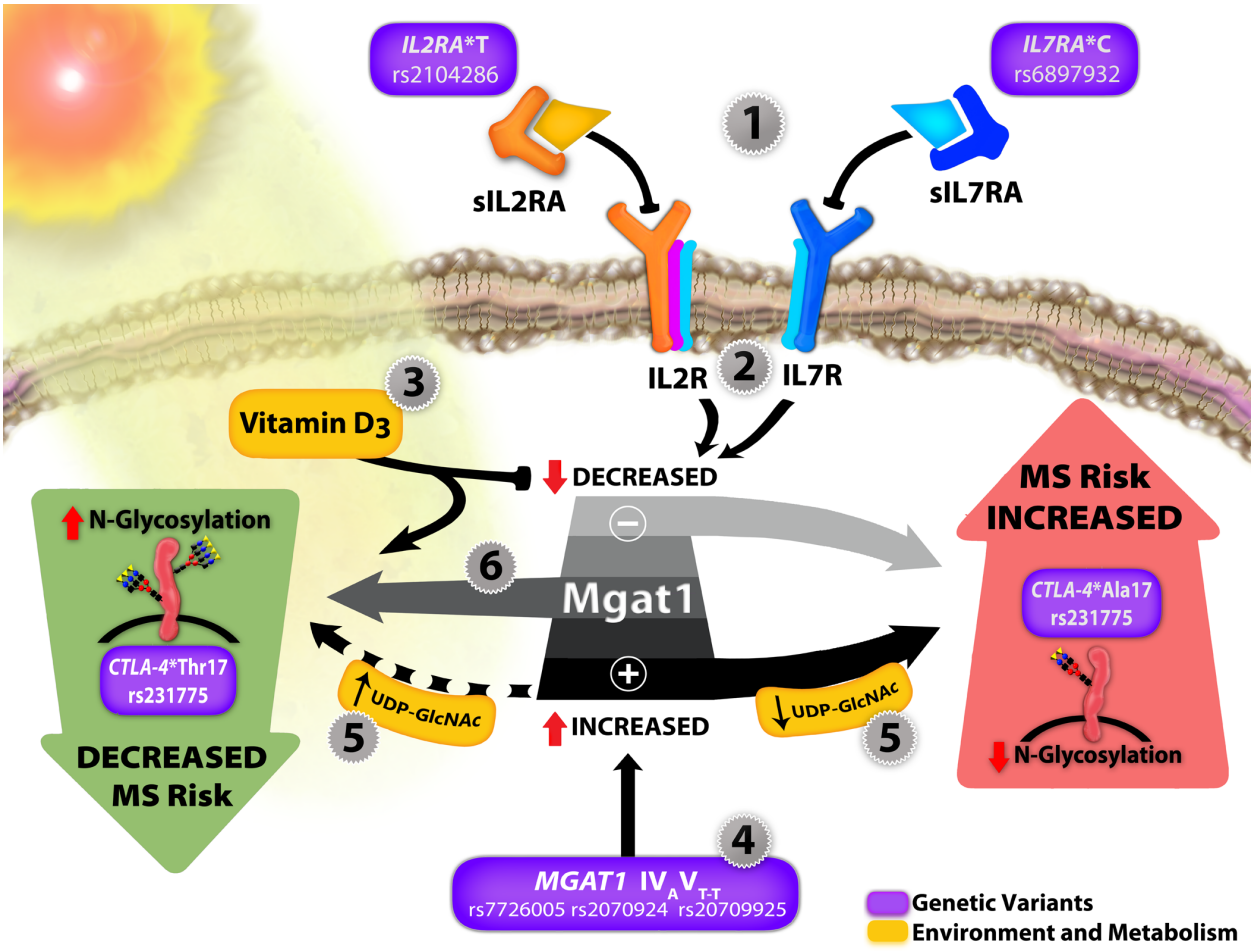

Figure 2.14. A model for environmental and genetic dysregulation of N-glycosylation in Multiple Sclerosis
Environmental and genetic interaction converges on the Golgi N-glycan branching enzyme Mgat1 and N-glycosylation of CTLA-4 in T cell blasts. Both down or up-regulation of Mgat1 activity decrease branching by limiting N-glycan or UDP-GlcNAc substrate to downstream enzymes, respectively. 1) Soluble receptors associated with the *IL2RA**T (rs2104286) and *IL7RA**C (rs6897932) MS risk alleles antagonize IL-2 and IL-7 signaling, leading to 2) down regulation of Mgat1, decreased branching and CTLA-4 surface levels and increased MS risk. 3) Vitamin D3 signaling counteracts this by enhancing Mgat1, leading to increased branching, CTLA-4 surface expression and decreased MS risk. 4) The *MGAT1* IVAVT-T haplotype (rs7726005, rs2070924, rs2070925) increases Mgat1, which decreases branching, CTLA-4 surface levels and increases MS risk conditional on 5) metabolic production of UDP-GlcNAc. 6) Combining genetic up-regulation of Mgat1 by the *MGAT1* IVAVT-T haplotype with genetic down-regulation of Mgat1 by the *IL2RA**T and *IL7RA**C MS risk alleles optimizes Mgat1 activity, thereby enhancing branching, CTLA-4 surface expression and mitigating MS risk. The *CTLA-4* Thr17Ala (rs231775) variant modifies these interactions by controlling the number of N-glycans attached to CTLA-4, with the Thr17 allele doubling N-glycan number to promote CTLA-4 surface retention and reduce MS risk when combined with *MGAT1* IVAVT-T, *IL2RA**TT and *IL7RA**CC.

microbial and pathogen glycans, chronically activating innate immune responses[42,43]. Neurodegeneration in MS may arise from increased sensitivity to apoptotic stimuli. Indeed, targeted deficiency of Mgat1 in neurons induces their apoptosis *in vivo* while Mgat5 deficiency enhances spontaneous neurodegeneration along with inflammatory demyelination[17,20]. Thus, genetic and environmental alterations in the N-glycosylation pathway likely conspire to promote MS through dysfunction of both immune (T cells, antigen presenting cells) and target cells (oligodendrocytes, neurons).

*IL2RA**T (rs2104286), *IL7RA**C (rs6897932) and Vitamin D_3 deficiency also associate with Type 1 diabetes (T1D)[28,44-46], while Non-Obese Diabetic (NOD) mice are deficient for branching in T cells but not B cells[20]. A second independent variant of *IL2RA* (rs11594656) also alters sIL2RA levels and associates with both MS and T1D[28], but paradoxically in opposite directions. *CTLA-4* Ala17 (rs231775) displays point association with T1D but not MS[34,47]. These considerations imply that defective N-glycosylation likely also contributes to T1D risk; however interactions between these variants and *MGAT1* $IV_AV_{T\text{-}T}$ may differ due to disparity in *CTLA-4* Ala17 (rs231775) frequencies between T1D and MS. Direct affects of branching deficiency on neuronal survival would also be expected to result in distinctive interactions in MS compared to T1D and other autoimmune diseases.

IL-7 and IL-2 both promote T cell growth, yet targeted deficiencies of these pathways in mice induce immunodeficiency and spontaneous autoimmunity, respectively[48,49]. Our data suggests that by having opposing effects on branching in resting and activated T cells, IL-2 and IL-7 enhance T cell growth early by lowering branching and TCR

activation thresholds but promote self-tolerance later by enhancing branching and CTLA-4 surface retention.

Prior to GWAS, many candidate gene studies proved unreliable. This failure likely arose from multiple issues such as very small sample size, lack of replication cohorts, poor selection of candidate genes (i.e. no evidence for regulating spontaneous disease in animals) and association testing in the absence of detailed functional characterization. We avoid these issues by initially ignoring association testing and performing a detailed biological screen for functional variants that induce phenotypes causal of disease in mice. Critically, only the single variant with the greatest biological effect is selected for subsequent association testing in large cohorts. This reverse approach also avoids the problem of multiple hypothesis testing inherent to GWAS. Indeed, the p-values we report (~10^{-5} – 10^{-7}) are orders of magnitude better than the genome wide significance level of ~$5x10^{-8}$ that corrects to ~0.02 after adjusting for multiple hypothesis testing in a typical GWAS with ~550,000 SNPs[50].

As the N-glycan branching pathway includes at least ~30 genes likely to also harbor variants that alter branching, the additive risk reported here probably underestimates the true magnitude of genetic dysregulation of N-glycosylation in MS. Indeed, the top hit in a recent GWAS for variants regulating disease severity in MS was *MGAT5*[51]. More broadly, our data suggest an alternative to the rare allele – common disease hypothesis by implicating genetic and environmental interaction of common factors that additively converge to disrupt a critical biochemical pathway regulating disease.

References

1. Steinman,L. Multiple sclerosis: a two-stage disease. *Nat. Immunol.* **2**, 762-764 (2001).

2. Smolders,J., Damoiseaux,J., Menheere,P. & Hupperts,R. Vitamin D as an immune modulator in multiple sclerosis, a review. *J. Neuroimmunol.* **194**, 7-17 (2008).

3. Hafler,D.A. *et al.* Risk alleles for multiple sclerosis identified by a genomewide study. *N. Engl. J. Med.* **357**, 851-862 (2007).

4. Manolio,T.A. *et al.* Finding the missing heritability of complex diseases. *Nature* **461**, 747-753 (2009).

5. Gorlov,I.P., Gorlova,O.Y., Sunyaev,S.R., Spitz,M.R. & Amos,C.I. Shifting paradigm of association studies: value of rare single-nucleotide polymorphisms. *Am. J. Hum. Genet.* **82**, 100-112 (2008).

6. McClellan,J. & King,M.C. Genetic heterogeneity in human disease. *Cell* **141**, 210-217 (2010).

7. Dickson,S.P., Wang,K., Krantz,I., Hakonarson,H. & Goldstein,D.B. Rare variants create synthetic genome-wide associations. *PLoS. Biol.* **8**, e1000294 (2010).

8. Surolia,I. *et al.* Functionally defective germline variants of sialic acid acetylesterase in autoimmunity. *Nature* **466**, 243-247 (2010).

9. Culverhouse,R., Suarez,B.K., Lin,J. & Reich,T. A perspective on epistasis: limits of models displaying no main effect. *Am. J. Hum. Genet.* **70**, 461-471 (2002).

10. Ebers,G.C. *et al.* A population-based study of multiple sclerosis in twins. *N. Engl. J. Med.* **315**, 1638-1642 (1986).

11. Baranzini,S.E. *et al.* Genome, epigenome and RNA sequences of monozygotic twins discordant for multiple sclerosis. *Nature* **464**, 1351-1356 (2010).

12. Schachter,H. The 'yellow brick road' to branched complex N-glycans. *Glycobiology* **1**, 453-461 (1991).

13. Kornfeld,R. & Kornfeld,S. Assembly of asparagine-linked oligosaccharides. *Annu. Rev. Biochem.* **54**, 631-664 (1985).

14. Dennis,J.W., Nabi,I.R. & Demetriou,M. Metabolism, cell surface organization, and disease. *Cell* **139**, 1229-1241 (2009).

15. Lau,K.S. *et al.* Complex N-glycan number and degree of branching cooperate to regulate cell proliferation and differentiation. *Cell* **129**, 123-134 (2007).

16. Grigorian,A. *et al.* Control of T Cell-mediated autoimmunity by metabolite flux to N-glycan biosynthesis. *J. Biol. Chem.* **282**, 20027-20035 (2007).

17. Ye,Z. & Marth,J.D. N-glycan branching requirement in neuronal and postnatal viability. *Glycobiology* **14**, 547-558 (2004).

18. Demetriou,M., Granovsky,M., Quaggin,S. & Dennis,J.W. Negative regulation of T-cell activation and autoimmunity by Mgat5 N-glycosylation. *Nature* **409**, 733-739 (2001).

19. Chen,I.J., Chen,H.L. & Demetriou,M. Lateral Compartmentalization of T Cell Receptor Versus CD45 by Galectin-N-Glycan Binding and Microfilaments Coordinate Basal and Activation Signaling. *J. Biol. Chem.* **282**, 35361-35372 (2007).

20. Lee,S.U. *et al.* N-glycan processing deficiency promotes spontaneous inflammatory demyelination and neurodegeneration. *J. Biol. Chem.* **282**, 33725-33734 (2007).

21. Grigorian,A., Torossian,S. & Demetriou,M. T-cell growth, cell surface organization, and the galectin-glycoprotein lattice. *Immunol. Rev.* **230**, 232-246 (2009).

22. Gregory,S.G. *et al.* Interleukin 7 receptor alpha chain (IL7R) shows allelic and functional association with multiple sclerosis. *Nat. Genet.* **39**, 1083-1091 (2007).

23. Lundmark,F. *et al.* Variation in interleukin 7 receptor alpha chain (IL7R) influences risk of multiple sclerosis. *Nat. Genet.* **39**, 1108-1113 (2007).

24. Cummings,R.D. & Kornfeld,S. Characterization of the structural determinants required for the high affinity interaction of asparagine-linked oligosaccharides with immobilized Phaseolus vulgaris leukoagglutinating and erythroagglutinating lectins. *J. Biol. Chem.* **257**, 11230-11234 (1982).

25. Chen,H.L., Li,C.F., Grigorian,A., Tian,W. & Demetriou,M. T cell receptor signaling co-regulates multiple Golgi genes to enhance N-glycan branching. *J. Biol. Chem.* **284**, 32454-32461 (2009).

26. Tulsiani,D.R., Harris,T.M. & Touster,O. Swainsonine inhibits the biosynthesis of complex glycoproteins by inhibition of Golgi mannosidase II. *J. Biol. Chem.* **257**, 7936-7939 (1982).

27. Rose,T., Lambotte,O., Pallier,C., Delfraissy,J.F. & Colle,J.H. Identification and biochemical characterization of human plasma soluble IL-7R: lower concentrations in HIV-1-infected patients. *J. Immunol.* **182**, 7389-7397 (2009).

28. Maier,L.M. *et al.* IL2RA genetic heterogeneity in multiple sclerosis and type 1 diabetes susceptibility and soluble interleukin-2 receptor production. *PLoS. Genet.* **5**, e1000322 (2009).

29. Maier,L.M. *et al.* Soluble IL-2RA levels in multiple sclerosis subjects and the effect of soluble IL-2RA on immune responses. *J. Immunol.* **182**, 1541-1547 (2009).

30. Chen,W. & Stanley,P. Five Lec1 CHO cell mutants have distinct Mgat1 gene mutations that encode truncated N-acetylglucosaminyltransferase I. *Glycobiology* **13**, 43-50 (2003).

31. Unligil,U.M. *et al.* X-ray crystal structure of rabbit N-acetylglucosaminyltransferase I: catalytic mechanism and a new protein superfamily. *EMBO J.* **19**, 5269-5280 (2000).

32. Anjos,S., Nguyen,A., Ounissi-Benkalha,H., Tessier,M.C. & Polychronakos,C. A common autoimmunity predisposing signal peptide variant of the cytotoxic T-lymphocyte antigen 4 results in inefficient glycosylation of the susceptibility allele. *J. Biol. Chem.* **277**, 46478-46486 (2002).

33. Maurer,M. *et al.* A polymorphism in the human cytotoxic T-lymphocyte antigen 4 (CTLA4) gene (exon 1 +49) alters T-cell activation. *Immunogenetics* **54**, 1-8 (2002).

34. Bagos,P.G., Karnaouri,A.C., Nikolopoulos,G.K. & Hamodrakas,S.J. No evidence for association of CTLA-4 gene polymorphisms with the risk of developing multiple sclerosis: a meta-analysis. *Mult. Scler.* **13**, 156-168 (2007).

35. Noseworthy,J.H. Progress in determining the causes and treatment of multiple sclerosis. *Nature* **399**, A40-A47 (1999).

36. Munger,K.L. *et al.* Vitamin D intake and incidence of multiple sclerosis. *Neurology* **62**, 60-65 (2004).

37. Tsoukas,C.D., Provvedini,D.M. & Manolagas,S.C. 1,25-dihydroxyvitamin D3: a novel immunoregulatory hormone. *Science* **224**, 1438-1440 (1984).

38. Lemire,J.M. & Archer,D.C. 1,25-dihydroxyvitamin D3 prevents the in vivo induction of murine experimental autoimmune encephalomyelitis. *J. Clin. Invest* **87**, 1103-1107 (1991).

39. Veldman,C.M., Cantorna,M.T. & DeLuca,H.F. Expression of 1,25-dihydroxyvitamin D(3) receptor in the immune system. *Arch. Biochem. Biophys.* **374**, 334-338 (2000).

40. Zella,J.B., McCary,L.C. & DeLuca,H.F. Oral administration of 1,25-dihydroxyvitamin D3 completely protects NOD mice from insulin-dependent diabetes mellitus. *Arch. Biochem. Biophys.* **417**, 77-80 (2003).

41. Salvatore,S. *et al.* A pilot study of N-acetyl glucosamine, a nutritional substrate for glycosaminoglycan synthesis, in paediatric chronic inflammatory bowel disease. *Aliment. Pharmacol. Ther.* **14**, 1567-1579 (2000).

42. Green,R.S. *et al.* Mammalian N-glycan branching protects against innate immune self-recognition and inflammation in autoimmune disease pathogenesis. *Immunity.* **27**, 308-320 (2007).

43. Ilarregui,J.M. *et al.* Tolerogenic signals delivered by dendritic cells to T cells through a galectin-1-driven immunoregulatory circuit involving interleukin 27 and interleukin 10. *Nat. Immunol.* **10**, 981-991 (2009).

44. Wellcome Trust Case Control Consortium. Genome-wide association study of 14,000 cases of seven common diseases and 3,000 shared controls. *Nature* **447**, 661-678 (2007).

45. Todd,J.A. *et al.* Robust associations of four new chromosome regions from genome-wide analyses of type 1 diabetes. *Nat. Genet.* **39**, 857-864 (2007).

46. Hypponen,E., Laara,E., Reunanen,A., Jarvelin,M.R. & Virtanen,S.M. Intake of vitamin D and risk of type 1 diabetes: a birth-cohort study. *Lancet* **358**, 1500-1503 (2001).

47. Kavvoura,F.K. & Ioannidis,J.P. CTLA-4 gene polymorphisms and susceptibility to type 1 diabetes mellitus: a HuGE Review and meta-analysis. *Am. J. Epidemiol.* **162**, 3-16 (2005).

48. Malek,T.R. The biology of interleukin-2. *Annu. Rev. Immunol.* **26**, 453-479 (2008).

49. Peschon,J.J. *et al.* Early lymphocyte expansion is severely impaired in interleukin 7 receptor-deficient mice. *J. Exp. Med.* **180**, 1955-1960 (1994).

50. Clarke,G.M. *et al.* Basic statistical analysis in genetic case-control studies. *Nat. Protoc.* **6**, 121-133 (2011).

51. Brynedal,B. *et al.* MGAT5 alters the severity of multiple sclerosis. *J. Neuroimmunol.* **220**, 120-124 (2010).

52. McDonald,W.I. *et al.* Recommended diagnostic criteria for multiple sclerosis: guidelines from the International Panel on the diagnosis of multiple sclerosis. *Ann. Neurol.* **50**, 121-127 (2001).

53. Oksenberg,J.R. *et al.* Mapping multiple sclerosis susceptibility to the HLA-DR locus in African Americans. *Am. J. Hum. Genet.* **74**, 160-167 (2004).

Acknowledgments

The authors thank the National Institute of Diabetes and Digestive and Kidney Diseases, the General Clinical Research Center, UCI (funded by National Center for Research Resources) and Peter Gregersen, Stacy Caillier, Stephen L. Hauser, Jorge R. Oksenberg for DNA samples/genotyping; Anup Datta and Margie Murnan (University of California, San Diego) for mass spectroscopy and Wen Hsin Chang for assistance. Research was supported by grants from Canadian Arthritis Network; Canada Research Chair and McLaughlin Centre of Molecular Research Chair to K.A.S.; National Institutes of Health (NIH) to K.G.C., A.G. (F32AI081456), and C.F.L. (T32AI-060573); Canadian Institutes of Health to K.A.S. and J.W.D; and National Multiple Sclerosis Society, Wadsworth Foundation and National Institute of Allergy and Infectious Disease (R01AI082266, R01AI053331) to M.D.

Chapter 3

Golgi proofreading homeostatically controls cell growth and differentiation

Statement of contribution

In this study I designed and performed all experiments, analyses of data and interpretation of results, except for mass spectromety of *N*-glycan (Figure 3.4) which was done with the assistance of Anne Dell and Stuart Haslam.

Summary

Essential biological systems frequently employ proofreading mechanisms to maintain cell homeostasis. Cell growth, differentiation and diseases states are regulated by the interaction of galectins with branched N-glycans at the cell surface. Galectins bind N-acetyllactosamine units (LacNAc: Galβ1,4GlcNAc) in branched N-glycans attached to surface glycoproteins, forming a molecular lattice that controls receptor clustering/surface-retention/signaling. LacNAc density and galectin avidity for N-glycans increase proportional to the number of LacNAc branches initiated via the sequential action of the medial Golgi branching enzymes Mgat1, 2, 4, and 5. Mgat5 deficiency marginally reduces LacNAc content by limiting N-glycans to three branches, yet results in T-cell hyperactivity and autoimmunity. However, restricting N-glycans to a single branch via Mgat2 deficiency or mannosidase II inhibition does not produce a more hyperactive state. Rather, a marked increase in poly-LacNAc extension maintains LacNAc content and galectin binding to N-glycans, thereby preventing further increases in T cell activity and autoimmunity; phenotypes reversed by targeted deficiency of the poly-LacNAc extension enzyme B3GnT2 or complete blockade of branching. Homeostatic maintenance of LacNAc content in N-glycans appears to be a general mechanism, being present in epithelial, mesenchymal and stem cells. These data define Golgi proofreading and LacNAc content, rather than unique N-glycan structures, as critical regulators of the galectin lattice, cell homeostasis and autoimmunity.

Introduction

Self-correcting mechanisms have evolved to maintain the integrity of critical biological pathways in the face of disruptive insults and stochastic uncertainty. Such mechanisms range from proofreading in DNA replication and translation to functional and genetic redundancy of important cellular apparatuses. The galectin-glycoprotein lattice is a dynamic cell surface structure which globally regulates receptor localization and signaling[1-3]. Its importance is underscored by its role in basic cellular processes such as signaling, apoptosis, endocytosis, differentiation, and cell growth, as well as its association with a wide range of human diseases including autoimmunity, cancer and diabetes. Here we present a homeostatic mechanism employed by the Golgi apparatus that acts to maintain the galectin-glycoprotein lattice in the face of dysregulated Golgi function.

The lattice forms due to the multivalent interactions between extracellular galectins, a family of sugar binding proteins, and the disaccharide N-acetyllactosamine (LacNAc) present on glycoproteins[4-6]. The vast majority of secreted and cell surface proteins are co or post-translationally modified by the addition of sugars. As these proteins transit through the ER and Golgi, their glycans undergo dramatic remodeling, producing a vast and heterogeneous array of glycoforms[7,8]. In the medial Golgi a group of enzymes, Mgat1, 2, 4, and 5, act successively to produce N-glycans with one, two, three, or four N-acetlyglucosamine (GlcNAc) branches[9]. The subsequent addition of galactose by a family of galactosyl transferase (GalT) enzymes produces the disaccharide and galectin substrate LacNAc. Alternating action of B3GnT and GalT enzymes can produce a linear polymer of LacNAc (poly-LacNAc) at any given branch

(Figure 3.1). The number and length of branches depends on the relative activity of the Golgi enzymes and availability of UDP-GlcNAc. Although, the affinity of galectin binding to a LacNAc monomer is relatively weak, increased LacNAc valency through branching and poly-LacNAc extension can dramatically increase galectin avidity leading to a major impact on cell surface dynamics[6]. In T cells for example, the avidity of TCR for peptide-MHC is similar to that of galectin for poly-LacNAc branched glycans(~10^5M). In this case galectin-TCR interactions directly oppose ligand induced TCR clustering and signaling, thereby negatively regulating antigen-dependent T cell growth.

Deficiency in the branching enzyme β1,6-N-acetylglucosaminyltransferaseV (Mgat5) reduces avidity for galectin, enhancing antigen dependent and independent TCR clustering/signaling leading to development of spontaneous autoimmune disease[3,10-12]. Based on the current model of the galectin-glycoprotein lattice, more severe reductions in branching should weaken the lattice further and result in greater T cell hyperactivity. Surprisingly, limiting branching to a single branch with Mgat2 deficiency revealed that the Golgi apparatus has a remarkable capacity to buffer challenges to the strength of the galectin-glycoprotein lattice.

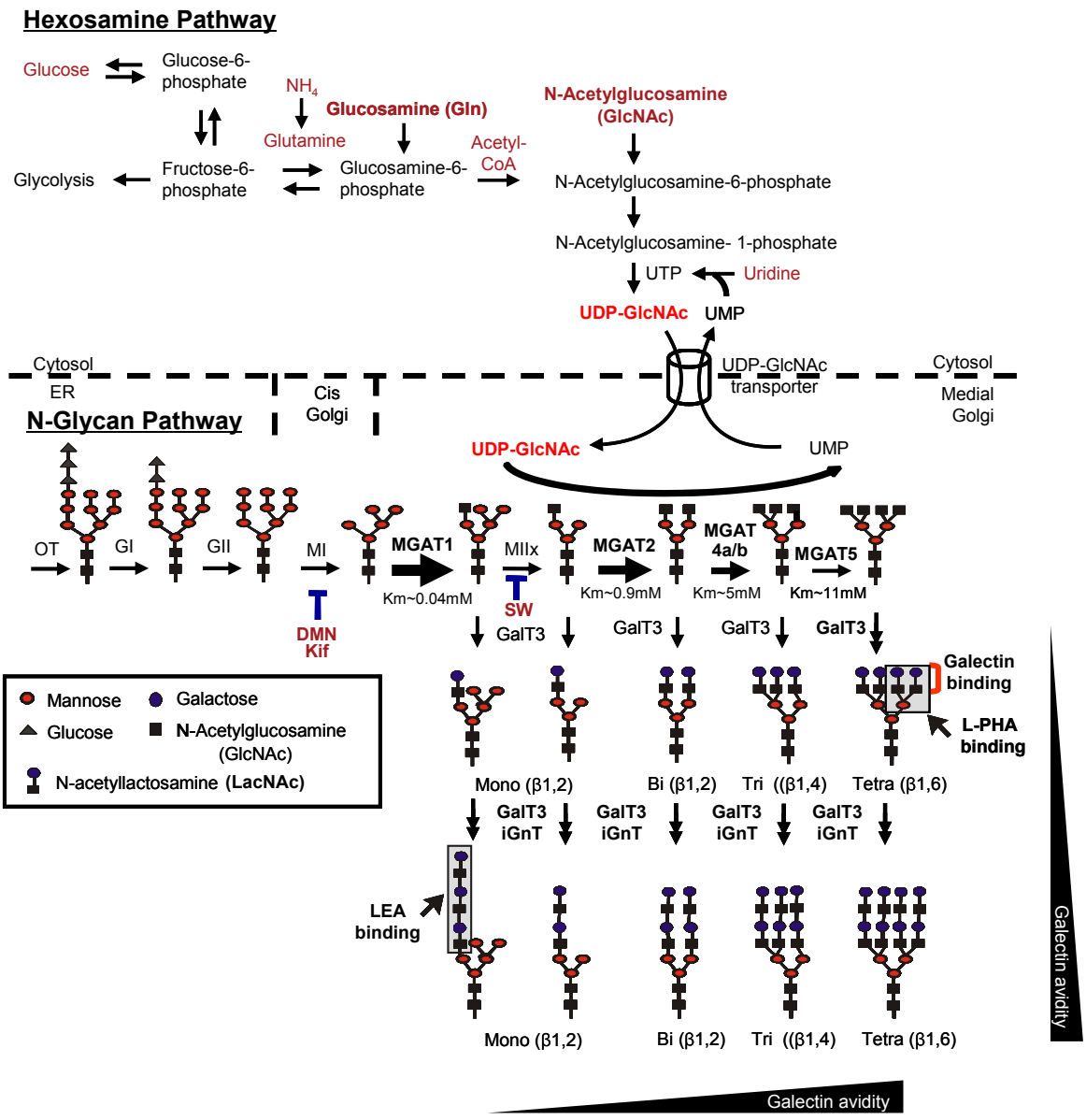

Figure 3.1. Hexosamine and N-glycan biosynthetic pathways in mammals.
Utilizing the hexosamine pathway product, UDP-GlcNAc, the Golgi enzymes Mgat1, 2, 4a/b, and 5 are responsible for genrating mono-, bi-, tri-, and tetra-antennary branched N-glycans, respectively. GlcNAc branches are further modified to create N-acetyllactosamine units which serve as binding sites for galectins and L-PHA. The alternating action of GalT and iGnT enzymes produce additional LacNAc units by extending existing branches. The number of N-glycans attached to a glycoprotein and the number of LacNAc units per glycan determine strength of galectin binding, allowing for differential incorporation of glycoproteins into the lattice. Mgat1, 2, 4 and 5 = N-acetylglucosaminyltransferases I, II IV and V; MII/MIIx = mannosidase II/IIx, MIa,b,c = mannosidase I,a,b,c, SW = swainsonine; DMN = deoxymannorjirimycin; Kif = kifunensine. Additional structural diversity via addition of sialic acid, fucose, N-acetylgalactosamine and/or sulfate is not shown.

Methods

Reagents, Mice and Flow Cytometry

Isolated human $CD3^+$ T cells purified by negative selection (RosetteSep, StemCell Technologies) were stimulated with plate-bound anti-CD3 (OKT3, eBioscience). Procedures with human subjects were approved by the Institutional Review Board of the University of California, Irvine. $Mgat2^{f/f}$ (006892), $Mgat1^{f/f}$ (006891) and Lck-Cre (003802) mice were obtained from Jackson Laboratory. $B3GnT2^{+/-}$ (11605) embryos were from the MMRRC and were rederived by the UC Irvine Transgenic Mouse Facility. Inter-breeding generated all other mice. Mice were selected randomly for experiments and approved by the Institutional Animal Care and Use Committee of the University of California, Irvine. Human cells were stained with anti-CD4, anti-CD69 (eBioscience) and/or L-PHA-FITC (*Phaseolus Vulgaris* Leukoagglutinin, Vector Labs) as previously described. Mouse cells were stained with anti-CD4 (RM 4-5), anti-CD8 (53-6.7), and anti-CD69 (H1.2F3) (eBioscience). Proliferation was assessed by 5,6-carboxyfluorescein diacetate succinimidyl ester (CFSE; Molecular Probes) at 1uM in PBS (20 min., 4^oC) and stimulated with plate-bound anti-CD3e. Cells were cultured in RPMI-1640 media supplemented with 10% fetal bovine serum, 2μM L-glutamine, 100 U/ml penicillin/streptomycin and 2μM 2-mercaptoethanol. Where indicated, 40 mM GlcNAc (Ultimate Glucosamine, Wellesley Therapeutics Inc.) and 10 mM uridine (Sigma) were added to cells in culture at time 0. For flow cytometric analysis of glycan expression, cells were stained with 2 ug/ml L-PHA-FITC, ConA-FITC, LEA-FITC or biotinylated versions of these lectins followed by DyLight649 labelled streptavidin(Vector Labs). Data analysis was performed using FlowJo software.

RNA Isolation and Microarray

$CD4^+$ T cells isolated from $Mgat2^{f/f}$ mice and L-PHA^-CD4^+ T cells isolated from $Mgat2^{f/f}$/Lck-Cre mice were used analysis. The RNeasy mini kit (Qiagen, Valencia, CA) was used for RNA extraction. Gene expression was assessed using the Affymetrix Mouse Gene 1.0 ST arrays in triplicate. Array data were quantified with Expression Console version 1.1 software (Affymetrix, Inc.) using the PLIER Algorithm default values. Expression values were then filtered as present/absent at expression 100. The Cyber-T web server was used for data analysis and to compare samples.

Galectin-3 Binding

Recombinant mouse galectin-3 (R&D systems) was labeled using an Alexa Fluor 488 protein labeling kit (Life Technologies). Cells were stained for flow cytometry using 3ug labeled galectin-3 per test. Staining was carried out for 30 minutes at room temperature followed by one wash and fixation with paraformaldehyde. For the lactose control samples, 50mM lactose was included in all steps.

PNGase F Treatment of Live Cells

Purified mouse T cells were washed twice in HBSS and resuspended in 100ul of G7 reaction buffer. 2500 units of glycerol free PNGase F (New England Biolabs) was added to the cells and the reaction was allowed to proceed for up to four hours at 37 degrees Celsius. Cells were then washed with HBSS and immediately stained for flow cytometry.

Enzymatic assays

B3GnT enzyme activity was measured using a glycosyltransferase activity kit (R&D systems). Five million Jurkat cells grown with or without SW were washed three times with Tris buffered saline and lysed with 300ul of lysis buffer (10mM Tris pH 7.5, 2mM

$MnCl_2$, 4mM $CaCl_2$, 0.5% Triton-X, with protease inhibitors). The lysate was cleared of insoluble material by centrifugation and dialyzed overnight in an identical solution to remove cellular phosphate. Enzyme activity was measured following the instructions of the kit. Briefly, 25ul of lysate was mixed with 25ul of reaction mixture to give a final concentration of 6mM N-acetyllactosamine, 5mM UDP-GlcNAc, and 6ng/ul coupling phosphatase. The reaction was allowed to proceed for two hours at 37°C, followed by visualization of released phosphate by a malachite green reagent as indicated in the kit. Absorbance at 620nm was determined using a plate reader and converted using a phosphate standard run in parallel. Background was determined and subtracted by parallel reactions that lacked the specific acceptor N-acetyllactosamine but contained UDP-GlcNAc and coupling phosphatase.

MALDI-TOF mass spectroscopy

Control and SW treated Jurkat cells were lysed with 1% SDS in 100mM Tris pH7.4, dialyzed to remove SDS, digested with trypsin to generate glycopeptides and treated with PNGaseF to release N-glycans. N-glycans were desialylated by mild acid digestion prior to permethylation and mass spectroscopy.

Experimental Autoimmune Encephalomyelitis

EAE was induced by subcutaneous immunization of randomly selected female mice at days 0 with 100μg of bovine MOG35-55 (AnaSpec) emulsified in Complete Freund's Adjuvant containing 4mg/ml heat-inactivated *Mycobacterium tuberculosis* (H37RA;Difco). On days 0 and 2, mice received 150ng of pertussis toxin(List Biological Laboratories) by intraperitoneal injection. Mice were examined daily for clinical signs of EAE over the next 30 days with observer blinded to treatment conditions. Mice were

scored daily as follows: 0, no disease; 1, loss of tail tone; 2, hindlimb weakness; 3, hindlimb paralysis; 4, forelimb weakness or paralysis and hindlimb paralysis; 5, moribund or dead. Kifunensine was given orally via the drinking water starting 3 days before immunization. All mice were housed with 12 hr light/dark cycles.

Results

Mgat2 deficiency in T cells does not result in greater hyperactivity than Mgat5 deficiency

To further investigate the role of branching in T cell function, T cell specific Mgat2 deficient mice were generated by crossing Lck/Cre mice with Mgat2 floxed mice. Loss of Mgat2 limits glycans to a single GlcNAc branch and as a result of the sequential nature of the branching pathway also impacts a greater number of cell surface glycans than Mgat5 deletion[13]. Examination of peripheral T cells from $Mgat2^{f/f}$/Lck-Cre+ mice indicated loss of Mgat2 in most but not all T cells as assayed by L-PHA binding (Figure 3.2A). L-PHA (*Phaseolus vulgaris, leukoagglutinin*) is a plant lectin that binds specifically to β1,6GlcNAc-branched N-glycans, structures lost with Mgat2 deletion[3,14]. The effect of Mgat2 deficiency on T cell function was evaluated by stimulating with plate bound anti-CD3 and assaying activation by CD69 expression at 24 hours and proliferation by CFSE dilution at 72 hours. Surprisingly, Mgat5 and Mgat2 deficient T cells displayed a similar degree of activation and proliferation despite the much more dramatic reduction in branching in Mgat2 deficient T cells (Figure 3.2B and 3.2C). This suggested that either the β1,6GlcNAc branch produced by Mgat5 is uniquely important for regulating T cell activation or that a compensatory mechanism maintains lattice strength when the number of N-glycan branches is severely reduced. To evaluate for differences in total surface LacNAc content between Mgat2 and Mgat5 deficient T cells, Galectin-3 binding was measured. Mgat5 deletion resulted in a significant reduction in the ability of T cells to bind Galectin-3 (Figure 3.2D), consistent with previously published results[3]. However, Mgat2 deficiency produced no additional decrease in

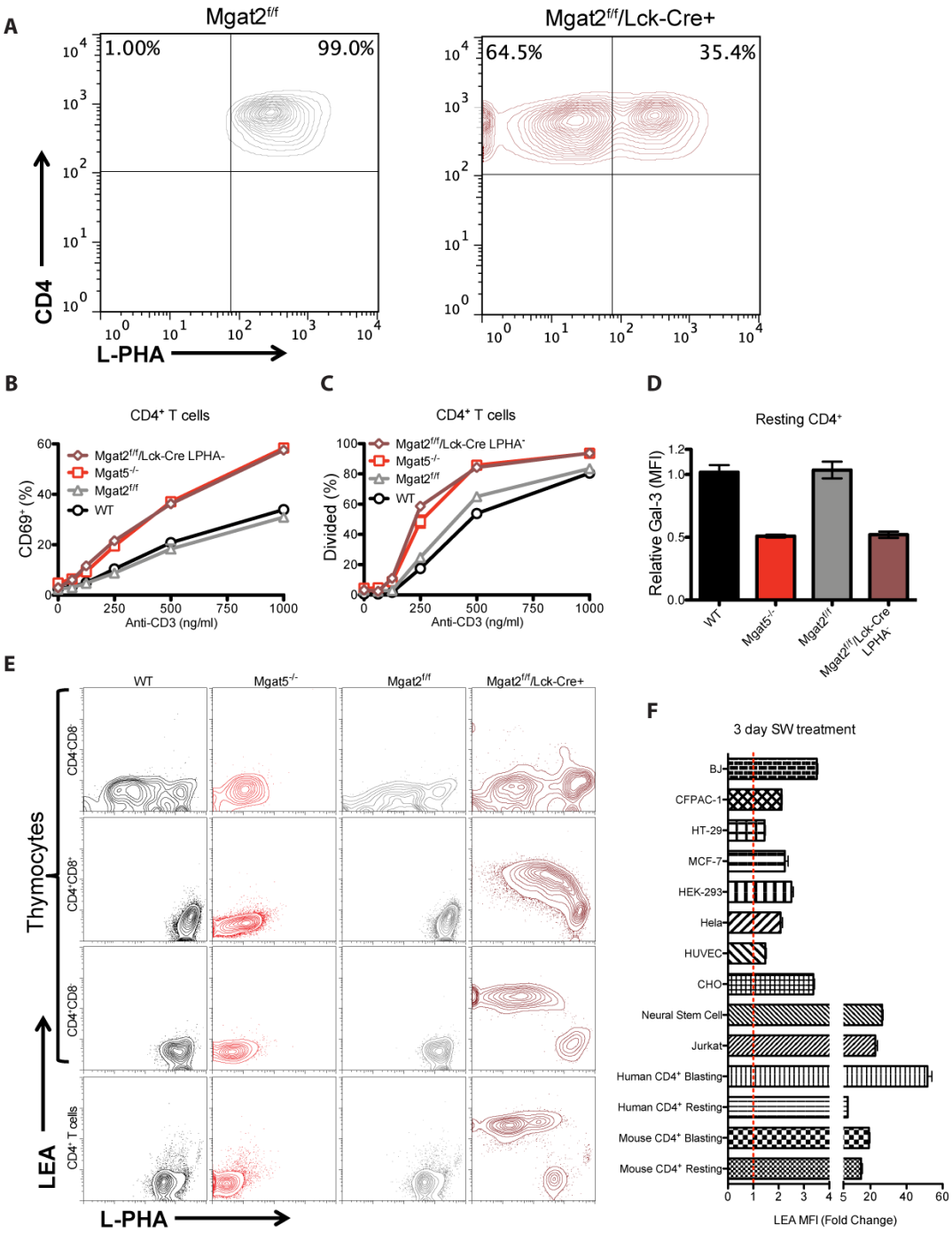

Figure 3.2. Compensation limits hyperactivity of Mgat2 deficient T cells
(A) T cells isolated from mice of the indicated genotypes were analyzed for L-PHA binding by FACS, gating on $CD4^+$ cells. **(B,C)** T cells from mice of the indicated genotypes were activated with plate bound anti-CD3 for 24 **(B)** or 72 **(C)** hours. $CD4^+$ cells were analyzed for CD69 expression **(B)** or CFSE dilution **(C)** by FACS, gating on L-PHA^- cells where indicated. **(D)** T cells of the indicated genotypes were analyzed for galectin-3 binding by FACS, gating on L-PHA^- cells where indicated. Each mutant was normalized to its control. **(E)** Thymocytes and T cells of the indicated genotypes were analyzed for L-PHA and LEA binding by FACS. (**F**) Cells were treated in culture with or without 500nM SW for 72 hours followed by analysis of LEA binding by FACS. Fold increase in LEA MFI of the SW treated sample compared to the untreated sample is presented. The red line marks one fold or no change.

galectin-3 binding (Figure 3.2D), suggesting comparable LacNAc content at the cell surface.

Inhibition of branching results in linear extension of the remaining branch to maintain LacNAc content

Since the branching pathway enzymes act sequentially, only a single branch remains in the absence of Mgat2. We thus hypothesized that compensatory maintenance of cell surface LacNAc content would need to occur by linear extension of the remaining branch producing poly-LacNAc structures (Figure 3.1). To test this prediction, T cells and thymocytes from wild type, Mgat5$^{-/-}$, Mgat2$^{f/f}$ and Mgat2$^{f/f}$/Lck-Cre mice were stained with L-PHA as well as the tomato lectin Lycopersicon Esculentum (LEA). LEA binds to poly-LacNAc structures containing at least three repeating LacNAc units[15,16]. Wild type and Mgat5$^{-/-}$ T cells and thymocytes expressed low levels of poly-LacNAc. However, in Mgat2$^{f/f}$/Lck-Cre mice, loss of L-PHA staining was accompanied by a ~100 fold increase in LEA staining. The loss of L-PHA binding and the increase in LEA binding appeared to occur concurrently during the double positive stage of thymocyte development, when the Lck driven Cre is first expressed, and were maintained through the single positive stage and in peripheral T cells (Figure 3.2E). Treatment of various cell types with swainsonine (SW), a mannosidase II inhibitor which blocks N-glycan processing between Mgat1 and Mgat2 indicated that lattice homeostasis was a general feature of many cell types (Figure 3.2F). Although all cell types assayed displayed an increase in LEA, the response was greater in white blood cells and neural precursor cells than in cells of epithelial origin.

Poly-LacNAc can occur on O-glycans and glycolipids in addition to N-glycans[17,18]. Furthermore, LEA has been reported to bind to high-mannose structures in addition to poly-LacNAc[19]. To investigate the structural basis for the increase in LEA staining, Mgat2 deficient T cells were treated with PNGase F, an amidase which specifically cleaves between the innermost GlcNAc and asparagine residue of N-glycans while leaving O-glycans and glycolipids intact[20]. PNGase F treatment of live cells incompletely removes N-glycans, with a four hour treatment of Mgat2$^{+/+}$ T cells reducing cell surface L-PHA binding by ~50% (Figure 3.3A). Nevertheless, the same treatment resulted in a >80% reduction in LEA staining intensity in Mgat2 deficient T cells, suggesting that the vast majority of LEA staining was due to cell surface N-glycans (Figure 3.3A). To further evaluate this question, we directly compared thymocytes derived from Mgat2$^{f/f}$Lck-Cre and Mgat1$^{f/f}$Lck-Cre mice. Mgat1 deficiency blocks all branching and poly-LacNAc extension in N-glycans and unlike Mgat2 deficiency, Mgat1 deficient thymocytes do not show an increase in LEA staining concurrent with the loss in L-PHA staining (Figure 3.3B). Similar to Mgat2 deficiency, treatment of CHO cells with SW increases LEA staining. However, LEA staining did not increase in SW treated Mgat1 deficient CHO (Lec1) cells (Figure 3.3C). Furthermore, increased LEA staining induced by Mgat2 deficiency in mouse T cells or SW treatment of Jurkat T cells are both reversed by the mannosidase I inhibitors deoxymannorjirimycin (DMN) and kifunensine, which block the N-glycan pathway prior to Mgat1 (Figure 3.3D). Moreover, MALDI-TOF mass spectroscopy analysis of N-glycans derived from swainsonine treated Jurkat T cells confirmed increased poly-LacNAc extension on hybrid N-glycans. Endo-β-galactosidase

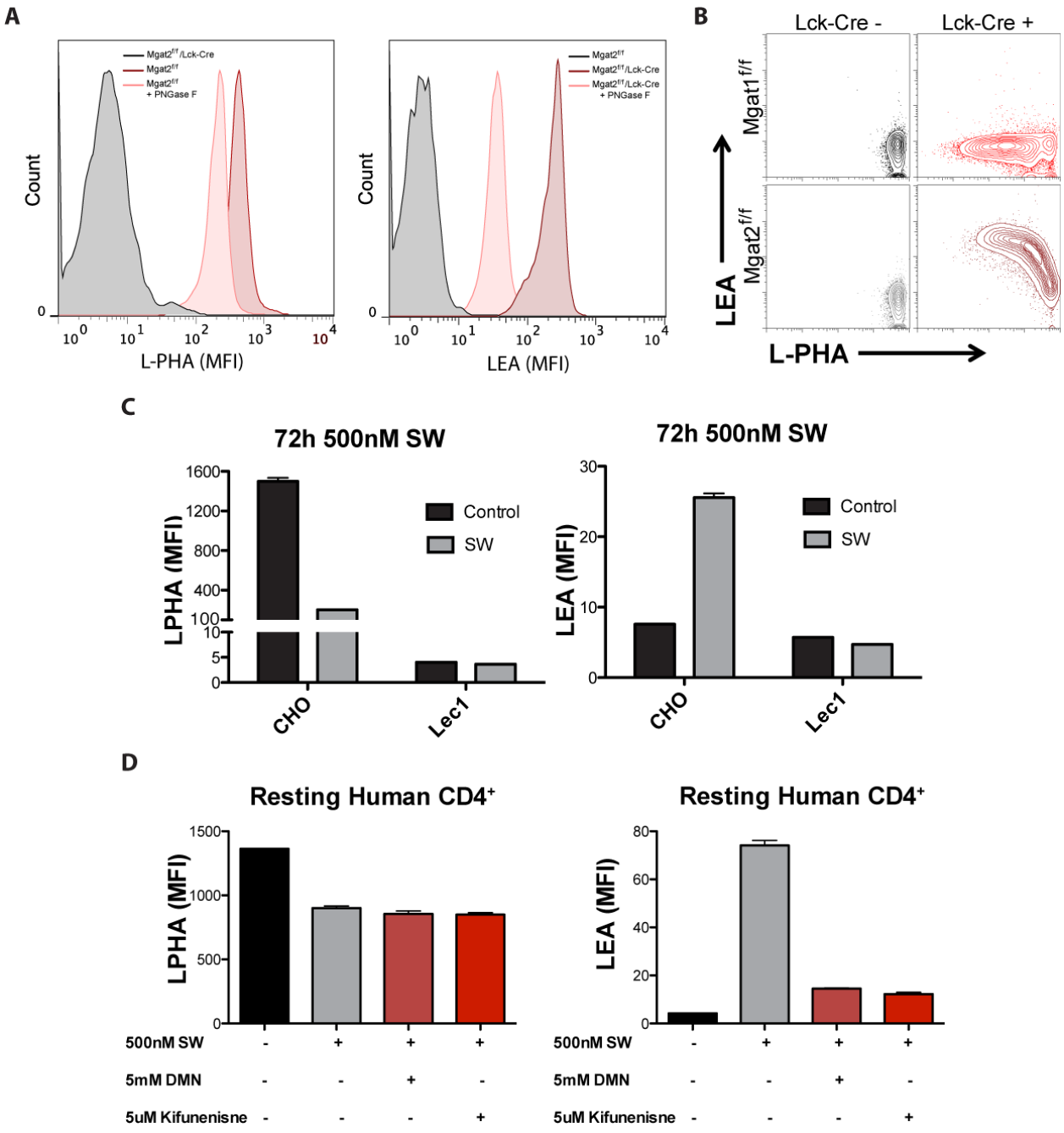

Figure 3.3. Branching deficiency induces poly-LacNAc on N-glycans
(A) T cells isolated from mice of the indicated genotypes were treated for 4 hours with 2500 units of PNGase F and analyzed for L-PHA binding by FACS, gating on $CD4^+$ cells. **(B)** Thymocytes of the indicated genotypes were analyzed for L-PHA and LEA binding by FACS, gating on double positive cells. **(C)** CHO and Lec1 cells were grown in the presence or absence of 500nM SW for 3 days followed by analysis for LEA and L-PHA binding by FACS. **(D)** Primary human T cells were treated with the indicated conditions for 3 days without stimulation and analyzed for lectin binding by FACS gating on live, non-blasting $CD4^+$ cells.

cuts internal β(1-4) galactose linkages in poly-LacNAc structures, producing GlcNAc β(1-3)Gal and Gal β (1-4)GlcNAc β(1-3)Gal, the latter representing the terminal most cut. The ratio of these two structures can be used to assess the relative length of poly-LacNAc structures, with a higher ratio indicating longer chains. Endo-β-galactosidase treatment of N-glycans derived from Jurkat T cells treated with or without SW revealed much higher levels of GlcNAc β(1-3)Gal relative to Gal β (1-4)GlcNAc β(1-3)Gal, indicating SW induced long poly-LacNAc chains in N-glycans (Figure 3.4). Together, these data indicate that induction of severe branching deficiency results in homeostatic up-regulation of poly-LacNAc structures on N-glycans.

Lattice homeostasis opposes T cell hyperactivity and autoimmunity

To assess the functional consequences of poly-LacNAc up-regulation, we reversed the response to SW by blocking all branching using the mannosidase I inhibitors DMN or kifunensine and subsequently measured lattice strength, T cell activation, and proliferation. Whereas SW treatment alone moderately reduced galectin-3 binding, the addition of kifunensine dramatically reduced galectin-3 binding of Jurkat T cells (Figure 3.5A). To assess the effects on T cell activation and proliferation, primary human T cells were pretreated with PBS, SW, SW + DMN or SW + kifunensine for three days to establish baseline differences in cell surface glycans and then activated with plate bound anti-CD3. Activation and proliferation were measured via CD69 expression at 24 hours and CFSE dilution at 72 hours, respectively (Figure 3.5B and 3.5C). As previously shown, SW treatment alone caused significant increases in both activation

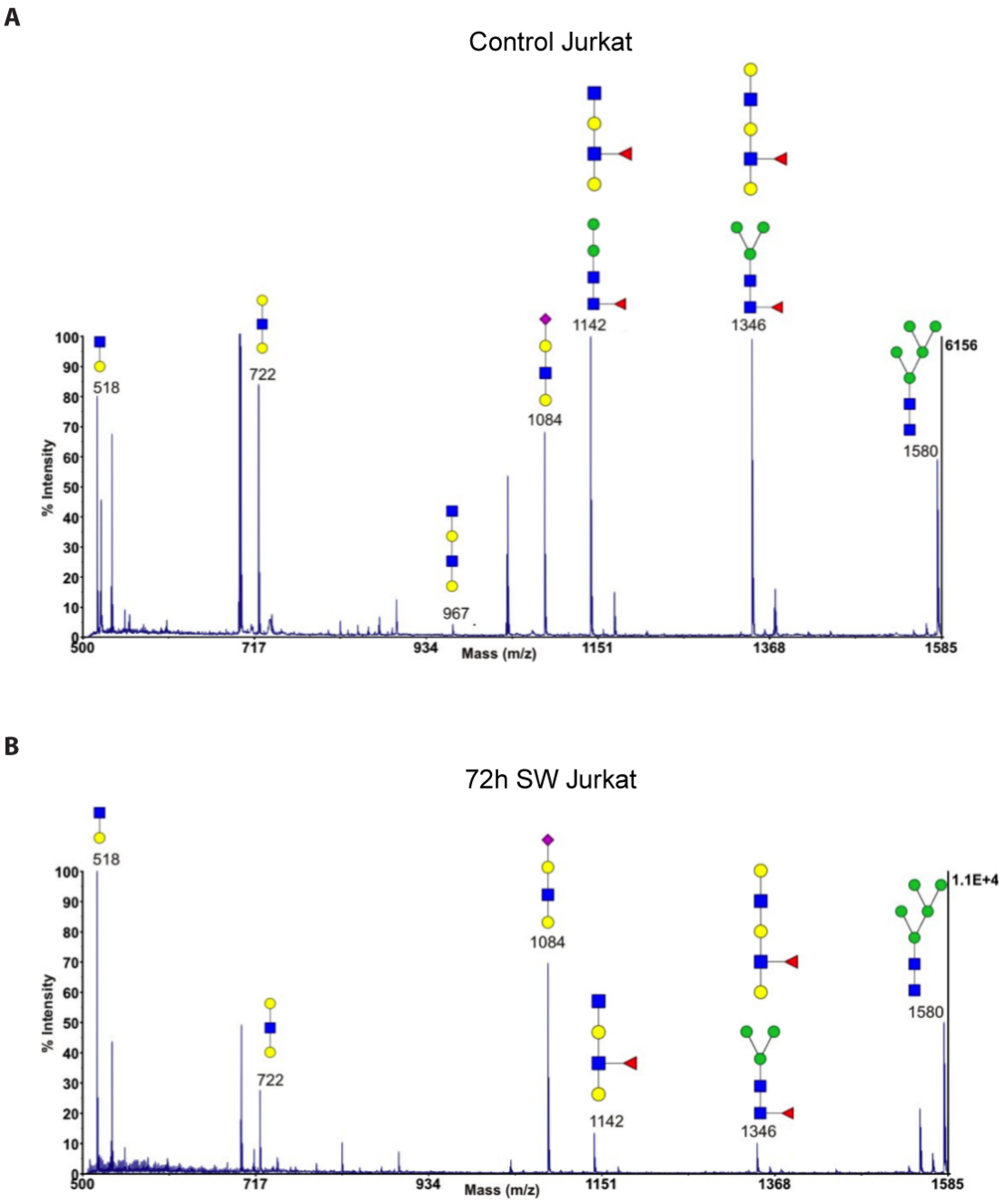

Figure 3.4. Mass spectrometry of N-glycans confirms poly-LacNAc induction by SW
(A,B) Mass spectrometric analysis of endo-β-galactosidase treated N-glycans from control **(A)** and SW treated **(B)** Jurkat cells. Endo-β-galactosidase cleaves internal β(1-4) galactose linkages of poly-LacNAc structures.

and proliferation. However, the addition of kifunensine or DMN resulted in much greater hyperactivity, particularly at lower doses of anti-CD3. Careful titration of kifunensine in the presence of SW showed a dose dependent decrease in LEA binding without further reducing LPHA binding (Figure 3.5D and 3.5E). Indeed, subsequent treatment with plate bound anti-CD3 and measurement of CD69 expression showed a corresponding dose dependent increase in T cell activation (Figure 3.5F).

To further evaluate the role of homeostatic induction of poly-LacNAc up-regulation in T cell function, mouse T cells deficient in both Mgat2 and B3GnT2 were generated. B3GnT2 is one of the major enzymes responsible for poly-LacNAc branch extension in mouse T cells and poly-LacNAc upregulation is expected to be limited in its absence[21]. Indeed, T cells from Mgat2$^{f/f}$/Lck-Cre/B3GnT2$^{-/-}$ mice showed significantly reduced LEA staining and galectin-3 binding when compared to Mgat2 deficient T cells, confirming reversal of poly-LacNAc extension (Figure 3.6A and 3.6B). Directly comparing T cell activation between these lines showed that both genetic and pharmacological inhibition of glycomic homeostasis resulted in significantly increased T cell hyperactivity (Figure 3.6C and 3.6D).

Since the galectin lattice has been shown to inhibit autoimmunity, we next sought to determine the functional consequences of glycomic homeostasis in regulating the course and severity of experimental autoimmune encephalomyelitis (EAE). EAE was induced in female Mgat2$^{f/f}$ and Mgat2$^{f/f}$/Lck-Cre mice by immunization with MOG 35-55 peptide and adjuvant, a model that mimics the autoimmune CNS pathology of multiple sclerosis[22]. Mice were treated with either vehicle or kifunensine in the drinking water from day -3 to 7, with day 0 indicating time of immunization. As expected vehicle treated

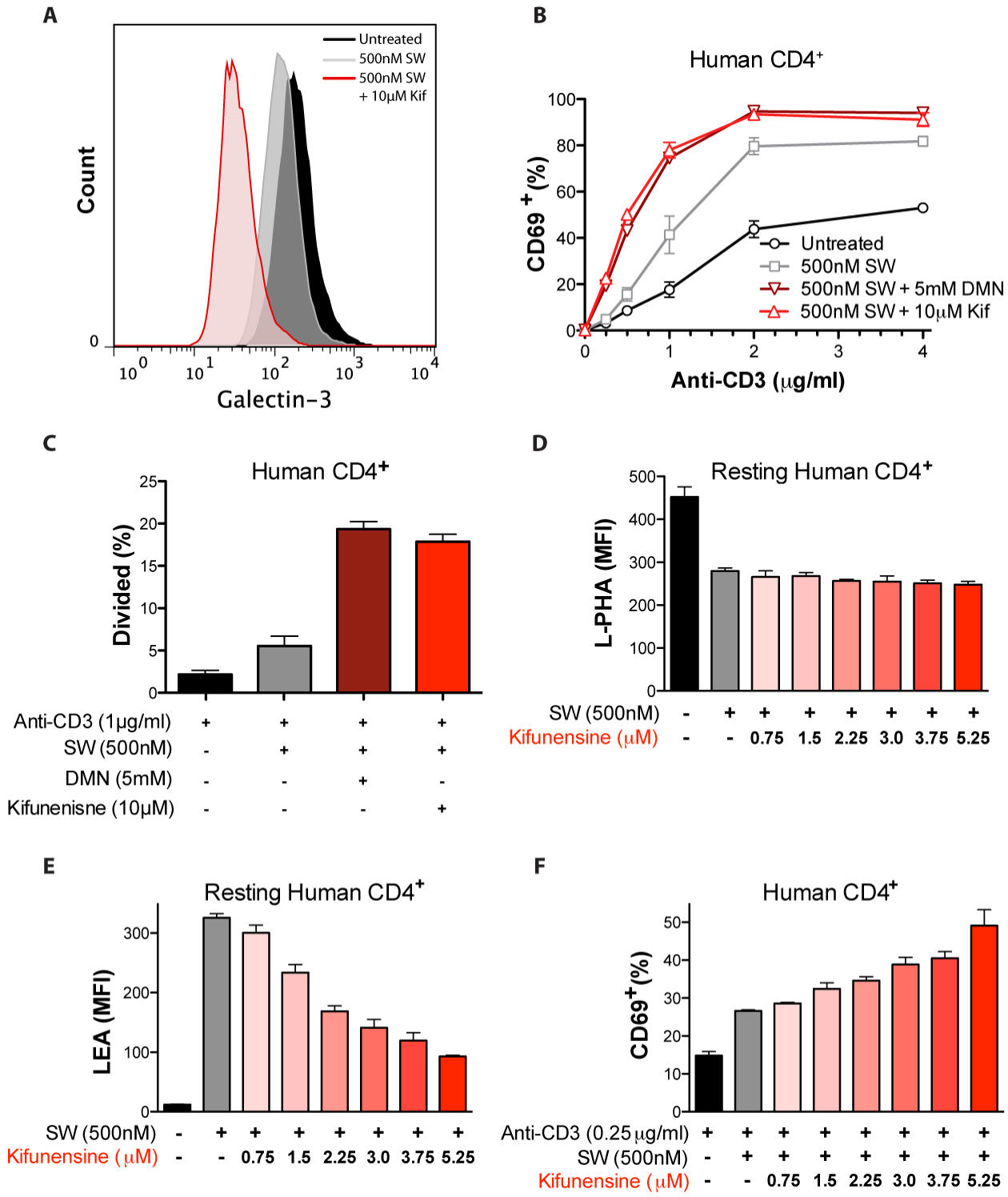

Figure 3.5. Poly-LacNAc compensation opposes human T cell activation
(A) Human T cells were treated as indicated for 72 hours in culture and analyzed for galectin-3 binding by FACS, gating on $CD4^+$ cells. **(B-F)** Human T cells were treated as indicated for 72h in culture without stimulation to establish baseline differences in glycan expression. Cells were analyzed for L-PHA **(D)** and LEA **(E)** binding by FACS, gating on $CD4^+$ cells. Cells treated in parallel were then activated with plate bound anti-CD3 for 24 **(B,F)** or 72 **(C)** hours. Cells were analyzed for CD69 expression **(B,F)** or CFSE dilution **(C)** by FACS, gating on $CD4^+$ cells.

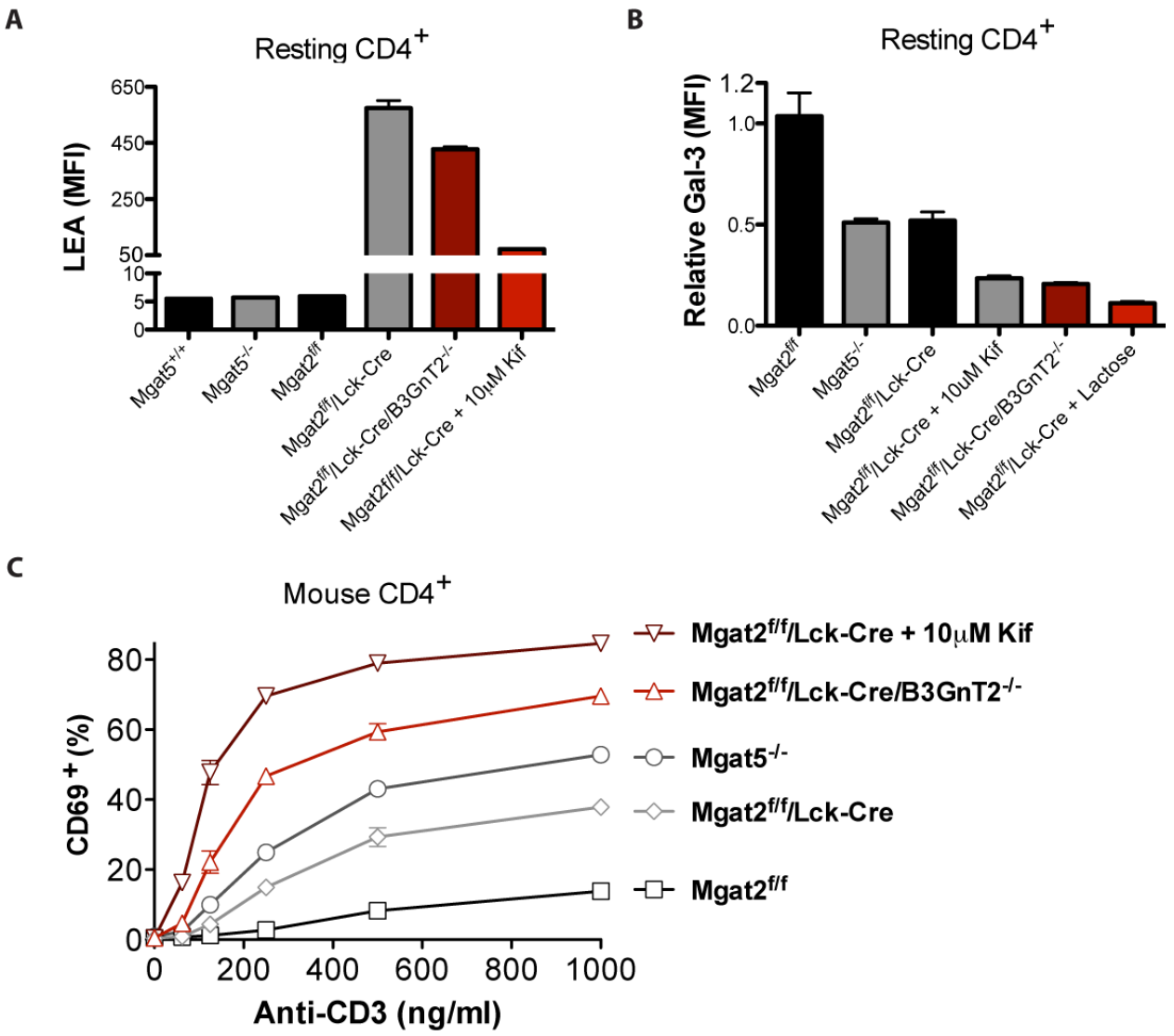

Figure 3.6. Poly-LacNAc compensation opposes mouse T cell activation
(A,B) T cells were isolated from mice of the indicated genotypes and analyzed for LEA **(A)** or galectin-3 **(B)** binding by FACS, gating on $CD4^+$ cells. **(C)** T cells isolated from mice of the indicated genotypes were activated for 24 hours with plate bound anti-CD3 and analyzed for CD69 expression by FACS.

Mgat2$^{f/f}$/Lck-Cre mice displayed a significantly more severe course of EAE than vehicle treated Mgat2$^{f/f}$ mice. Kifunensine treatment of Mgat2$^{f/f}$/Lck-Cre mice resulted in a dramatic increase in clinical score early in the disease course (Figure 3.7A).

At day 30, splenocytes were isolated and analyzed from representative mice from each group. Kifunensine treated mice had more CD25+ T cells as well as more Th1 and Th17 cells compared to vehicle treated mice (Figure 3.7B and 3.7C). Kifunensine treatment also dramatically increased pro-inflammatory recall responses when splenocytes were restimulated with MOG 35-55 *in vitro* (Figure 3.7D). Taken together these data demonstrate a major role for glycomic homeostasis in maintaining normal T cell growth, differentiation and self-tolerance.

Glycomic homeostasis is modulated but not driven by TCR signaling and UDP-GlcNAc concentration

Glycan analysis of tissues from glycosylation pathway deficient mice has revealed the presence of minor but unusual structures. It has been suggested this reflects compensation mediated by communication between the cell surface and the Golgi. We thus began our investigations of the molecular mechanism underlying lattice homeostasis by considering a feedback loop linking TCR signaling and cell surface LacNAc content. It is well established that the galectin-glycoprotein lattice negatively regulates TCR signaling, while TCR signaling promotes lattice strength[3,23]. It therefore stands to reason that compensation in the context of branching deficiency may be a feedback response driven by increased TCR signaling. Such a mechanism, which depends on a cell surface sensor of Golgi activity/branching implies a temporal lag

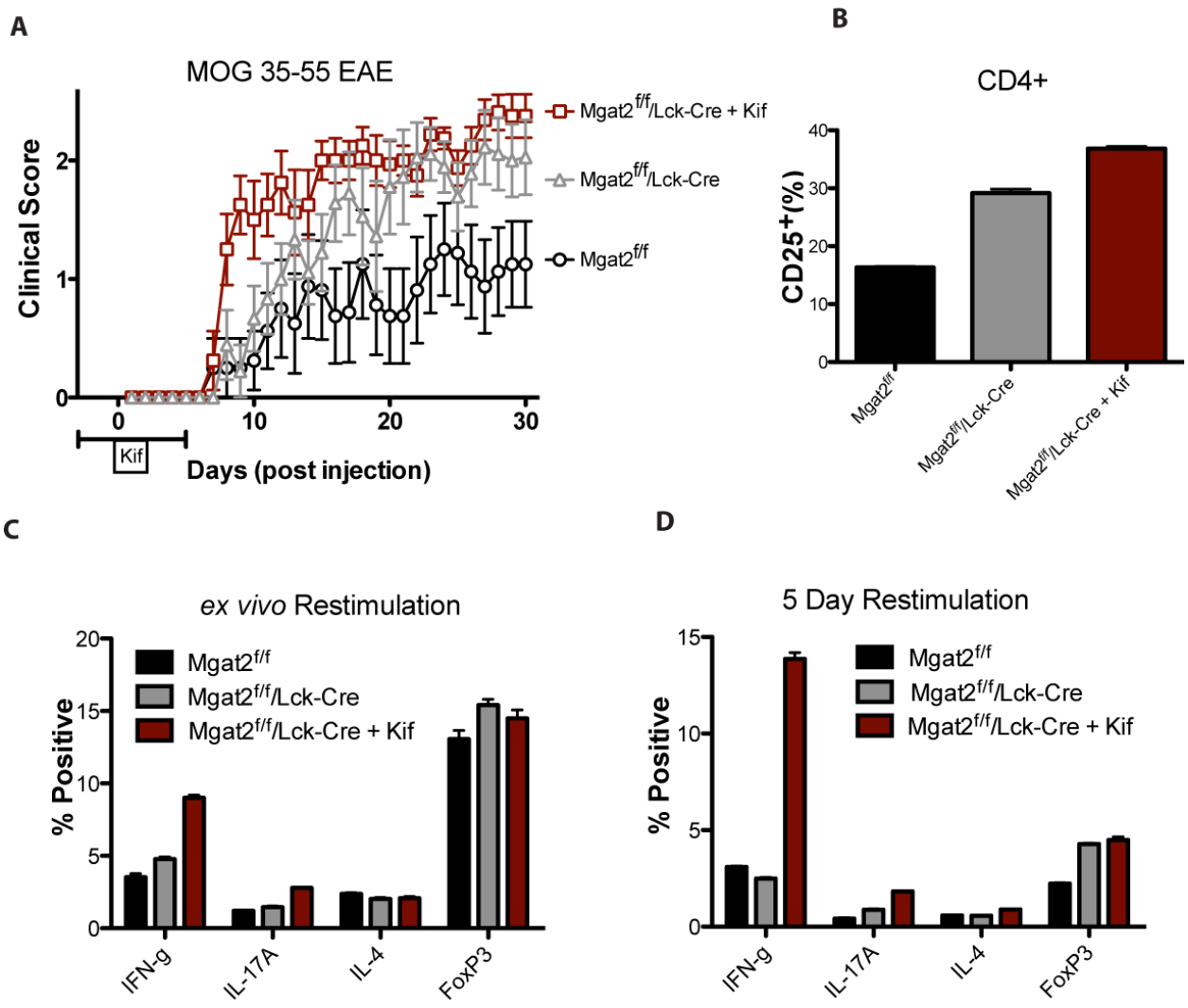

Figure 3.7. Poly-LacNAc compensation inhibits severity of EAE and pro-inflammatory T cells *in vivo*
(A) EAE was induced in age matched female C57BL/6 mice of the indicated genotypes/treatments by immunization with MOG 35-55 peptide emulsified in Complete Freund's adjuvant and pertussis toxin. Mice were treated with kifunensine via oral supplementation of the drinking water at 0.2 mg/ml from day -3 to 5, with day 0 indicating time of immunization (n = 9 per group). **(B,C)** At day 30, splenocytes were isolated from representative mice of each group and analyzed for CD25 expression **(B)** or cytokine expression **(C)** by FACS, gating on $CD4^+$ cells. **(D)** Alternatively splenocytes were activated *in vitro* for 5 days with 20µg/ml MOG 35-55 peptide, followed by analysis of cytokine expression by FACS to assay recall responses.

phase during which a defect is detected, a signal is sent, and the proper response is generated by the Golgi. With this prediction in mind, Jurkat cells were treated with SW for various times and analyzed for changes in cell surface glycosylation by LPHA, LEA and ConA, the latter a plant lectin that binds high-mannose structures increased by branching deficiency (Figure 3.8A and 3.8B). Although the increase in LEA binding trailed slightly behind an increase in ConA binding, it began to increase very soon after SW treatment, indicating an almost immediate compensatory response. Loss of L-PHA staining exhibited the smallest slope, possibly reflecting the preferential cell surface retention of highly branched glycoproteins (Figure 3.8C).

Since the increase in LEA staining exhibited some delay, the role of TCR signaling in driving poly-LacNAc induction was assessed. Blocking TCR signaling either genetically, with TCR and Lck deficient Jurkat lines, or pharmacologically, with MAP kinase inhibitors, only partially reduced the magnitude of the poly-LacNAc response induced by SW (Figure 3.8D and 3.8E). Furthermore, activating downstream TCR signaling with PMA and ionomycin increased poly-LacNAc up-regulation induced by SW but had no effect in the absence of SW (Figure 3.8F). Thus, TCR signaling appears to be neither necessary nor sufficient for the poly-LacNAc response, but does contribute to its magnitude in the context of deficient branching.

Since nearly every cell surface receptor is glycosylated, there are a large number of possible cell surface sensors which could function to drive compensation. However, we reasoned that regardless of the upstream components, a mechanism that acts to increase poly-LacNAc production must do so by either increasing substrate (UDP-GlcNAc or glycoprotein) for the reaction or by increasing the activity of responsible

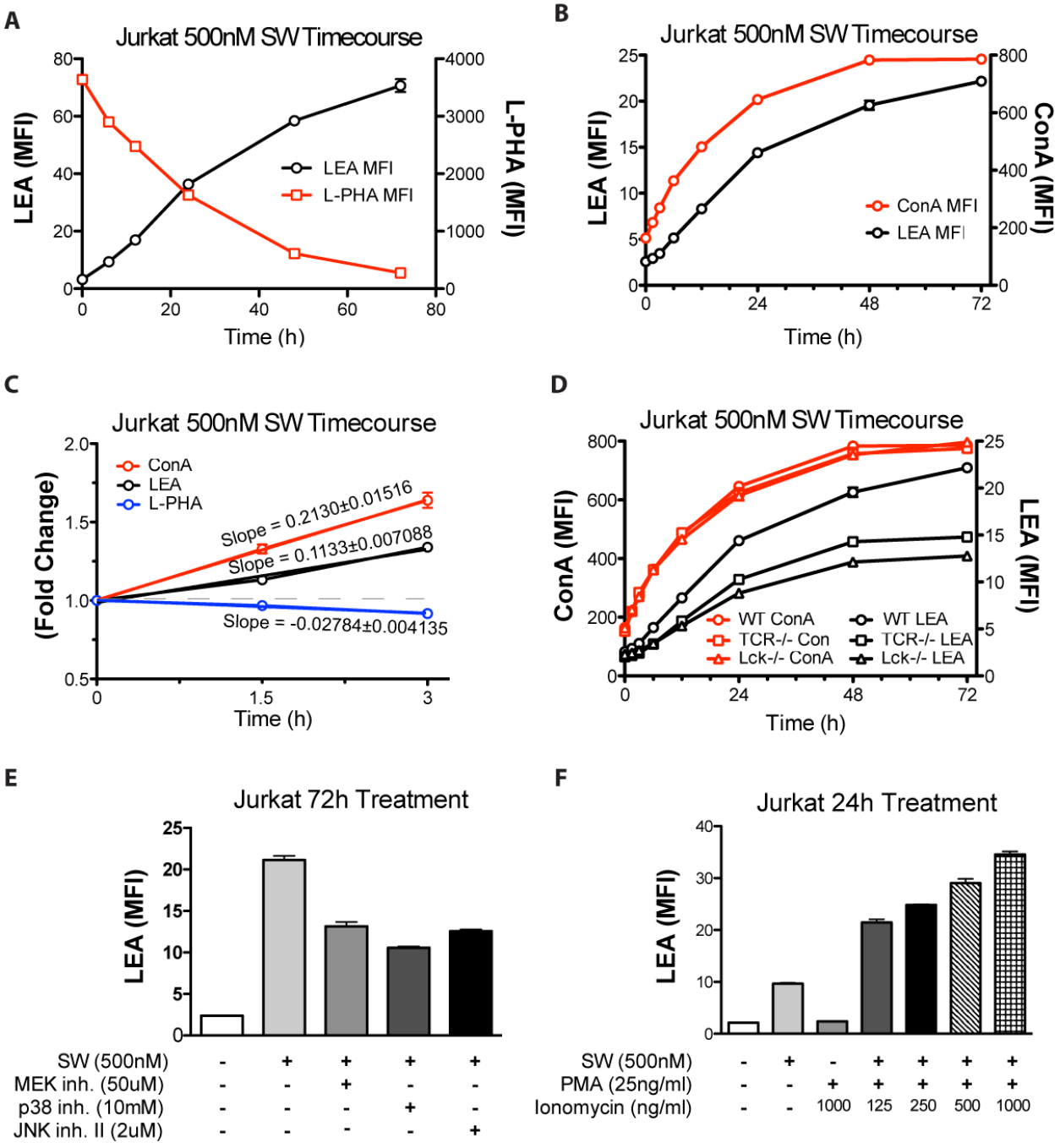

Figure 3.8. TCR signaling is neither necessary nor sufficient for poly-LacNAc induction
(A-C) Jurkat T cells were treated as with SW for indicated times and analyzed for lectin binding by FACS. **(D)** WT, $TCR^{-/-}$ and $Lck^{-/-}$ Jurkat cells were treated with SW for the indicated times and analyzed for lectin binding by FACS. **(E,F)** Jurkat cells were treated as indicated for 72 hours **(E)** or 24 hours **(F)** and analyzed for LEA binding by FACS.

enzymes. It has previously been reported that B3GnT enzymes show little preference for the various glycoforms upon which they can act. This is supported by recent studies which show that all branches are equally likely to be extended with poly-LacNAc[24]. Thus it is unlikely that an increase in mono-antennary glycans could account for the observed compensatory response. In fact, all else being equal, branching deficiency is expected to reduce B3GnT activity by severely reducing glycan acceptors.

On the other hand, it is possible that the sugar nucleotide substrate UDP-GlcNAc either accumulates in the absence of Mgat2-5 activity or is driven by a feedback mechanism that targets the hexosamine pathway. We therefore sought to compare UDP-GlcNAc levels in $Mgat2^{+/+}$ and $Mgat2^{-/-}$ T cells. Since $Mgat2^{f/f}$/Lck-Cre mice exhibit incomplete Cre mediated deletion of Mgat2, we isolated $LPHA^{low}$ LEA^{hi} T cells from $Mgat2^{f/f}$/Lck-Cre mice by including biotinylated-LPHA in a T cell negative selection cocktail produced by StemCell technologies. Measurement of UDP-GlcNAc levels by mass spectrometry in $Mgat2^{+/+}$ and $Mgat2^{-/-}$ T cells showed no difference (Figure 3.9A). Meaurement of UDP-GlcNAc levels in Jurkat cells treated with or without SW and Kifunensine by either mass spectrometry or a colorimetric assay also showed no increase in total cellular UDP-GlcNAc (Figure 3.9B and 3.9C). In addition, treatment of Jurkat cells with GlcNAc and uridine increased LEA staining in the presence but not absence of SW, despite a 3-4 fold increase in cellular UDP-GlcNAc concentrations in the absence of SW (Figure 3.9B, 3.9C and 3.9D). Much like TCR signaling, increased UDP-GlcNAc levels are thus neither necessary nor sufficient to induce poly-LacNAc but may drive poly-LacNAc when branching is inhibited. Not surprisingly, poly-LacNAc

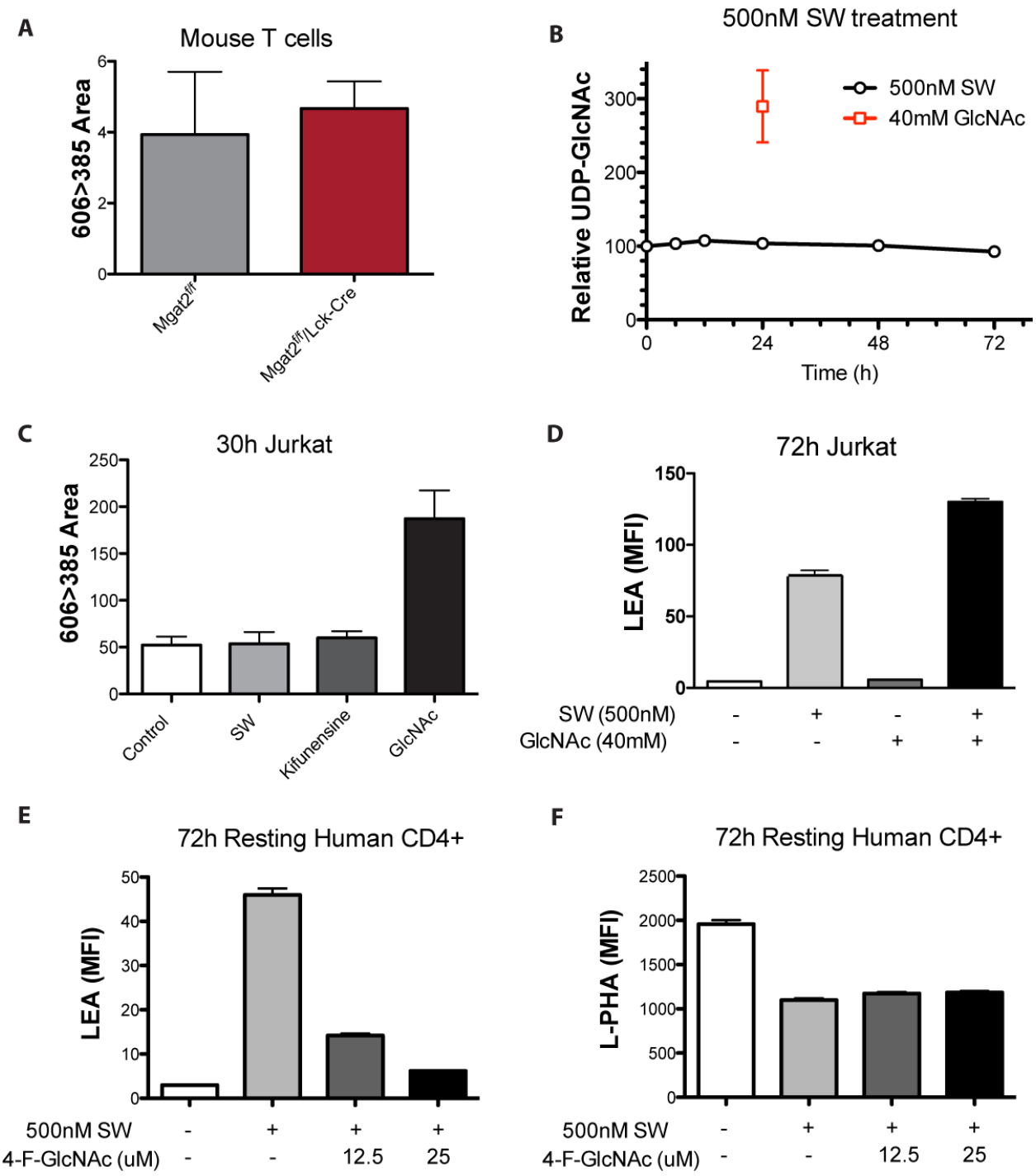

Figure 3.9. Poly-LacNAc induction is not dependent on increased UDP-GlcNAc levels
(A-C) UDP-GlcNAc levels were measured in mouse T cells of the indicated genotypes **(A)**, or Jurkat cells treated as indicated **(B, C)** via mass spectrometry **(A, C)** or a spectrophotometric method **(B)**. **(D-F)** Jurkat cells **(D)** or human T cells isolated from blood **(E, F)** were treated as indicated for 72 hours and analyzed for lectin binding by FACS.

induction was blocked by 4-Fluoro-GlcNAc, a drug which is known to inhibit poly-LacNAc production by reducing UDP-GlcNAc levels (Figure 3.9E and Figure 3.9F).

iGnT enzyme activity is unchanged in response to branching deficiency

Having ruled out increased substrate levels we sought to determine whether poly-LacNAc compensation was driven by increased enzyme activity. We began by probing gene expression changes using microarray profiling of purified $Mgat2^{+/+}$ and $Mgat2^{-/-}$ CD4+ T cells isolated from $Mgat2^{f/f}$ and $Mgat2^{f/f}$/Lck-Cre mice, respectively. Surprisingly, although gene expression changes were detected (Table 3.1), there were no significant changes observed in glycosylation genes known to impact poly-LacNAc production (Table 3.2). Hexosamine pathway genes responsible for UDP-GlcNAc production were also unchanged, consistent with the UDP-GlcNAc measurements (Table 3.2). As expected, the microarray showed dramatically decreased Mgat2 levels in the $Mgat2^{-/-}$ sample (Table 3.1).

Comparing B3GnT2 protein levels in Jurkat cells treated with or without SW also showed no difference (Figure 3.10A). Finally, to account for post-translational regulation as well as contribution from other B3GnT enzymes, total iGnT enzyme activity in lysates from control and SW treated Jurkat cells was measured. No difference was observed between control and SW treated samples (Figure 3.10B). Spiking in recombinant B3GnT2 resulted in an equal increase in enzyme activity, confirming that enzyme activity in the SW treated sample was not being artificially masked (Figure 3.10B). Thus, increased B3GnT enzyme activity is not responsible for homeostatic up-regulation of poly-LacNAc induced by branching deficiency.

Table 3.1. List of top 50 differentially expressed genes

Gene Symbol	Gene Description	p Value	Fold Change
Rpl36al	ribosomal protein L36A-like	4.44E-16	-15.6258
Mgat2	mannoside acetylglucosaminyltransferase 2	9.43E-14	-27.8780
Fn1	fibronectin 1	5.83E-12	-7.5845
Cpm	carboxypeptidase M	3.54E-10	3.1233
Zbtb16	zinc finger and BTB domain containing 16	5.45E-10	-3.3239
Mmp9	matrix metallopeptidase 9	1.58E-09	-3.9658
Serpinb10-ps	serine (or cysteine) peptidase inhibitor, clade B (ovalbumin), member 10, pseudogene	4.39E-09	-5.0634
Zfp69	zinc finger protein 69	4.63E-09	-2.1283
Cd93	CD93 antigen	1.04E-08	-2.3236
Atp8a2	ATPase, aminophospholipid transporter-like, class I, type 8A, member 2	2.64E-08	-2.2711
Gpr141	G protein-coupled receptor 141	3.83E-08	-3.4035
Penk	preproenkephalin	5.28E-08	3.8411
Clec7a	C-type lectin domain family 7, member a	8.21E-08	-2.4336
Lyz1	lysozyme 1	1.06E-07	-3.4287
Mpeg1	macrophage expressed gene 1	1.18E-07	-4.3408
Klra2	killer cell lectin-like receptor, subfamily A, member 2	1.33E-07	-4.4037
Kit	kit oncogene	2.44E-07	-2.3150
Plbd1	phospholipase B domain containing 1	2.47E-07	-2.9529
Lyz2	lysozyme 2	2.83E-07	-3.6156
Pld4	phospholipase D family, member 4	3.00E-07	-4.1375
Ace	angiotensin I converting enzyme (peptidyl-dipeptidase A) 1	3.36E-07	-3.3758
Sirpa	signal-regulatory protein alpha	3.40E-07	-3.9975
Clec12a	C-type lectin domain family 12, member a	3.54E-07	-4.4547
Tlr13	toll-like receptor 13	4.15E-07	-6.5477
Tnfrsf21	tumor necrosis factor receptor superfamily, member 21	4.86E-07	-3.4333
Tgfbi	transforming growth factor, beta induced	5.57E-07	-3.6315
Adrbk2	adrenergic receptor kinase, beta 2	5.98E-07	-2.0416
Il12rb2	interleukin 12 receptor, beta 2	7.32E-07	-2.6927
Csf1r	colony stimulating factor 1 receptor	7.57E-07	-5.9870
Xcl1	chemokine (C motif) ligand 1	9.55E-07	-2.0969
Mlh1	mutL homolog 1 (E. coli)	9.66E-07	-2.0854
Sulf2	sulfatase 2	1.01E-06	-2.9791
Igsf6	immunoglobulin superfamily, member 6	1.04E-06	-3.0615
Gpr56	G protein-coupled receptor 56	1.10E-06	-2.2352
Fcna	ficolin A	1.23E-06	-4.7706
Clec4a1	C-type lectin domain family 4, member a1	1.29E-06	-5.5202
Gm11428	predicted gene 11428	1.33E-06	-2.5636
Kcnj16	potassium inwardly-rectifying channel, subfamily J, member 16	1.35E-06	-2.5828
Coro2a	coronin, actin binding protein 2A	1.80E-06	1.5820
Clec4a3	C-type lectin domain family 4, member a13	1.88E-06	-4.7329
Muc13	mucin 13, epithelial transmembrane	1.91E-06	-2.0524
Abcd2	ATP-binding cassette, sub-family D (ALD), member 2	2.49E-06	-2.2046
Cd68	CD68 antigen	2.56E-06	-2.6229
Cd34	CD34 antigen	2.65E-06	-1.9429
Cxcr6	chemokine (C-X-C motif) receptor 6	2.68E-06	-3.3244
Mpo	myeloperoxidase	2.80E-06	-15.0742
Car1	carbonic anhydrase 1	2.95E-06	-10.5252
Pira11	paired-Ig-like receptor A11	3.03E-06	-3.3245
Emr1	EGF-like module containing, mucin-like, hormone receptor-like sequence 1	3.18E-06	-6.1010
Pira1	paired-Ig-like receptor A1	3.23E-06	-3.6538

Gene symbol, gene description, p value and fold change of Mgat2 deficient CD4+ cells relative to control are shown. Data are ordered by p value.

Table 3.2. List of N-glycan branching, poly-LacNAc production, and hexosamine pathway genes

Gene Symbol	Gene Description	p Value	Fold Change
Man1a	mannosidase 1, alpha	0.3602	1.0628
Man1a2	mannosidase, alpha, class 1A, member 2	0.4885	-1.0551
Man1b1	mannosidase, alpha, class 1B, member 1	0.4397	-1.0627
Man1c1	mannosidase, alpha, class 1C, member 1	0.4053	1.0748
Man2a1	mannosidase 2, alpha 1	0.8150	-1.0168
Man2a2	mannosidase 2, alpha 2	0.3647	-1.0787
Man2b1	mannosidase 2, alpha B1	0.0800	-1.1350
Man2b2	mannosidase 2, alpha B2	0.6465	1.0331
Man2c1	mannosidase, alpha, class 2C, member 1	0.9826	1.0016
Mgat1	mannoside acetylglucosaminyltransferase 1	0.1005	-1.1846
Mgat2	**mannoside acetylglucosaminyltransferase 2**	**0.0000**	**-27.8780**
Mgat3	mannoside acetylglucosaminyltransferase 3	0.1757	1.1377
Mgat4a	mannoside acetylglucosaminyltransferase 4, isoenzyme A	0.1486	-1.2068
Mgat4b	mannoside acetylglucosaminyltransferase 4, isoenzyme B	0.2248	1.1345
Mgat4c	mannosyl (alpha-1,3-)-glycoprotein beta-1,4-N-acetylglucosaminyltransferase, isozyme C (putative)	0.5695	1.0539
Mgat5	mannoside acetylglucosaminyltransferase 5	0.4045	1.0666
Mgat5b	mannoside acetylglucosaminyltransferase 5, isoenzyme B	0.1450	1.1347
B3gnt1	UDP-GlcNAc:betaGal beta-1,3-N-acetylglucosaminyltransferase 1	0.5597	-1.0587
B3gnt2	UDP-GlcNAc:betaGal beta-1,3-N-acetylglucosaminyltransferase 2	0.1503	1.1219
B3gnt3	UDP-GlcNAc:betaGal beta-1,3-N-acetylglucosaminyltransferase 3	0.4031	1.1072
B3gnt4	UDP-GlcNAc:betaGal beta-1,3-N-acetylglucosaminyltransferase 4	0.2923	1.1100
B3gnt5	UDP-GlcNAc:betaGal beta-1,3-N-acetylglucosaminyltransferase 5	0.1758	1.1742
B3gnt6	UDP-GlcNAc:betaGal beta-1,3-N-acetylglucosaminyltransferase 6 (core 3 synthase)	0.5565	1.0511
B3gnt7	UDP-GlcNAc:betaGal beta-1,3-N-acetylglucosaminyltransferase 7	0.8028	1.0237
B3gnt8	UDP-GlcNAc:betaGal beta-1,3-N-acetylglucosaminyltransferase 8	0.6157	1.0443
B3gnt9-ps	UDP-GlcNAc:betaGal beta-1,3-N-acetylglucosaminyltransferase 9, pseudogene	0.2841	1.0856
B3gntl1	UDP-GlcNAc:betaGal beta-1,3-N-acetylglucosaminyltransferase-like 1	0.7979	-1.0241
B4galt1	UDP-Gal:betaGlcNAc beta 1,4- galactosyltransferase, polypeptide 1	0.8003	1.0166
B4galt2	UDP-Gal:betaGlcNAc beta 1,4- galactosyltransferase, polypeptide 2	0.1023	1.1487
B4galt3	UDP-Gal:betaGlcNAc beta 1,4-galactosyltransferase, polypeptide 3	0.6938	-1.0304
B4galt4	UDP-Gal:betaGlcNAc beta 1,4-galactosyltransferase, polypeptide 4	0.1378	1.1624
B4galt5	UDP-Gal:betaGlcNAc beta 1,4-galactosyltransferase, polypeptide 5	0.8380	1.0131
B4galt6	UDP-Gal:betaGlcNAc beta 1,4-galactosyltransferase, polypeptide 6	0.0645	-1.2196
B4galt7	xylosylprotein beta1,4-galactosyltransferase, polypeptide 7 (galactosyltransferase I)	0.4116	-1.0764
Gck	glucokinase	0.0548	1.1856
Hk1	hexokinase 1	0.8593	1.0129
Hk2	hexokinase 2	0.4688	1.0771
Hk3	hexokinase 3	0.0236	-1.2237
Adpgk	ADP-dependent glucokinase	0.4033	-1.0787
Gpi1	glucose phosphate isomerase 1	0.7826	-1.0173
Gfpt1	glutamine fructose-6-phosphate transaminase 1	0.2410	-1.0941
Gfpt2	glutamine fructose-6-phosphate transaminase 2	0.0289	1.2116
Gnpda1	glucosamine-6-phosphate deaminase 1	0.6667	-1.0364
Gnpda2	glucosamine-6-phosphate deaminase 2	0.9474	1.0054
Gnpnat1	glucosamine-phosphate N-acetyltransferase 1	0.3646	-1.0839
Nat9	N-acetyltransferase 9 (GCN5-related, putative)	0.2253	1.0995
Pgm1	phosphoglucomutase 1	0.7697	-1.0243
Pgm2	phosphoglucomutase 2	0.7135	-1.0360
Pgm2l1	phosphoglucomutase 2-like 1	0.8036	-1.0167
Pgm3	phosphoglucomutase 3	0.6032	-1.0529
Pgm5	phosphoglucomutase 5	0.2374	1.1326
Uap1	UDP-N-acetylglucosamine pyrophosphorylase 1	0.6555	1.0402
Uap1l1	UDP-N-acteylglucosamine pyrophosphorylase 1-like 1	0.2637	-1.1092
Nagk	N-acetylglucosamine kinase	0.2907	-1.1126
Gale	galactose-4-epimerase, UDP	0.5196	1.0579
Gne	glucosamine (UDP-N-acetyl)-2-epimerase/N-acetylmannosamine kinase	0.2860	-1.0808

Gene symbol, gene description, p value and fold change of Mgat2 deficient CD4+ cells relative to control are shown. The microarray confirms loss of Mgat2 expression, highlighted in bold.

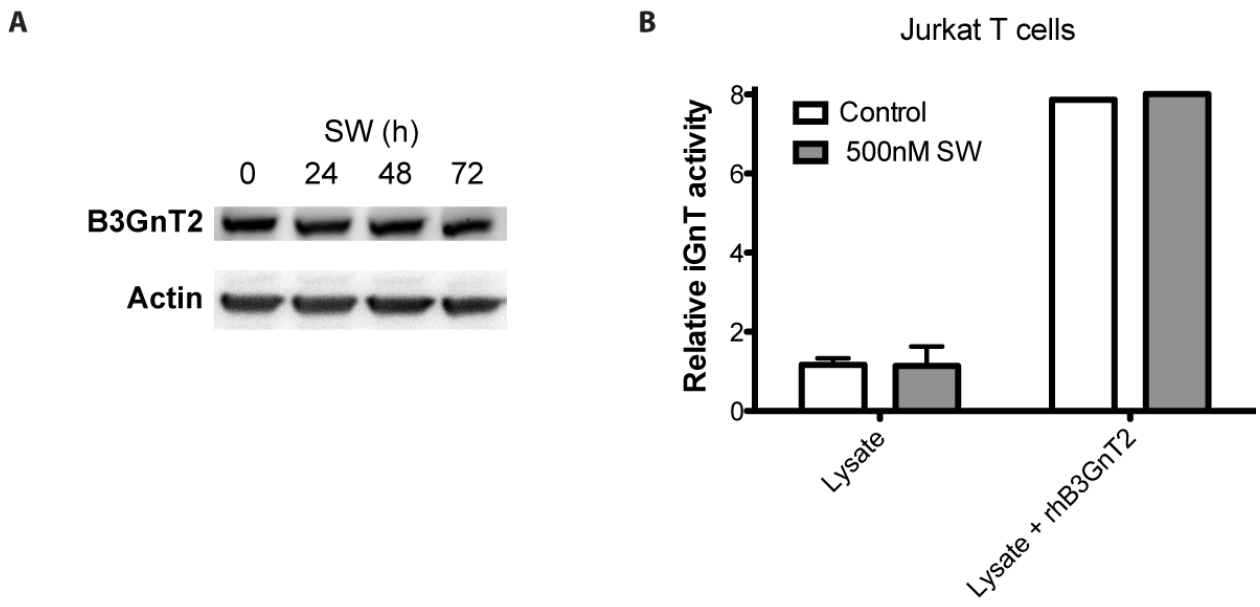

Figure 3.10. Poly-LacNAc induction cannot be accounted for by increased iGnT activity
(A) Jurkat cells were treated with 500nM SW for the indicated periods of time, lysed with RIPA buffer and immunoblotted for B3GnT2. Protein loading was normalized via BCA assay and confirmed by immunoblotting for actin. **(B)** Jurkat cells treated with and without SW for 72 hours were lysed, dialyzed, and used for iGnT enzyme activity measurements with and without addition of 5ug/ml rhB3gnT2.

Discussion

In summary, our results indicate that a Golgi mediated mechanism maintains lattice strength in response to branching deficiency by increasing LacNAc content via poly-LacNAc structures. The similar degree of hyperactivity between Mgat5 and Mgat2 deficient T cells suggests that poly-LacNAc extended mono-antennary structures are functionally equivalent to tri-antennary structures. Importantly blockade of mannosidase II and Mgat2 deficiency produced a similar phenotype, which was blocked by both mannosidase I inhibition and Mgat1 deficiency, despite targeting distinct biochemical steps and resulting in distinct structures. This outlines the importance of GlcNAc branches and N-acetyllactosamine units rather than strict chemical or structural specificity in determining both the homeostatic response and the functionality of the glycans produced. These results are the most direct to date in support of a model of N-glycosylation that emphasizes the importance of functional units such as LacNAc groups rather than unique structures. In other words these results provide direct evidence for functional redundancy across various glycoforms. Of note, although these differing glycoforms are clearly overlapping, they are not strictly equivalent. This likely reflects effects specific for distinct geometries of LacNAc presentation rather than unique biological function.

A clear understanding of the network of interacting factors that coalesce to determine the state of the galectin-glycoprotein lattice is required for the successful exploitation of its therapeutic potential. Interventions must be able to overcome or at least take into account the homeostatic cellular response to the initial disturbance. The failure of SW as an anti-cancer therapeutic for example may be due to its

ineffectiveness against compensatory poly-LacNAc production[25,26]. This work suggests that therapeutic strategies aimed at disrupting the lattice must block branching and extension simultaneously or target a more proximal regulator such as UDP-GlcNAc metabolism or transport. In light of these findings, the lattice approach to cancer treatment may merit re-visitation. Conversely, a deeper understanding of the central regulatory machinery that determines total LacNAc content will also be required for therapeutic approaches that seek to strengthen the lattice.

This study did not positively identify the molecular mechanism driving homeostatic upregulation of poly-LacNAc. However, several key insights allow us to propose a potential mechanism. As previously stated we detect no difference in total iGnT activity or UDP-GlcNAc concentrations between control and branching deficient T cells. However, it has long been appreciated that the glycosylation enzymes are organized in order of action from *cis* to *trans* along the secretory pathway. Mgat1 and Mgat2 are localized to the medial Golgi while GalT and B3GnT1 have been shown to be present in the *trans*-Golgi[27]. It has also been shown that the CMP-sialic acid transporter has a relatively restricted localization within the Golgi suggesting that sugar-nucleotide donors may be preferentially supplied to specific Golgi compartments[28]. We thus propose that one possible mechanism involves localization of UDP-GlcNAc. We suggest that UDP-GlcNAc supply may be restricted to an early Golgi compartment, thus preferentially driving branching over extension. However, if branching is inhibited, its shift from the *medial* to *trans* Golgi by cisternal maturation[29] may drive poly-LacNAc production despite unchanged total UDP-GlcNAc levels. This is consistent with our observation that increased total UDP-GlcNAc levels fail to drive poly-LacNAc when the

branching pathway is intact, yet significantly raise poly-LacNAc levels in the presence of SW. In the former case, *medial* Golgi branching enzymes likely consume the increased UDP-GlcNAc, resulting in more branching rather than extension. On the other hand, when branching is inhibited, increased UDP-GlcNAc can drive further poly-LacNAc production. Such a mechanism would take advantage of the compartmentalization of the Golgi apparatus to allow use of a single substrate to be prioritized to specific enzymes while still allowing for proofreading. Further, this would imply that metabolism, via production of UDP-GlcNAc, can serve as the central regulator of a complex glycosylation machinery.

Indeed the organization of the Golgi and the preferential supply of UDP-GlcNAc to the Mgat enzymes imply that branching is normally prioritized above extension. Our model suggests that at least under some circumstances extension may act as a backup mechanism to catch unused UDP-GlcNAc in the Golgi. This may also explain the lack of evolutionary pressure to produce genetic redundancy in the Mgat enzymes and the dramatically more severe phenotype seen with Mgat1 deficiency compared to other Mgat genes[30,31].

Finally, the presence of functional groups (LacNAc) as subcomponents of glycans combined with our current understanding of Golgi transport may help explain the curious use of three different nucleotides to charge the array of sugars used in glycosylation. Under our model, UDP-GlcNAc unused in the medial Golgi would progress to the trans Golgi. Its use in the trans Golgi would produce UMP which could preferentially drive antiport of UDP-Galactose into the Golgi to ensure further extension of poly-LacNAc rather than capping by CMP-Sialic acid. Were sialic acid also charged

with UDP rather than CMP, UDP-GlcNAc usage would drive UDP-Sialic acid antiport and capping equally with UDP-Galactose and extension.

References

1 Dennis, J. W., Nabi, I. R. & Demetriou, M. Metabolism, cell surface organization, and disease. *Cell* **139**, 1229-1241, doi:10.1016/j.cell.2009.12.008 (2009).

2 Lau, K. S. *et al.* Complex N-glycan number and degree of branching cooperate to regulate cell proliferation and differentiation. *Cell* **129**, 123-134, doi:10.1016/j.cell.2007.01.049 (2007).

3 Demetriou, M., Granovsky, M., Quaggin, S. & Dennis, J. W. Negative regulation of T-cell activation and autoimmunity by Mgat5 N-glycosylation. *Nature* **409**, 733-739, doi:10.1038/35055582 (2001).

4 Ahmad, N. *et al.* Galectin-3 precipitates as a pentamer with synthetic multivalent carbohydrates and forms heterogeneous cross-linked complexes. *The Journal of biological chemistry* **279**, 10841-10847, doi:10.1074/jbc.M312834200 (2004).

5 Brewer, C. F., Miceli, M. C. & Baum, L. G. Clusters, bundles, arrays and lattices: novel mechanisms for lectin-saccharide-mediated cellular interactions. *Current opinion in structural biology* **12**, 616-623 (2002).

6 Hirabayashi, J. *et al.* Oligosaccharide specificity of galectins: a search by frontal affinity chromatography. *Biochimica et biophysica acta* **1572**, 232-254 (2002).

7 Kornfeld, R. & Kornfeld, S. Assembly of asparagine-linked oligosaccharides. *Annual review of biochemistry* **54**, 631-664, doi:10.1146/annurev.bi.54.070185.003215 (1985).

8 Schachter, H. The 'yellow brick road' to branched complex N-glycans. *Glycobiology* **1**, 453-461 (1991).

9 Schachter, H. Biosynthetic controls that determine the branching and microheterogeneity of protein-bound oligosaccharides. *Biochemistry and cell biology = Biochimie et biologie cellulaire* **64**, 163-181 (1986).

10 Chen, I. J., Chen, H. L. & Demetriou, M. Lateral compartmentalization of T cell receptor versus CD45 by galectin-N-glycan binding and microfilaments coordinate basal and activation signaling. *The Journal of biological chemistry* **282**, 35361-35372, doi:10.1074/jbc.M706923200 (2007).

11 Grigorian, A. *et al.* Control of T Cell-mediated autoimmunity by metabolite flux to N-glycan biosynthesis. *The Journal of biological chemistry* **282**, 20027-20035, doi:10.1074/jbc.M701890200 (2007).

12 Lee, S. U. *et al.* N-glycan processing deficiency promotes spontaneous inflammatory demyelination and neurodegeneration. *The Journal of biological chemistry* **282**, 33725-33734, doi:10.1074/jbc.M704839200 (2007).

13 Wang, Y. *et al.* Modeling human congenital disorder of glycosylation type IIa in the mouse: conservation of asparagine-linked glycan-dependent functions in mammalian physiology and insights into disease pathogenesis. *Glycobiology* **11**, 1051-1070 (2001).

14 Cummings, R. D. & Kornfeld, S. Characterization of the structural determinants required for the high affinity interaction of asparagine-linked oligosaccharides with immobilized Phaseolus vulgaris leukoagglutinating and erythroagglutinating lectins. *The Journal of biological chemistry* **257**, 11230-11234 (1982).

15 Merkle, R. K. & Cummings, R. D. Relationship of the terminal sequences to the length of poly-N-acetyllactosamine chains in asparagine-linked oligosaccharides from the mouse lymphoma cell line BW5147. Immobilized tomato lectin interacts with high affinity with glycopeptides containing long poly-N-acetyllactosamine chains. *The Journal of biological chemistry* **262**, 8179-8189 (1987).

16 Kawashima, H., Sueyoshi, S., Li, H., Yamamoto, K. & Osawa, T. Carbohydrate binding specificities of several poly-N-acetyllactosamine-binding lectins. *Glycoconjugate journal* **7**, 323-334 (1990).

17 Watanabe, K., Hakomori, S. I., Childs, R. A. & Feizi, T. Characterization of a blood group I-active ganglioside. Structural requirements for I and i specificities. *The Journal of biological chemistry* **254**, 3221-3228 (1979).

18 Fukuda, M., Carlsson, S. R., Klock, J. C. & Dell, A. Structures of O-linked oligosaccharides isolated from normal granulocytes, chronic myelogenous leukemia cells, and acute myelogenous leukemia cells. *The Journal of biological chemistry* **261**, 12796-12806 (1986).

19 Oguri, S. Analysis of sugar chain-binding specificity of tomato lectin using lectin blot: recognition of high mannose-type N-glycans produced by plants and yeast. *Glycoconjugate journal* **22**, 453-461, doi:10.1007/s10719-005-5329-4 (2005).

20 Maley, F., Trimble, R. B., Tarentino, A. L. & Plummer, T. H., Jr. Characterization of glycoproteins and their associated oligosaccharides through the use of endoglycosidases. *Analytical biochemistry* **180**, 195-204 (1989).

21 Togayachi, A. *et al.* Polylactosamine on glycoproteins influences basal levels of lymphocyte and macrophage activation. *Proceedings of the National Academy of Sciences of the United States of America* **104**, 15829-15834, doi:10.1073/pnas.0707426104 (2007).

22 Grigorian, A. *et al.* N-acetylglucosamine inhibits T-helper 1 (Th1)/T-helper 17 (Th17) cell responses and treats experimental autoimmune encephalomyelitis. *The Journal of biological chemistry* **286**, 40133-40141, doi:10.1074/jbc.M111.277814 (2011).

23 Chen, H. L., Li, C. F., Grigorian, A., Tian, W. & Demetriou, M. T cell receptor signaling co-regulates multiple Golgi genes to enhance N-glycan branching. *The Journal of biological chemistry* **284**, 32454-32461, doi:10.1074/jbc.M109.023630 (2009).

24 Antonopoulos, A. *et al.* Loss of effector function of human cytolytic T lymphocytes is accompanied by major alterations in N- and O-glycosylation. *The Journal of biological chemistry* **287**, 11240-11251, doi:10.1074/jbc.M111.320820 (2012).

25 Goss, P. E., Reid, C. L., Bailey, D. & Dennis, J. W. Phase IB clinical trial of the oligosaccharide processing inhibitor swainsonine in patients with advanced malignancies. *Clinical cancer research : an official journal of the American Association for Cancer Research* **3**, 1077-1086 (1997).

26 Goss, P. E., Baptiste, J., Fernandes, B., Baker, M. & Dennis, J. W. A phase I study of swainsonine in patients with advanced malignancies. *Cancer research* **54**, 1450-1457 (1994).

27 Lee, P. L., Kohler, J. J. & Pfeffer, S. R. Association of beta-1,3-N-acetylglucosaminyltransferase 1 and beta-1,4-galactosyltransferase 1, trans-Golgi enzymes involved in coupled poly-N-acetyllactosamine synthesis. *Glycobiology* **19**, 655-664, doi:10.1093/glycob/cwp035 (2009).

28 Zhao, W., Chen, T. L., Vertel, B. M. & Colley, K. J. The CMP-sialic acid transporter is localized in the medial-trans Golgi and possesses two specific endoplasmic reticulum export motifs in its carboxyl-terminal cytoplasmic tail. *The Journal of biological chemistry* **281**, 31106-31118, doi:10.1074/jbc.M605564200 (2006).

29 Glick, B. S. & Luini, A. Models for Golgi traffic: a critical assessment. *Cold Spring Harbor perspectives in biology* **3**, a005215, doi:10.1101/cshperspect.a005215 (2011).

30 Metzler, M. *et al.* Complex asparagine-linked oligosaccharides are required for morphogenic events during post-implantation development. *The EMBO journal* **13**, 2056-2065 (1994).

31 Ioffe, E. & Stanley, P. Mice lacking N-acetylglucosaminyltransferase I activity die at mid-gestation, revealing an essential role for complex or hybrid N-linked carbohydrates. *Proceedings of the National Academy of Sciences of the United States of America* **91**, 728-732 (1994).

Chapter 4

Conclusions, implications, and future directions

We have demonstrated that the galectin-glycoprotein lattice is highly regulated, by both intercellular and intracellular mechanisms. Cytokine and hormone signaling combined with metabolism appear to set *N*-glycan branching levels in T cells. In the case of IL-2 and IL-7 signaling, these cytokines keep branching low in resting T cells, thus promoting activation and growth. However, their regulation of branching is complex as they increase branching in stimulated T cells, in contrast to unstimulated T cells. Nevertheless, it is critical for such an important structure to be dynamic and respond to environmental cues. Our expectation is that we are just scratching the surface in understanding the complex network of factors that influence *N*-glycan branching and the galectin-glycoprotein lattice.

Understanding this regulatory network will undoubtedly highlight areas of susceptibility to dysregulation. As we have shown, understanding the effect of a combination of factors on the lattice can inform us about genetic interactions in disease risk. Since a great deal of risk in complex trait diseases may lie in complex genetic interactions, this should be an emphasis of future studies. Taking a purely genetic approach is unlikely to reveal these interactions due to an astronomical increase in tested hypotheses and the corresponding requirement for immense stringency to avoid false positives.

We have also demonstrated a cell-intrinsic mechanism that homeostatically maintains lattice integrity in the face of disruptive insults to the branching pathway. Thus, in addition to dynamic regulation by external factors, a cellular mechanism has evolved to respond to stress on the Golgi machinery, further highlighting the importance of regulating *N*-glycan LacNAc content.

A major implication of this work is that glycans that are structurally distinct (i.e. poly-LacNAc extended mono-antennary glycans vs. tri-antennary glycans) may nevertheless be functionally equivalent if they contain equivalent amounts of LacNAc and thus bind galectins equally at the cell surface. If true, this may collapse glycan diversity into a smaller group of structures, making the issue of dealing with glycoform complexity more feasible. For example, TCR is glycosylated on at least 7 sites[1]. If we assume that there are 15 possible glycans, then the number of TCR glycoforms, each a unique molecule, equals 15^7 or 170,859,375. If glycans can be collapsed into 7 groups based on LacNAc content, then the number is reduced to 7^7 or 823,543. Though still a large number, this is vastly more manageable. It may be possible in fact, that through further such studies exploring bioequivalence among glycans, a code can be deciphered based on interaction with the galectin lattice, collapsing complexity further.

An interesting open question involves the mechanism by which poly-LacNAc is induced when branching is inhibited. We have shown that it is an almost immediate response, but does not involve increased UDP-GlcNAc levels or iGnT activity. In our estimation, the most likely remaining possibility is therefore a change in localization of UDP-GlcNAc, B3GnT enzymes, or both. For a shift in localization to produce such a large effect implies that under branching sufficient conditions B3GnT enzymes have little access to UDP-GlcNAc. We know however, that UDP-GlcNAc must be abundant in the Golgi in order to supply the Mgat enzymes. Nevertheless, the Golgi is not one compartment but rather several compartments in series[2]. In fact, it is known that the glycosylation enzymes are organized along the Golgi in the order in which they act[3,4]. Thus the branching enzymes are present in an earlier compartment than the B3GnT

enzymes. It is therefore possible that the UDP-GlcNAc transporter is preferentially localized to the Mgat compartment but absent from the more *trans* B3GnT compartment.

Unfortunately, there are currently no commercially available UDP-GlcNAc transporter or B3GnT antibodies that have been validated for immunostaining. However, we have acquired a plasmid encoding for a DDK tagged version of SLC35A3, one of the two UDP-GlcNAc transporters expressed in Jurkat cells, as well as an mVenus tagged B3GnT2 construct. Experiments are under way to transfect Jurkat cells with these constructs and determine their sub-Gogli localization using co-localization analysis with known Golgi subcompartment markers by confocal microscopy. If indeed they are localized to different compartments, it raises the possibility that UDP-GlcNAc supply to the poly-LacNAc extending enzymes is restricted when branching is intact. If this is the case, we will determine whether co-localization of SLC35A3 and B3GnT2 increases with SW treatment. If the result is positive it can be further evaluated with mislocalization experiments. If it is negative on the other hand, it is possible that the other transporters or B3GnT enzymes are involved. Since it would be challenging to look at all of these combinations individually, a better approach may be to subfractionate the Golgi apparatus and assay for a shift in iGnT enzyme activity between the fractions. Movement of a UDP-GlcNAc transporter between fractions can be evaluated by immunoblotting as western validated antibodies against the UDP-GlcNAc transporters are commercially available.

A final possibility is that branching deficiency induces co-localization of UDP-GlcNAc and a B3GnT enzyme without causing redistribution of the transporter or the

enzyme. The current model of Golgi transport involves progression or maturation of entire cisternae along the secretory pathway while some form of retrograde transport maintains relative distribution of resident Golgi proteins[5]. Under such a model, if UDP-GlcNAc is normally supplied to a compartment upstream of B3GnT2, then in the event that branching is severely inhibited, unused UDP-GlcNAc could move downstream by cisternal maturation driving poly-LacNAc production by B3GnT enzymes. Such an organization would impart an inherent proofreading ability to the Golgi based solely on its architecture, without the need to redistribute glycosylation machinery.

Thus the most direct experiment would be to measure UDP-GlcNAc levels in the B3GnT2 compartment of branching intact versus branching deficient cells. However, this is challenging for several reasons. Firstly, there are no tools available to visualize UDP-GlcNAc localization in cells with sub-Golgi resolution. Secondly, UDP-GlcNAc lacks reactive groups for standard fixation reagents. As a small molecule it is also unlikely to be trapped, and would therefore leak out of cells in response to fixation or permeabilization. The most feasible approach is thus to isolate various Golgi compartments by either immuno-isolation or density gradient methods followed by UDP-GlcNAc measurement by mass spectrometry. However, this approach requires cell lysis/homogenization as well as lengthy isolation procedures. The integrity and permeability of isolated vesicles for UDP-GlcNAc and its stability throughout the procedure are critical for success, yet difficult to predict. Nevertheless, I reckon it’s still worth a shot.

1 Rudd, P. M. *et al.* Roles for glycosylation of cell surface receptors involved in cellular immune recognition. *Journal of molecular biology* **293**, 351-366, doi:10.1006/jmbi.1999.3104 (1999).

2 Dunphy, W. G. & Rothman, J. E. Compartmental organization of the Golgi stack. *Cell* **42**, 13-21 (1985).

3 Dunphy, W. G. & Rothman, J. E. Compartmentation of asparagine-linked oligosaccharide processing in the Golgi apparatus. *The Journal of cell biology* **97**, 270-275 (1983).

4 Kleene, R. & Berger, E. G. The molecular and cell biology of glycosyltransferases. *Biochimica et biophysica acta* **1154**, 283-325 (1993).

5 Glick, B. S. & Luini, A. Models for Golgi traffic: a critical assessment. *Cold Spring Harbor perspectives in biology* **3**, a005215, doi:10.1101/cshperspect.a005215 (2011).